Analysis of Avian Bone Response to Mechanical Loading Using a Computational Connected Network

Li Yuan Mi

A dissertation submitted to the Faculty in Engineering in partial fulfillment of the requirements for the degree of Doctor of Philosophy,

The City University of New York

2004

INFORMATION TO USERS

The quality of this reproduction is dependent upon the quality of the copy submitted. Broken or indistinct print, colored or poor quality illustrations and photographs, print bleed-through, substandard margins, and improper alignment can adversely affect reproduction.

In the unlikely event that the author did not send a complete manuscript and there are missing pages, these will be noted. Also, if unauthorized copyright material had to be removed, a note will indicate the deletion.

ProQuest Information and Learning Company
300 North Zeeb Road
P.O. Box 1346
Ann Arbor, MI 48106-1346

This manuscript has been read and accepted for the Graduate Faculty in Engineering in satisfaction of the dissertation requirement for the degree of Doctor of Philosophy.

April 19, 2004
Date

Mitra Basu
Professor Mitra Basu
Chair of Examining Committee

April 27, 2004
Date

Mumtaz K. Kassir
Professor Mumtaz K. Kassir
Executive Officer

Professor Stephen C. Cowin

Professor Susannah P. Fritton

Professor Michael Anshel

Professor Jonathan J. Kaufman
Supervisory Committee

The City University of New York

Abstract

ANALYSIS OF AVIAN BONE RESPONSE TO MECHANICAL LOADING USING A COMPUTATIONAL CONNECTED CELLULAR NETWORK

Li Yuan Mi

Mentor: Professor Mitra Basu, Co-mentor: Professor Stephen S. Cowin

The hypothesis that mechanical loading induced signals are transmitted and integrated by a connected cellular network (CCN) before reaching bone surfaces where adaptation occurs is investigated in this study. Our objective is to develop a computational connected cellular network (CCCN) model to explore how bone cells transmit the signals through intercellular communication. The intercellular communication signal is selected as the bone fluid shear stress induced by bending and axial loading in transverse sections of avian long bones in two animal adaptation experiments (Gross et al. J Bone Miner Res 12:982-988, 1997 and Judex et al. J Bone Miner Res 12:1737-1745, 1997). The distribution of the fluid shear stress is computed using a mathematical model based on the microstructure of the avian bones. The computed fluid shear stress is found to be correlated with the radial strain gradient obtained in the experiments. However, experimentally determined bone response shows no linear spatial correlation with the absolute value of averaged shear stress. These results suggest that the radial strain gradient is the driving force for bone fluid flow in the radially distributed lacunar-canalicular system and that bone formation is not linearly related to the loading induced local stimulus.

A CCCN model is developed to study the intercellular communication within a grid

of bone cells by correlating bone adaptation responses in the experiments with the computed fluid shear stress. Intercellular communication patterns extracted by adjusting cell sensitivities (loading and signal thresholds) and connection weights indicate the cell population responsible for perceiving the loading induced signal and regulating bone formation in the CCCNs. The averaged cell sensitivities and connection weights are shown to be inversely correlated with the averaged fluid shear stress across the bone section. Network results suggest that the loading threshold play an important role in regulating the bone response. The proposed CCCN model provides a unique and important tool to analyze intercellular communication and to discover the underlying relationship between input and output data in biological structures.

Acknowledgements

I would like to thank my advisor Professor Mitra Basu for her guidance and encouragement throughout this work. Her clear and concise scientific writing style has deep influence on me. I thank Professor Stephen C. Cowin for introducing this research direction to me and for his help in the computation of bone fluid shear stress.

I am grateful to Dr. Ted Gross and Dr. Stefan Judex for kindly providing the experimental data. Thanks to Dr. John Currey and Dr. Stephen Doty for the preparation and histological examination of turkey bone sections.

I would like to acknowledge Dr. Jonathan J. Kaufman, Dr. Liyun Wang, Dr. Lidan You, Dr. Peng Guo, Xiaobing Zhang and Qianhong Wu for inspiring and helpful discussions.

Thanks to the people and friends who helped me directly or indirectly to have this dissertation completed. Special thanks to Hang Wan, Dr. Jianjun Feng and Dr. Zhexuan Wang.

I am forever indebted to my Chinese parents Xinghua Wu and Ming Mi who have embraced every dream I have had and to my American parents Barbara and Harold Levine who have been my support of living and studying in the states and resources of adapting to a new culture. This work would not have been possible without their unconditional love, endless patience and tremendous help in every possible way.

This dissertation is dedicated to my Chinese and American parents.

Contents

List of Tables

List of Figures

Chapter 1 Introduction

As a connective tissue, bone is a composite material with fluid and solid phases, providing chief support for the body, attachment for muscles and storage for calcium. The fluid phase (25%) consists of mainly blood and extracellular fluid, and the solid phase (75%) consists of bone cells and extracellular bone matrix (Piekarski, 1973). There are two types of bone cells, namely osteoclasts (bone resorption cells) and osteoblasts (bone forming cells). Osteoblasts have two sub-types of cells. One is osteocytes which are osteoblasts encased in the bone matrix during bone tissue production. The other is bone lining cells, which are inactive osteoblasts in terms of forming bone. Osteoblasts and bone lining cells reside on vascular and bone surfaces. The interaction between the solid and fluid phases provides a basis for mechanical, metabolic and adaptive behavior of bone.

By microstructure, bone can be classified as cortical, or compact, and trabecular, or cancellous bone. Cortical bone is a dense material that is primarily found at the diaphyses of long bones. Trabecular bone is a porous material that is found at the epiphyses, surrounded by a thin layer of cortical bone. Cortical and trabecular bones differ in the development, architecture, function, blood supply and fractures (Jee, 1999).

The most important characteristic of bone, as well as many other biological structures, is self-renewal, an ability of responding to external influences, including mechanical loading. There are two types of self-renewal procedure in bone, namely modeling and remodeling. Modeling occurs during bone growth and healing, changing bone structure

by independent actions of osteoblasts and osteoclasts. Remodeling occurs from bone growth through death, causing no significant changes in bone structure by coupled actions of osteoblasts and osteoclasts at the same site (Freemont, 1993). This study is focused on mechanical loading induced remodeling of matured cortical bones.

The objective of this study is to develop a computational model to investigate intercellular communication between bone cells in response to cellular level stimuli induced by mechanical loading. In this chapter, a review is presented regarding the possible mechanical stimuli responsible for bone remodeling, features of bone responses to mechanical loading observed in experiments, and previously developed computational models depicting cortical bone remodeling. Next, the structure of the extracellular bone matrix, a site suggested to perceive mechanical loading stimuli, is described. Finally, we outline the procedure and results of two animal experiments by Gross et al. (1997) and Judex et al. (1997), which provide data for our computational model.

1.1 Mechanical stimuli and bone response

For over a century, extensive research has been done to analyze the relationship between mechanical loading and bone response. Animal experiments have been employed to identify mechanical loading parameter(s) as the possible mechanical stimuli that signal bone tissue to deposit, resorb or simply maintain its structure. Many mechanical parameters of dynamic loading have been found experimentally to be able to maintain bone mass or to induce surface bone formation. The possible mechanical stimuli are presented here at the tissue level and the cellular level. Experimental results of bone surface formation

in the time and space domains at the tissue level are described as well.

1.1.1 Mechanical stimuli and bone response at the tissue level

Animal experiments of cortical bone remodeling induced by mechanical loading suggest the following specific mechanical parameter(s) to be the possible stimuli that initiate bone response:

- *Strain magnitude:* Bone formation or bone formation rate is found to be proportional to the peak strain magnitude above 1000 $\mu\varepsilon$ (O'Connor et al., 1982; Rubin and Lanyon, 1985; Turner et al., 1994; Hsieh et al., 2001).

- *Loading frequency:* When strain magnitude and number of loading cycles per day are constants, bone formation is proportional to loading frequency from 0 to 2 Hz (Turner et al., 1995). When loading frequency increases from 1 to 30 Hz, the smallest strain magnitude required for bone maintenance decreases from 1200 to 100 $\mu\varepsilon$ (Qin et al., 1998).

- *Number of loading cycles:* If the applied loading force and strain magnitude increases, the number of loading cycles required to initiate bone formation decreases (Cullen et al., 2001).

- *Strain rate:* Bone formation is found in proportional to strain rate (O'Connor et al., 1982; Turner et al., 1995; Mosley and Lanyon, 1998).

- *Strain gradient:* Loading induced bone formation is correlated in the space domain to the circumferential strain gradient (Gross et al., 1997; Judex et al., 1997).

- *Strain distribution:* Functionally isolated avian bone experiments show that external loading with a physiological strain magnitude and altered strain distribution can prevent remodeling and maintain bone mass (Rubin and Lanyon, 1984).

- *Strain history:* Animal experimental studies and strain analyses suggest that the bone adaptation maybe related to the changes in cyclic strain history (Carter, 1984).

- *Strain energy density:* It is hypothesized that the heat energy generated during cyclic loading may lead to the chemical reactions initiating bone remodeling (Carter et al., 1987; Huiskes et al., 1987).

- *Microdamage:* Animal experiments indicate that loading within the physiological range with relatively few load cycles can produce substantial microdamage, which may be a significant factor in initiating intracortical bone remodeling (Burr et al., 1985).

Bone tissue response in the time domain: The response of bone to exterior mechanical loading involves different timescales. The tissue response of actively depositing bone induced by a short period (in minutes) of mechanical loading was found in a few days (Pead et al., 1988). Bone response is observed to be able to continue for months before reaching a steady state. In a four-point bending experiment on an adult rat tibia, periosteal bone formation was elevated transiently for 6-12 weeks (Cullen et al., 2000).

In addition, bone tissue exhibits saturation to mechanical stimuli in animal experiments. An experiment with the isolated turkey ulna model showed that only four loading cycles a day are sufficient to maintain bone mass, and 36 loading cycles are adequate

to initiate bone formation (Rubin and Lanyon, 1984). It is demonstrated that loading applied with discrete bouts, separated by recovery periods, is more effective in enhancing bone biomechanical and structural properties (Robling et al., 2002; Srinivasan et al., 2002). Bone tissue shows saturation to a long term loading as well. In the above four-point bending experiment, loading that continued beyond week 12 is found to only maintains the current bone status (Cullen et al., 2000).

Bone tissue response in the space domain: Bone tissue response happens on one of the four surfaces, namely periosteal, endosteal, osteonal, and trabecular surfaces (Frost, 1990). Mechanical loading induced bone formation is observed predominantly at the periosteal surface for mature animals (Rubin and Lanyon, 1984; Raab-Cullen et al., 1994; Gross et al., 1997; Judex et al., 1997; Hsieh et al., 2001; Srinivasan et al., 2002). Occasionally loading induced bone formation occurs not only at the periosteal surface, but also at the endosteal surface (Rubin and Lanyon, 1985; Qin et al., 2003).

Bone tissue response to mechanical loading is site-specific at different surfaces. Even at the same surface, bone formation is observed to be nonuniformly distributed at cross sections (Loitz and Zernicke, 1992; Gross et al., 1997; Judex et al., 1997).

1.1.2 Mechanical stimuli and bone cell response at the cellular level

At the cellular level, bone is described as a mechanosensory and mechanotransduction system. Mechanosensory concerns the detection of a loading stimulus by bone cells, and connects two domains, namely the loading stimulus acting on bone cells and the

cell response, or signal, to the stimulus. Mechanotransduction involves the cell-cell transmission of the signal until it reaches action cells.

Mechanosensory: The main objective of mechanosensory system is to translate mechanical forces into mechanobiological, mechanochemical, biochemical and electromechanical signals. However, the mechanism of the translation is still unclear. Four changes are generated by a dynamic loading on bone, namely the direct cell deformation, hydrostatic pressure, fluid shear stress, and electrical fields (Cowin, 1999). The direct cell deformation may lead to cell response involving stretch activated ion channels, which may initiate cellular electrical events (French, 1992) and the transmembrane integrin molecule which provides a stimulus to activate osteocytic gene expression (Jones et al., 1991). The other three changes are related to loading induced bone fluid flow. The change of hydrostatic pressure enhances molecular transport from the blood supply to bone cells and consequently regulates cell activity and metabolic functions (Piekarski and Munro, 1977; Jacobs et al., 1998). Fluid shear stress is proposed as the stimulus acting on the membranes of osteocytic processes in bone's lacunar-canalicular system (Weinbaum et al., 1994) (more details below). The electrical fields can be induced by fluid flow generated streaming currents and potentials, formed by a diffuse double layer of fluid electrolyte with positive charges (Pollack et al., 1984; Salzstein and Pollack, 1987). The generated electrical field can activate voltage sensitive ion channels and modulate osteocyte membrane permeability (Lanyon and Hartman, 1977; Cowin et al., 1991; Harrigan and Hamilton, 1993).

Although the nature of the stimulus that activates bone cells is still debated, more attention has been given to the fluid shear stress as the stimulus at the cellular level.

Bone cells have been shown to be more responsive to fluid flow than mechanical strain (Owan et al., 1997; Smalt et al., 1997). In addition, fluid shear stress, not streaming potentials (Klein-Nulend et al., 1995; Bakker et al., 2001) or the molecular transport induced by hydrostatic pressure change (Bakker et al., 2001), is shown to be responsible for the increased bone cell activities. In this study, we chose the fluid shear stress as the stimulus at the cellular level.

Osteocytes are suggested to be the sensor cells in bone mechanosensory system. In vivo, the activity of osteocytes, osteoblasts and bone lining cells is observed to be increased immediately (in minutes) after a short period of dynamic loading (Skerry et al., 1989; Pead et al., 1988; Dodds et al., 1993). In vitro, osteocytes, osteoblasts and bone lining cells are shown to be responsive to fluid flow by significantly increased signaling molecules, including prostaglandins (Reich and Frangos, 1991; Ajubi et al., 1996), intracellular calcium (Williams et al., 1994; Hung et al., 1995), inositol trisphosphate (Reich and Frangos, 1991), nitric oxide (Klein-Nulend et al., 1995; Bakker et al., 2001) and gene expression (Klein-Nulend et al., 1997; Ogata, 1997). However, osteocytes have been demonstrated as the most mechanosensitive cells in bone, compared to osteoblasts and lining cells (Klein-Nulend et al., 1995; Zaman et al., 1999; Westbroek et al., 2000).

Mechanotransduction: The function of bone mechanotransduction system is to transmit signals detected by sensor cells (osteocytes) to action cells (osteoblasts and osteoclasts) through intercellular communication. It has been shown that two neighboring bone cells are connected to each other through gap junctions, channels assembled by two matching rings of proteins penetrating the membrane of each cell. Gap junctions enable the direct exchange of ions and small compounds between two cells; thus allowing

a bone cell to have intercellular communication with its neighboring cells (Civitelli et al., 1993; Jones et al., 1993; Donahue et al., 1995). Gap junctions are formed primarily by connexin43 (Cx43) in bone. Osteocytes are observed in vivo with strong expressers of Cx43, both on the cell bodies and on their dendritic processes (Jones et al., 1993). Intercellular communication through gap junctions has been revealed experimentally in osteocytes (Jones et al., 1993; Palumbo et al., 1990), osteoblasts (Doty, 1981; Chiba et al., 1994; Donahue et al., 1995; Lecanda et al., 1998; Saunders et al., 2001; Romanello et al., 2003) and between osteocytes and osteoblasts (Doty, 1981; Yellowley et al., 2000).

Mechanical loading is found to be able to modulate the function of gap junctions. The intercellular communication through gap junctions involves cellular electrical events initiated by stretch and voltage activated ion channels (K^+, Ca^{2+}, Na^+ and Cs^+) and action potentials (Ypey et al., 1992; Rawlinson et al., 1996; Mikuni-Takagaki, 1999). In vitro experiments indicate that mechanical loading enhances gap junctional communication between osteoblastic cells (Ziambaras et al., 1998), and that intercellular coupling between osteocytes increases in proportional to fluid shear stress level (Jiang and Cheng, 2001).

1.2 Computational modeling of cortical bone response

The object of computational and theoretical modeling of bone adaptation is to quantitatively understand the relationship between mechanical loading and bone response. One type of computational modeling of cortical bone response is to describe the time-dependent change of bone surfaces and material properties. The mechanical stimuli

involved in this type of computational modeling are at the tissue level, including strain, strain energy density, stress and fatigue microdamage. A general assumption of this type of modeling is that bone is a linear elastic material (Hart et al., 1984).

Strain: Based on the assumption, an adaptive elasticity model was developed to estimate the changes of bone density and shape under altered loading or in response to implantation of a bone prosthesis (Cowin and Hegedus, 1976; Cowin and Firoozbakhsh, 1981). Local strain differences, estimated remodeling equilibrium strain and remodeling rate parameters were used to predict the change of the bone surface over time.

Strain energy density: Instead of using strain as the remodeling equilibrium parameter, Huiskes et al. (1987) chose strain energy density to develop a two-dimensional finite-element model for bone adaptation simulation. A threshold of mechanical stimuli is implemented in the model to control the initiation of bone adaptation. Bone surface change can be computed using a remodeling rate with small computational time steps.

Stress: A finite-element model was employed in another computational model to simulate the change of bone shape based on the assumption that the stress distribution at bone surface is homogeneous (Mattheck and Huber-Betzer, 1991). Bone surface change is defined to be linearly related to a surface rate constant and the difference between the von Mises equivalent stress and a reference value of the stress.

Fatigue microdamage: Fatigue microdamage was hypothesized to be the regulating signal for bone to attain an optimal strength in another computational model (Prendergast and Taylor, 1994). Bone adaptation rate is described to be proportional to the microdamage difference compared to that at the remodeling equilibrium over a

time period.

The other type of modeling of cortical bone response recognizes the important roles of bone cells in bone adaptation. The bone adaptation is suggested to be dependent on cellular activity, number, and the surface areas (Martin, 1972). Strain remodeling potential, a parameter determined by the function of strain history, is used to describe the cellular population. If the cellular population is linearly dependent on the strain remodeling potential, the simplified model is equivalent to the linear relationship between strain and surface modeling in Cowin and Van Buskirk (1979).

1.3 Bone connected cellular network (CCN)

Close study of bone structure shows that bone is a well-organized tissue. Osteocytes, the most abundant living cells in mature bones, are embedded in the mineralized cavities called lacuna in the bone matrix. Each osteocyte has dozens of cell processes that lie in fine canals known as canaliculi, which connect either to other osteocytes or to surface osteoblasts, including lining cells. Even in newly formed bone matrix, osteocytes and cell processes remain connected with osteocytes in the preexisting bone matrix. Within each canaliculus, there are two long (each around 15 μm), thin osteocytic processes surrounded by bone fluid (Figure 1.1). These two osteocytic processes can be connected by gap junctions, through which osteocytes are extensively linked together in the lacunar-canalicular system, forming a connected cellular network (CCN) (Figure 1.2).

The CCN is hypothesized to be a mechanosensory and mechanotransduction system, in which the mechanical induced signals are most likely processed and integrated be-

fore reaching the action cells to regulate the bone renewal processes such as site, rate, direction, magnitude and duration (Moss and Cowin, 1997). Given the interconnected structure, the CCN is suggested to function as a network with osteocytes as nodes and osteocytic processes as connections. Each osteocyte, which functions as an information-processing unit with nonlinear capability, is connected via gap junctions to its neighbors. Cells in a CCN are organized in layers and the cell processes of all osteocytes in all layers have identical functions. The hypothesis that osteocytes may exhibit certain capabilities of neurons is supported by the reported possible involvement of the neurotransmitter glutamate, an important transmitter in the central neural system, in intercellular communication among bone cells (Mason et al., 1997; Patton et al., 1998; Gu and Publicover, 2000; Hinoi et al., 2001; Huggett et al., 2002) and the evidence of short- and long-term memory exhibited by bone cells and tissue (Turner et al., 2002; Spencer and Genever, 2003).

1.4 Animal experiments

Two animal bone adaptation experiments, namely a turkey experiment (Gross et al., 1997) and a rooster experiment (Judex et al., 1997), provide the data of loading conditions and bone formation for this study. Based on the experimental data of the loading conditions, fluid shear stress in the bone CCNs is computed in Chapter 3, which is the basis of developing the computational model of bone CCNs.

1.4.1 The turkey experiment (Gross et al., 1997)

The functionally isolated right radius of ten adult turkeys were subjected to mechanical loading, primarily of a bending type, during a 4-week period with 5 procedures per week. For comparison purposes, only one radius of each bird received a trapezoidal waveform with 10.8 Newton peak loading (see Appendix 2). Thin bone sections (125 μm) were extracted from the midshaft of both radii and digitally scanned to measure bone formation. The mid-diaphyseal cross section of each loaded bone was divided into 24 equal angle sectors and the bending-induced bone formation within each sector was determined by comparing the loaded bone sections to the control sections of the contralateral limb (the left radius) (Figure 1.3). No bone formation was observed in the absence of loading and non-uniform formation at the periosteal surface was found in the loaded bone.

Based on strain gauge data and finite element analysis, Gross et al. (1997) determined the bending induced normal circumferential, radial and longitudinal strain gradients in the cross section of the bone. The circumferential strain gradient was derived from the difference in normal strain at the midpoints between the periosteal and the endosteal surfaces of a sector divided by the linear distance between these two points (Figure 1.3). Radial and longitudinal strain gradients were calculated along radial and longitudinal directions, respectively, in the same manner. The strain energy density was obtained as the sum of all the components of strain multiplied by the components of the stress at a site bisecting each sector. Bone formation data and strain parameter data were averaged for all animals. The averaged bone formation is correlated with the averaged

strain gradients (in three directions) and the averaged strain energy density using a linear regression model.

1.4.2 The rooster experiment (Judex et al., 1997)

Eight adult roosters were subject to an exercise model of bone adaptation, namely running 1500 loading cycles/day on a treadmill for 3 weeks. Mid-diaphyseal transverse tarsometatarsus sections (300 μm) were cut from the left legs of the roosters and digitally scanned to measure bone formation. Five out of the eight roosters were observed having bone formation at the periosteal surface. The cross section of the tarsometatarsus was divided into 12 equal angle sectors and the loading induced bone formation within each sector was determined by comparing those sections to the corresponding sections of roosters in a control group.

Using the same method as in the turkey experiment, Judex et al. (1997) determined the loading induced mechanical parameters (normal circumferential, radial, longitudinal strain gradients, longitudinal normal strain and peak strain rate) in the mid-diaphyseal tarsometatarsus of six roosters in the control group. The averaged bone formation over all roosters is correlated with the averaged strain gradients using a linear regression model.

1.4.3 The results of the turkey and rooster experiments (Gross et al., 1997; Judex et al., 1997)

Both experiments used the linear regression model to correlate spatial locations and amounts of new bone. The model is a statistic tool to assess the variability of a collection of variables using the least square method. The correlation coefficient r or the square of this coefficient r^2 describes a strength, or a degree of a linear relationship between the actual and the predicted outputs, which enables us to specify to what extent the variables behave alike ($0 \leq r \leq 1$). A large value of the coefficient indicates a strong linear relationship. The correlation coefficient r between the averaged bone formation and the averaged mechanical loading parameters is shown in Table 1.1.

In the turkey experiment, the averaged circumferential strain gradient ($r^2 = 0.36$) is found more related to the averaged bone formation distribution in the space domain than the averaged radial ($r^2 = 0.24$) and the averaged longitudinal ($r^2 = 0.08$) strain gradients. The averaged strain energy density ($r^2 = 0.01$) is found to not be related to the averaged bone formation distribution. The combination of the averaged strain gradients in the circumferential, radial and longitudinal directions shows a better correlation to the averaged bone formation distribution ($r^2 = 0.63$).

In the rooster experiment, the averaged circumferential strain gradient shows a better correlation ($r^2 = 0.63$) with averaged bone formation, compared with the averaged strain rate ($r^2 = -0.28$). The averaged radial strain gradient has negative correlation ($r^2 = -0.72$) with the averaged bone formation. The averaged longitudinal strain gradient ($r^2 = 0.02$) and the averaged longitudinal normal strain ($r^2 = 0.06$) do not correlate

with the averaged bone formation. The combination of the averaged circumferential, radial and longitudinal strain gradients shows a better correlation to the averaged bone formation distribution ($r^2 = 0.72$).

1.5 Thesis objectives and organization

The objective of this study is to develop a computational model to explore how bone cells perceive mechanical loading induced signals through intercellular communication. In Chapter 2, a study employing a similarity between a bone connected cellular network (CCN) and a multilayer neural network is presented. A back-propagation neural network model is employed to simulate the function of a CCN and to capture the nonlinear relationship between mechanical loading and bone formation. Available experimental data is tested and the neural network model validates experimental results. In addition, a nonlinear dependency between mechanical loading parameters and bone formation has been discovered. This work was presented in a conference paper Mi et al. (2000a).

In Chapter 3, a mathematical model is developed to obtain the fluid shear stress induced by bending and axial loading in transverse sections of avian long bones in the two adaptation experiments by Gross et al. (1997) and Judex et al. (1997). The predicted fluid shear stress is found to be correlated with the radial strain gradient obtained in the experiments but bone formation shows no spatial correlation with the absolute value of averaged shear stress. These results suggest that the radial strain gradient is the driving force for bone fluid flow in the radially distributed lacunar-canalicular system and that bone formation is not linearly related to the loading induced local stimulus. This part of

study was presented in a conference paper (Mi et al., 2002a) and has been submitted for publication in *Biomechanics and Modeling in Mechanobiology* (Mi et al., 2004a). The obtained fluid shear stress provides a basis for the development of the computational model of bone CCN in Chapter 4.

In Chapter 4, a computational connected cellular network (CCCN) model is developed to study the intercellular communication within a grid of bone cells. The intercellular communication signal is computed as the loading induced bone fluid shear stress in Chapter 3. Experimentally determined bone adaptation responses in turkeys and roosters are correlated with the fluid shear stress by a learning algorithm that adjusts cell sensitivities (loading and signal thresholds) and connection weights. Communication patterns show the cell population responsible for perceiving the loading induced signal in the turkey and rooster CCCNs. With limited animal data sets, CCCNs extract a distinct intercellular communication pattern in which the averaged cell sensitivities and connection weights are inversely related to the averaged fluid shear stress across a bone section. The loading threshold is shown to play an important role in regulating bone response. The development of the learning algorithm was presented in a series of conference papers (Mi et al., 2000b, 2001; Basu et al., 2002; Mi et al., 2002b) and has been submitted for publication in *Biomechanics and Modeling in Mechanobiology* (Mi et al., 2004b).

Future work and final remarks about this research are presented in Chapter 5.

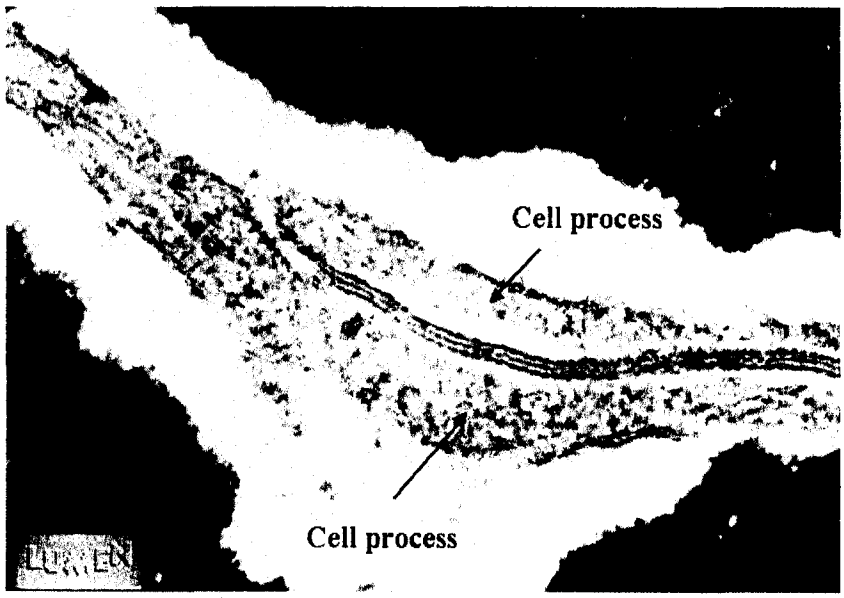

Figure 1.1: An image of two cell processes in a canalicular channel. Intercellular communication between the two cells can be established through gap junctions (From http://www.meddean.luc.edu).

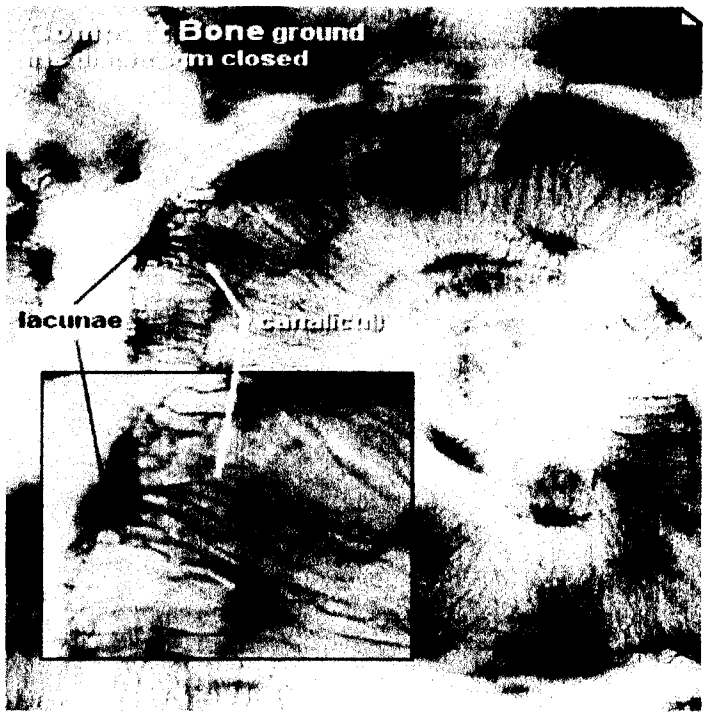

Figure 1.2: An image of the lacunar-canalicular system of an osteon in a human long bone. Osteocytes located in lacunae are embedded in bone matrix. The radially distributed canaliculi connect osteocytes to each other, forming a connected cellular network (CCN) (From http://www.meddean.luc.edu).

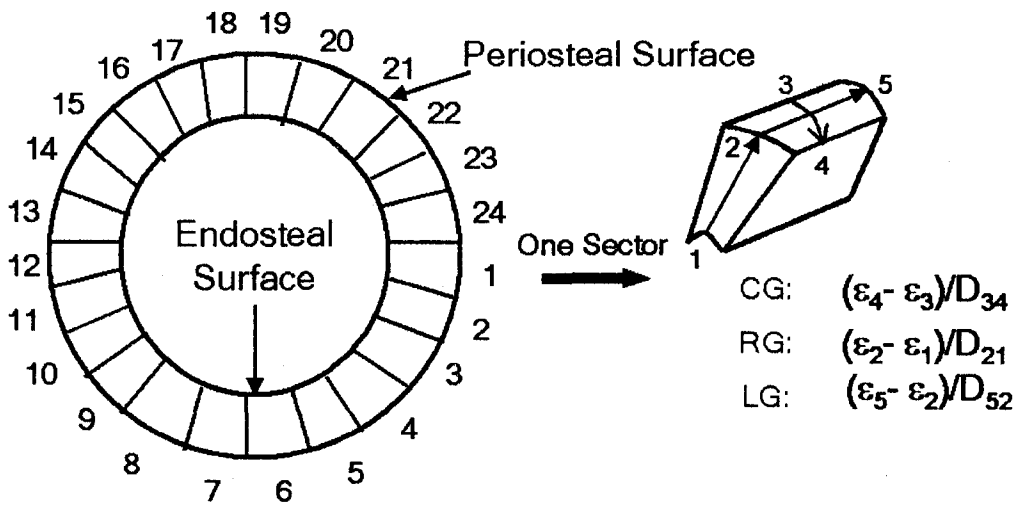

Figure 1.3: A diagram shows a turkey radius cross-section with the 24 sectors from the turkey experiment. Strain gradients in three directions are calculated for each of the 24 sectors. *CG*: Circumferential strain gradient, *RG*: Radial strain gradient, *LG*: Longitudinal strain gradient, ε_i: normal strain magnitude at surface i, D_{ij}: linear distance between surfaces i and j. (Adapted from Gross et al. (1997)).

Table 1.1: The square of correlation coefficient r between the averaged bone formation in the turkey and the rooster experiments and the averaged mechanical loading parameters (from Gross et al. (1997) and Judex et al. (1997)). CG_a: the averaged circumferential strain gradient, RG_a: the averaged radial strain gradient, LG_a: the averaged longitudinal strain gradient, SED_a: the averaged strain energy density, $NorLG_a$: the averaged longitudinal normal strain, SR_a: the averaged strain rate, $CG_a + RG_a + LG_a$: the combination of the averaged circumferential, radial, and longitudinal strain gradient.

Loading parameters	The turkey experiment (r^2)	The rooster experiment. (r^2)
CG_a	0.36	0.63
RG_a	0.24	-0.72
LG_a	0.08	0.02
SED_a	0.01	-
$NorLG_a$	-	0.06
SR_a	-	-0.28
$CG_a + RG_a + LG_a$	0.63	0.72

Chapter 2 Study of Site-Specific Bone Formation Using A Neural Network Model

Bone connected cellular network (CCN) has been proposed as a mechanosensory and mechanotransduction system, where the mechanical loading induced signals are perceived. The signals are sensed by bone cells and transmitted through intercellular communication within the network before reaching action cells (osteoblasts and osteoclasts) on surfaces where bone adaptation occurs. This study exploits a similarity between the CCN and a multilayer neural network to capture the nonlinear relationship between mechanical loading parameters and bone formation. The data from the turkey and the rooster experiments are tested and the neural network model validates experimental results. The correlation coefficient for each animal sample is shown to maintain its basic characteristics irrespective of the loading parameters. The study supports and validates the hypothesis that the signal transmission in a CCN during bone formation is a nonlinear process. In addition, a nonlinear dependency between certain loading parameters and bone formation has been observed.

2.1 Introduction

It has long been recognized that bones respond to external influences by changing their shape and density. Mechanical loading is considered an important influence that can

initiate bone adaptation response. Experiments with animals reveal that bone formation initiated by mechanical loading is site-specific (Churches and Howlett, 1982; Johnson et al., 2001; Gross et al., 1997; Judex et al., 1997; Skedros et al., 2003), i.e., large bone formation does not necessarily occur at the locations where the intensity of loading is large. Linear correlation model was not successful to capture the functional relationships in the space domain between various mechanical loading parameters and the bone adaptation response (Brown et al., 1990). This implies that bone response to mechanical loading may be a nonlinear process.

In the bone matrix, all bone cells except osteoclasts are extensively interconnected with each other to form a connected cellular network (CCN). It has been proposed that the signals sensed by osteocytes are processed and integrated through the CCN before activating osteoblasts and osteoclasts; and that a bone matrix is operationally analogous to a self-adapting and self-organizing system Moss and Cowin (1997).

This study implements a similarity between the CCN and a self-adapting network, a system with learning ability, to investigate the nonlinear relationship between mechanical loading parameters and bone formation. To a large extent, osteocytes as signal-sensing units and probably, signal-processing units in the CCN, function very much like the nonlinear interacting neurons in a neural network model. Each neuron in the neural network model functions as an information-processing unit with nonlinear capability, and an overall nonlinearity is incorporated throughout the model.

Neural networks, or artificial neural networks, aim to understand and simulate the function of the human brain, which is a highly complex, nonlinear and parallel processor.

They are systems composed of interconnected processing elements in a manner similar to that of the brain's neurons. Neural networks find abundant applications in diverse fields such as modeling, pattern recognition, signal and information processing. The advantage of neural networks becomes more evident in problems that are too elusive or too complex to be formulated explicitly in terms of mathematical equations.

There are three basic components in a neural network (Haykin, 1999), namely processing elements, or neurons; architecture, or network topology; and a method for learning input-output relationship, or a learning rule. A neuron receives data from other neurons in the network or from external input. The data is processed and new data is sent out by the neuron. The connection between two neurons is a weighted link, an adjustable value, which can be positive (excitatory) or negative (inhibitory). A neuron sums up all the weighted data from other neurons or external input and computes the output according to a threshold and an activation function.

The architecture of a neural network describes the way neurons are connected. There are several kinds of connections. For example, neurons can be all connected with each other, or they can be connected into two or more layers, where the output of a neuron can propagate forward only or with feedback.

A learning rule is the method to adjust weights in order to achieve the objective of a neural network. Learning can be done without (unsupervised learning) or with (supervised learning) a teacher (desired output data). In unsupervised learning, only input data is known and the neural network self-organizes itself in order to separate input data into different classes. In supervised learning, both input and the desired

output data is known and used in the training phase. Weights are adjusted to decrease the error signal (difference between the desired output and the computed output) until the error signal is sufficiently small.

We make use of a back-propagation neural network model to investigate the non-uniformity and site-specificity of bone formation. Data from the turkey and the rooster experiments described in Chapter 1 are used for the learning process, and the results are compared with those obtained from a linear model.

2.2 Neural network model development

An important and the most commonly used supervised learning rule is the back-propagation (BP) learning rule (Haykin, 1999), which can learn any functional relationship. It is composed of a hierarchy of computational elements, organized in a series of two or more mutually exclusive layers. The first, or input layer serves as a holding site for the values applied to the network. The last, or output layer is the point at which the final output of the network is read. Between these two extremes lie zero or more layers of *hidden* computational elements. Weighted links connect each element in one layer to only those in the next higher layer.

The BP learning algorithm consists of two phases, namely training phase and testing phase. The training phase has two distinct passes, namely the forward pass and the backward pass. In the forward pass, the output of the network for a particular input is computed on an element-by-element and layer-by-layer basis as connection weights remain fixed. The error (difference between actual and desired output) is computed

and this is proportionately propagated backward layer-by-layer to adjust the connection weights during the backward pass. This cycle is repeated until the error signal is within some acceptable range. At this point, the relationship between the network input and output is believed to have been encoded in the connection weights among computational elements/cells. This ends the training phase (for detailed BP learning algorithm, see Appendix 1). The trained BP network with fixed connection weights is ready to predict/classify new input vectors. This is the testing phase. We chose a BP network with one hidden layer as the model to capture the nonlinearity between loading parameters and the site-specific bone formation data.

2.2.1 Linear correlation of individual animals

In the turkey and the rooster experiments by Gross et al. (1997) and Judex et al. (1997), the linear relationship was obtained between the averaged bone formation and the averaged loading parameters. However, the linear relationship between bone formation and loading parameters of individual animals is unknown. In order to compare the results of a BP network, a linear regression model is used to compute the correlation of each animal in the two experiments.

2.2.2 BP network model for the turkey experiment

The BP network model for the turkey experiment has input, hidden and output layers (Figure 2.1). Since each bone cross section was divided into 24 sectors in the turkey experiment, the input of the BP network for the experiment is a 24-dimensional vector.

There are 16 neurons in the hidden layer and 24 neurons in the output layer. The sigmoid function is used as the activation function for the hidden layer. The number of neurons in the hidden layer and the form of the activation function are decided by the trial-and-error method. Four types of mechanical loading parameters (the circumferential strain gradient, the radial strain gradient, the longitudinal strain gradient, and the strain energy density) for each of the 24 sectors serve as four types of inputs. The measured bone formation in each of the 24 sectors from the turkey experiment serves as the outputs.

Among the ten experimental turkeys, one showed no response to mechanical loading (zero bone formation over all the 24 sectors) and is taken out of the data set. From a total of nine turkeys with bone response, one is chosen randomly as the testing data and the other eight as the training data. The network is reinitialized several times for the same training sample to avoid local minima. The correlation coefficient r (a measure of the similarity between the computed output of the network and the desired output from the experiment data) is computed for each testing sample.

2.2.3 BP network model for the rooster experiment

The BP network model for the rooster experiment is similar to the one used in the turkey experiment, except that the input is a 12-dimensional vector (corresponding to the 12 sectors in the cross section of the rooster bone) and that there are five neurons in the hidden layer and 12 neurons in the output layer.

In the rooster experiment, the bone formation and the mechanical loading data were

collected from a loading group (eight roosters) and a control group (six roosters), respectively. Among the eight roosters in the loading group, three showed no response to mechanical loading and are taken out of the data set. Five types of mechanical loading parameters, namely the circumferential strain gradient, the radial strain gradient, the longitudinal strain gradient, the longitudinal normal strain, and the strain rate were obtained from the six roosters in the control group. The five types of loading parameters and the bone formation serve as the input and the output of the BP network, respectively.

The fact that the bone formation and loading parameters were obtained from two different groups in the rooster experiment rules out the possibility of pairing up the bone formation and the loading parameters for the same rooster. A random pairing up is employed. From the six roosters in the control group, one rooster is chosen randomly as the testing sample, and the other five roosters as the training samples. The network is reinitialized several times for the same training group to avoid local minima. The correlation coefficient is computed between the loading parameters of the testing sample and the averaged bone formation of the loading group.

2.2.4 Validation

To validate the ability of the BP network of capturing the nonlinear relationship between the input and the output data, randomly generated data is used to test the function of the network. For each of the five mechanical loading parameters in the rooster experiment, 50 sets of the data with the same dimension within the same range are randomly generated

by a computer, among which 35 sets were randomly chosen as the training data with remaining sets serving as the testing data. Bone formation data is randomly generated in the same manner. The same BP network for the rooster experiment is used in the validation. Correlation coefficients are obtained for each type of mechanical loading.

2.3 Results

2.3.1 Linear correlation of individual animal

The correlation between the bone formation and the four types of loading parameters in the turkey experiment using a linear regression model is not strong (Figure 2.2). The correlation coefficient r above 0.5 is observed only for turkey No. 2 and 3 (with the circumferential strain gradient) and for turkey No. 1 (with the strain energy density). The correlation between the bone formation and other loading parameters for any turkey does not show any characteristic and appears rather random.

The correlation between the bone formation and the five types of loading parameters in the rooster experiment shows distinctive characteristics compared to the turkey group (Figure 2.3). A strong correlation ($r > 0.7$) between the bone formation and the circumferential strain gradient is observed for all roosters. The radial strain gradient shows a strong and negative ($r < -0.7$) correlation with the bone formation for all roosters. The rest of the loading parameters do not show correlation with the bone formation.

2.3.2 BP network results of the turkey experiment

The network converges (error reached a preset value) for all the turkey training data sets within a reasonable number of training cycles. The error generated by the network for turkey No. 3 with the longitudinal strain gradient as the input is shown in Figure 2.4.

The correlation coefficient between the network predicted bone formation and the loading parameters show relatively a larger value ($r > 0.5$) for several turkeys when they serve as the testing sample (Figure 2.5). Compared to other loading parameters, the circumferential strain gradient gives a better prediction of bone formation for turkey No. 2, 4, 5, 7 and 8. Other loading parameters show relatively good predictions of bone formation for fewer turkeys, including the strain energy density with turkey No. 2 and 4, the longitudinal strain gradient with turkey No. 3 and the radial strain gradient with turkey No. 9.

Another observation from the network results is that the correlation coefficient of the predicted bone formation maintains its characteristic irrespective of the loading parameter type for a few turkeys (Figure 2.5). For example, the correlation coefficient is consistently low for turkey No. 1 ($r < 0.38$ for all loading parameters) and turkey No. 7 ($r < 0.28$ for all loading parameters), while it is consistently high for turkey No. 2 ($r > 0.45$ for all loading parameters).

2.3.3 BP network results of the rooster experiment

The network converges (error reached a preset value) for all the rooster training data sets within a reasonable number of training cycles. The error generated by the network for rooster No. 1 with the circumferential strain gradient as the input is shown in Figure 2.6.

The network successfully predicts bone formation for all roosters (Figure 2.7). The correlation coefficient value between the predicted bone formation and the five loading parameters are high ($r > 0.65$) for every rooster. The circumferential and longitudinal strain gradients give the best prediction of bone formation ($r > 0.85$) for all roosters, compared with the longitudinal normal strain and strain rate.

The correlation coefficient for roosters shows similar characteristics to the network results of the turkey group. The correlation coefficient is consistently high irrespective of the loading parameters for certain testing samples, such as rooster No. 4 and 5, as opposed to others, such as rooster No. 1 and 6.

2.3.4 Validation

No correlation is found between the randomly generated input and output data (Figure 2.8). The correlation coefficients of all 15 sets of testing data show unsteady and random value for all five types of input.

2.4 Discussion

The bone response of turkeys appears to happen in a more complicated way than that of roosters. Although the averaged loading parameters (the circumferential strain gradient) show correlation to the averaged bone formation to a certain degree ($r = 0.6$) in the turkey experiment (Gross et al., 1997), the correlation between loading parameters and bone formation for each turkey using a linear regression model generally is low. The correlation between the loading parameters and the bone formation varies significantly among animal samples, which indicates the individual difference in bone response to an applied mechanical loading. The BP network captures a nonlinearity between certain loading parameters (the circumferential strain gradient and the strain energy density) and the bone formation for certain turkeys. Bone formation is predicted fairly accurately by the network with one specific loading parameter for a few turkeys, such as No. 2, 3, 4 and 9.

The correlation between all loading parameters and bone formation for each rooster using a linear regression model is low, except with the circumferential strain gradient. However, the BP network captures the nonlinear relationship between all five types of loading parameters and bone formation of the rooster group, and predicts accurately the bone formation for all rooster samples.

The difference in the bone response between the turkey group and the rooster group is unclear. One of the reasons may be the difference in the loading methods and patterns between the two animal groups. In the turkey group, loading was applied through a pair of pins with a loading machine and a functional isolation surgery was employed.

The loading applied on turkey radii was quite different in magnitude and distribution pattern from their physiological daily loading activities, such as wing flipping. In the rooster group, loading was applied through a noninvasive method, namely an exercise model of running on a treadmill. The applied loading on rooster legs may have larger magnitude than their physiological daily loading activities, such as walking or running (Konieczynski et al., 1998), however, the loading distribution pattern is most likely the same. The difference of the network results between the turkeys and the roosters may reflect the difference of avian bone response to different loading magnitude and pattern.

For both the turkey and the rooster network models, the correlation coefficient between input and bone formation changes with the types of input. This leads us to believe that each type of loading parameters affects the bone formation to a different extent. In both models, the circumferential strain gradient is found to have a stronger correlation with bone formation. This is in agreement with the result reported in Gross et al. (1997) and Judex et al. (1997).

Except for the circumferential strain gradient, the BP networks capture the nonlinear relationship between bone formation and other loading parameters. In the turkey group, the network results show that the strain energy density gives a good prediction of bone formation for turkey No. 2 and 4. This is not a surprising result as the strain energy density can be viewed as an information "pool" of the mechanical loading due to the fact that it is a scalar reflecting the contributions from all stresses and strain acting at a given location. In the rooster group, the network results show that all five types of loading parameters give good prediction of bone formation. We theorize that the relationship between the bone formation and all the loading parameters (except the circumferential

strain gradient, whose linear relationship with the bone formation was captured by the linear regression model) are nonlinear in nature.

The results of validating the BP network show that the correlation coefficients are randomly distributed for all testing data. It is clear that the random input data has no correlation with the random output data. Compared with the results of the BP network using the rooster experimental data, the results of the validation indicate that there is a significant difference between the random data and the experimental data, and that the BP network is able to capture the correlation between input and output data, if there is one. This observation is consistent with the conclusions reported in Ho and Basu (2000).

We have proposed a unique approach to model the relationship between bone formation and loading parameters. To the best of our knowledge, neural networks have never been used to explore the relationship between mechanical loading and bone formation. This proposed model for bone response reveals the individual response of each animal to different types of mechanical parameters. It supports and validates the long standing hypothesis that bone formation is a nonlinear process. A plausible conclusion that we can make from the proposed model's response in experiments with different groups of animals is that the method of loading may play a prominent role in the process of bone formation. This shows that a simple mathematical learning model is capable of capturing a complex biological phenomenon with considerable success.

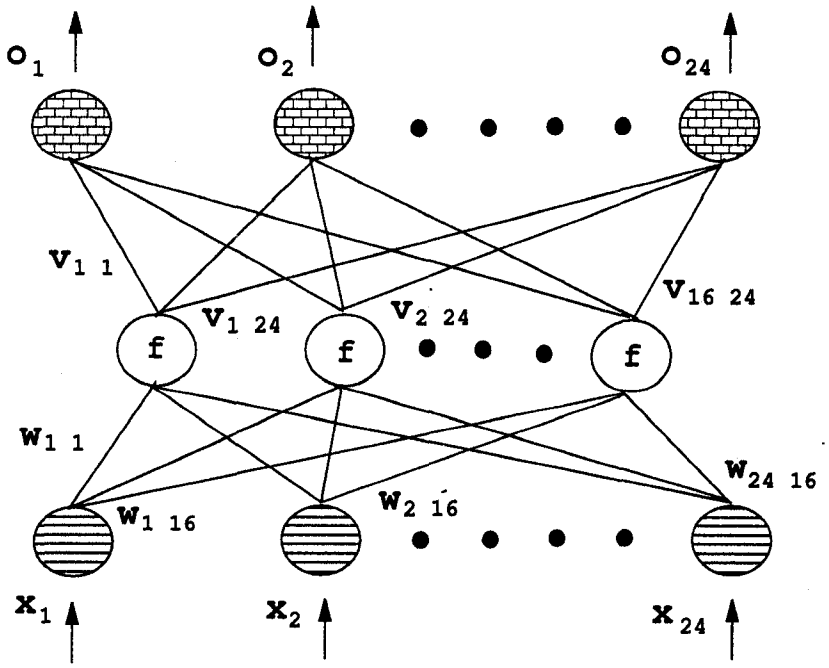

Figure 2.1: The BP network structure for the turkey experiment. There are three layers in the BP model, namely the input layer (the lower layer), the hidden layer (the middle layer) and the output layer (the upper layer). The BP network structure for the rooster experiment is the same as the one for the turkey experiment, except with different numbers of neurons in each layers. In the input and the output layer of the turkey BP network, there are 24 neurons (12 for the rooster BP network) in each layer, depicted as circles filled with lines and bricks, respectively. There are 16 neurons (5 for the rooster BP network) in the hidden layer and the active function for the hidden neurons is represented as f. Two sets of weights W and V connect each neuron in the hidden layer with each neuron in the input layer and the output layer, respectively.

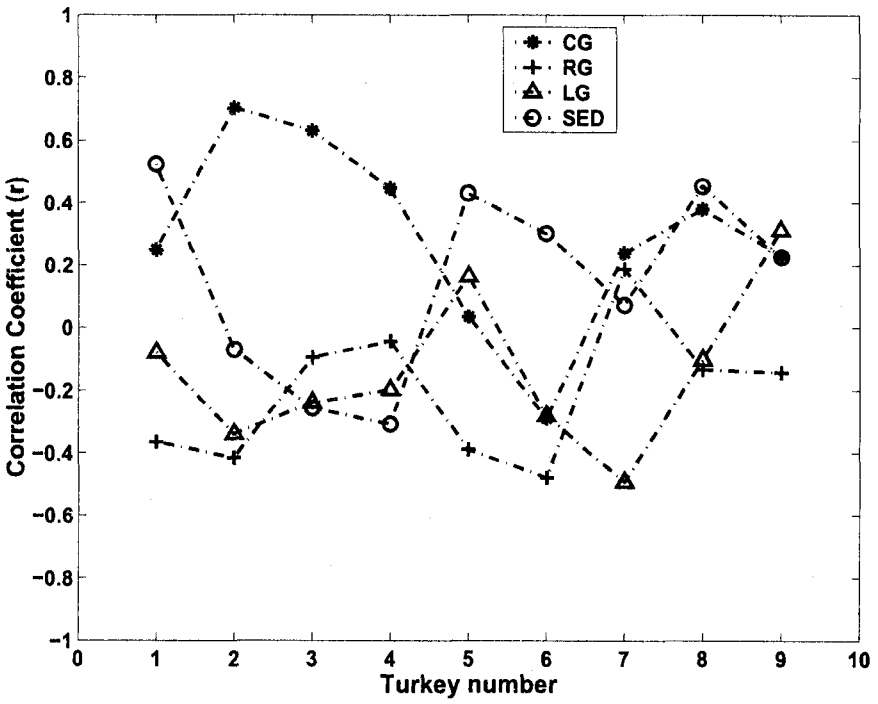

Figure 2.2: The correlation of each turkey using a linear regression model. The correlation coefficient r is computed between the bone formation and following loading parameters: the circumferential strain gradient (CG), the radial strain gradient (RG), the longitudinal strain gradient (LG) and the strain energy density (SED).

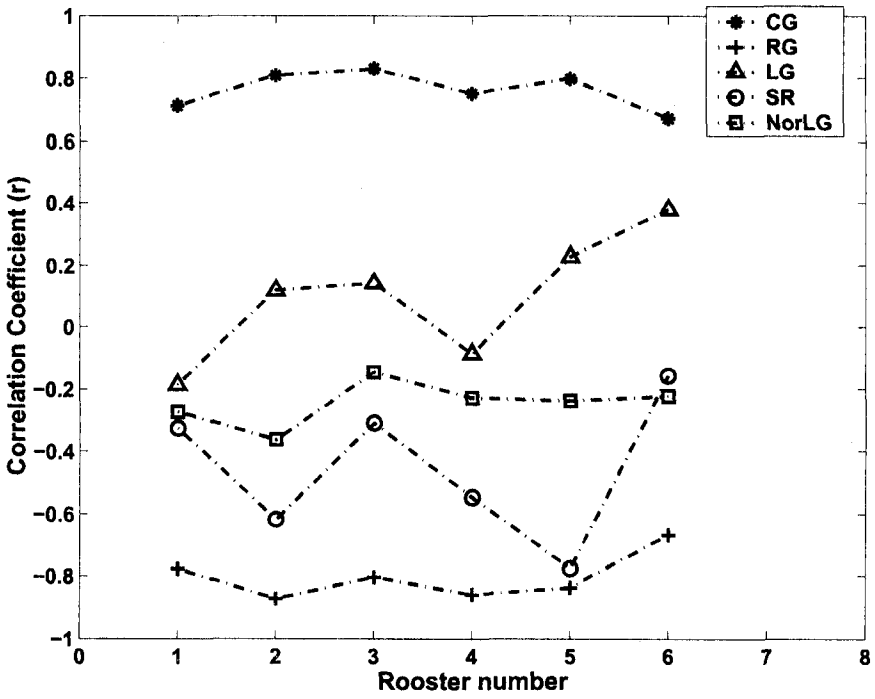

Figure 2.3: The correlation of each rooster using a linear regression model. The correlation coefficient r is computed between the bone formation and five types of loading parameters.

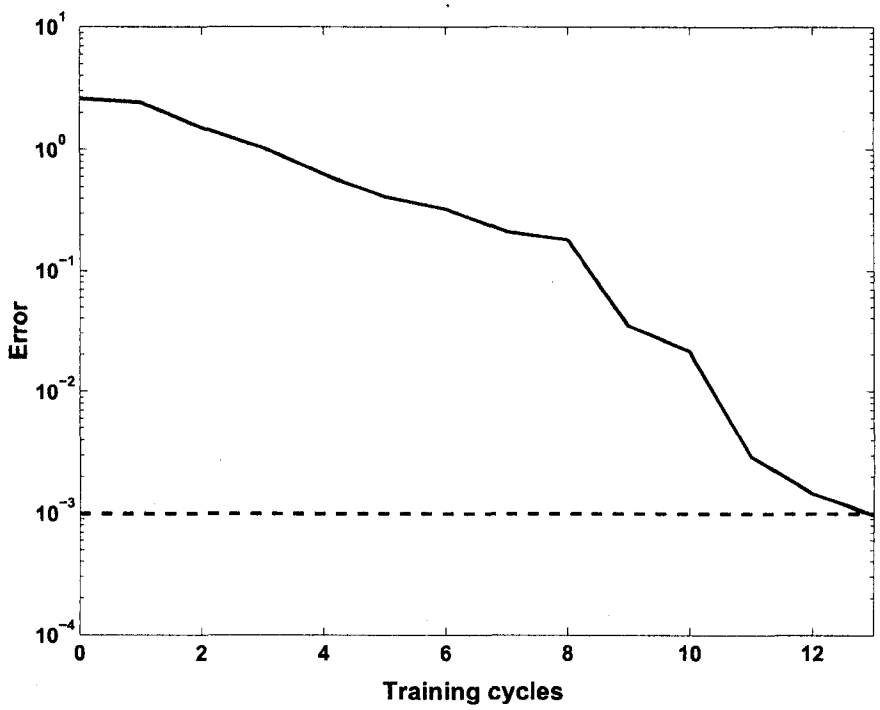

Figure 2.4: The error of the BP network with turkey No. 3 as the testing sample and the longitudinal strain gradient as the input. The error, represented by the solid line, decreases with the training cycle and reaches a preset value (0.001, represented by the dashed line) after 13 training cycles.

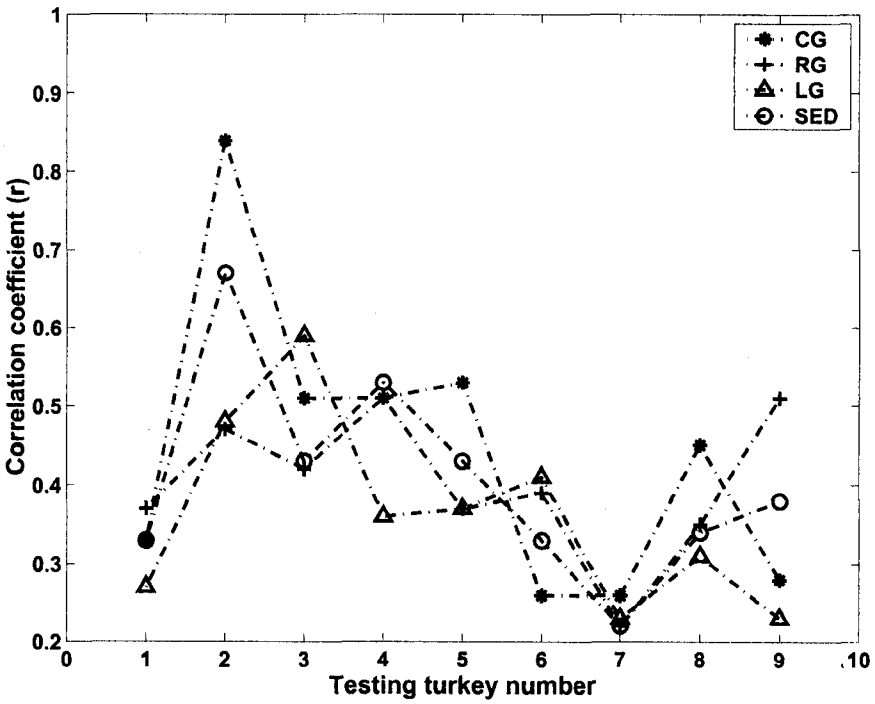

Figure 2.5: The correlation coefficient (r) between the network predicted bone formation and the loading parameters for the turkey served as the testing sample.

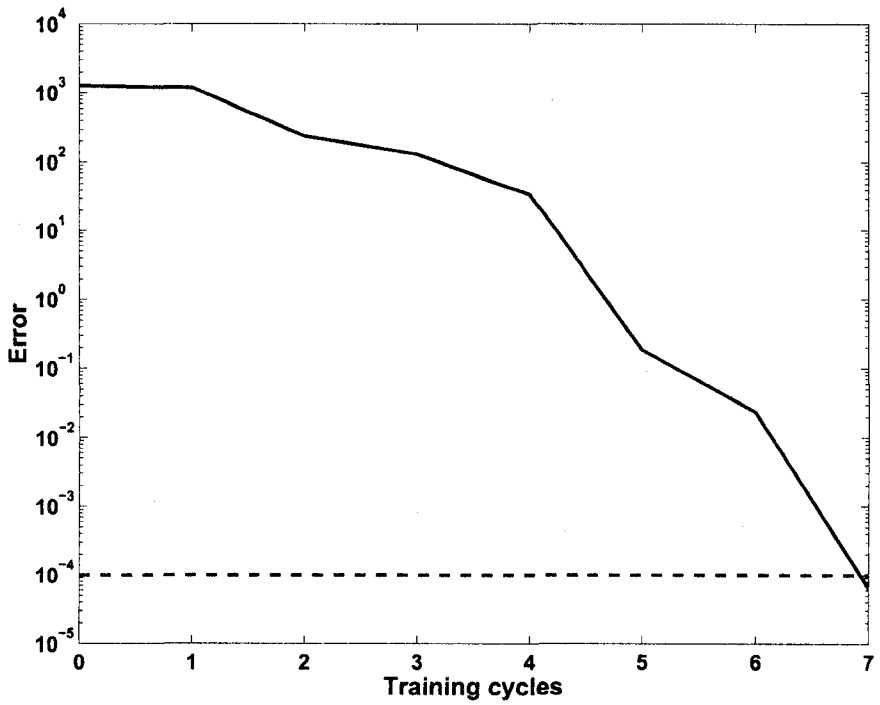

Figure 2.6: The error of the BP network with rooster No. 1 as the testing sample and the circumferential strain gradient as the input. The error, represented by the solid line, decreases with the training cycle and reaches a preset value (0.001, represented by the dashed line) after 7 training cycles.

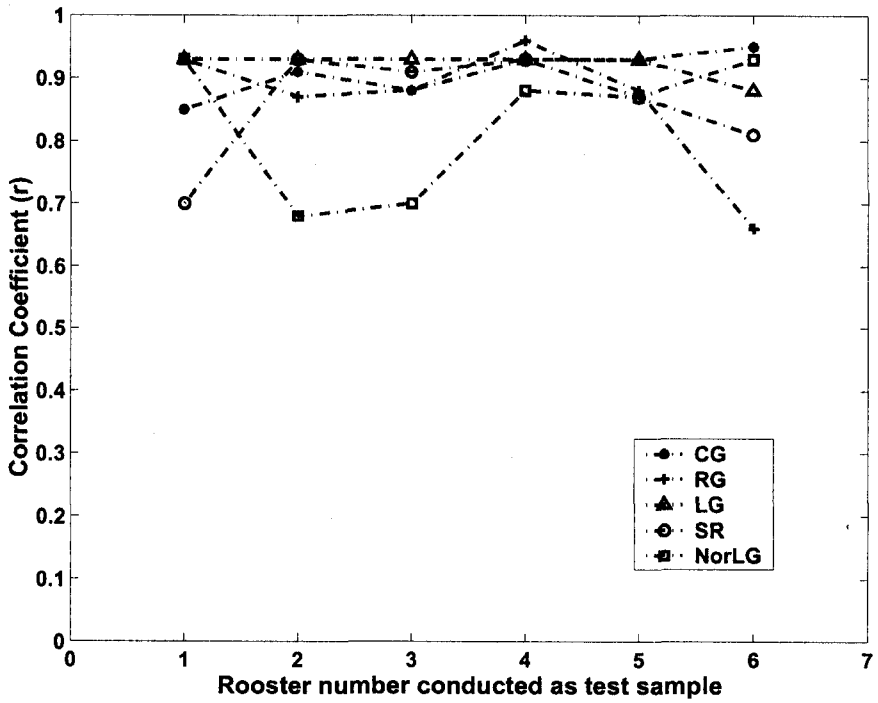

Figure 2.7: The correlation coefficient (r) between the network predicted bone formation and the loading parameters for the rooster served as the testing sample.

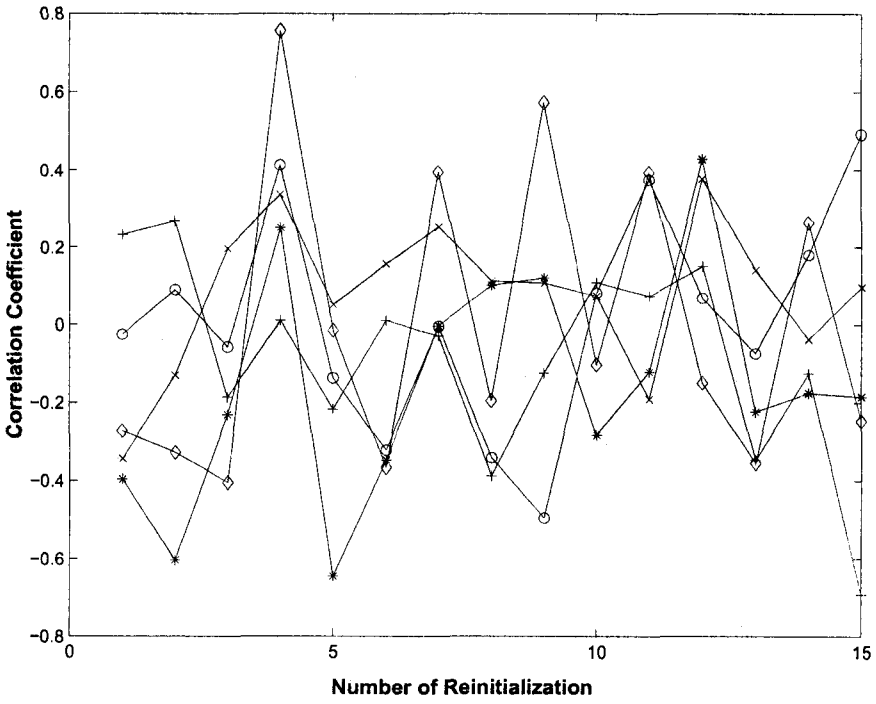

Figure 2.8: Correlation coefficient r between the randomly generated loading parameters and bone formation. Circumferential strain gradient: $*$ Radial strain gradient: $+$ Longitudinal strain gradient: $\circ$ Longitudinal normal strain: $\square$ Strain rate: $\triangle$

Chapter 3 Bone Fluid Shear Stress Induced by Bending and Axial Loading

3.1 Introduction

The fact that the structure of bones can be influenced by mechanical loading is well known; however the excitation signal that initiates the bone adaptation response induced by mechanical loading is still unclear. Different mechanical loading parameters at both the tissue and the cellular level have been suggested as the possible stimulus. The possible mechanical stimuli at the tissue level include strain magnitude (Frost, 1983; Rubin and Lanyon, 1985), strain gradient (Gross et al., 1997; Judex et al., 1997), strain rate (O'Connor et al., 1982; Turner et al., 1995; Mosley and Lanyon, 1998), strain energy density (Carter et al., 1987; Huiskes et al., 1987), loading frequency (McDonald et al., 1994; Turner et al., 1995; Qin et al., 1998), loading intensity and cycle number (Qin et al., 1998; Cullen et al., 2001), strain history (Carter, 1984), and fatigue microdamage (Burr et al., 1985). The suggested mechanical stimuli at the cellular level include the direct cell deformation (French, 1992), hydrostatic pressure change (Piekarski and Munro, 1977; Jacobs et al., 1998), fluid flow induced shear stress (Weinbaum et al., 1994) and the streaming currents and potentials (Lanyon and Hartman, 1977; Pollack et al., 1984; Salzstein and Pollack, 1987; Cowin et al., 1991; Harrigan and Hamilton, 1993). This study focus on the mechanical stimuli at the cellular level.

At the cellular level, bone fluid flow induced shear stress has been proposed to be the excitation of bone cells. Bone cells have been shown to be more responsive to fluid flow than mechanical strain (Owan et al., 1997; Smalt et al., 1997), which is related to the direct cell deformation. Observations from experimental data show that the fluid shear stress is responsible for the increased bone cell activities, not streaming potential (Klein-Nulend et al., 1995; Bakker et al., 2001) or the molecular transport induced by hydrostatic pressure change (Bakker et al., 2001). In this study, we choose the fluid shear stress as the mechanical stimulus at the cellular level.

Bone fluid shear stress acting on the osteocytic processes in the lacunar-canalicular system has been hypothesized to be the stimulus for the bone adaptation response induced by mechanical loading (Weinbaum et al., 1994; Hillsley and Frangos, 1994). Osteocytes, which are embedded in cavities called lacunae, have dozens of cell processes that lie in fine canals known as canaliculi. The canaliculi radiate from the lacunae and interconnect with canaliculi either of adjacent lacunae or of surface lining cells, including osteoblasts, forming the lacunar-canalicular system. When mechanical loading is applied, the interstitial fluid flows in the annular region, interior to the canaliculi and exterior to the osteocytic process, creating a shear stress acting around the exterior surface of the membrane of cell processes in the canaliculi. The hypothesis that fluid shear stress is the mechanical stimulus for bone cells is supported by the observations that osteocytes and osteoblasts are responsive to fluid flow in *in vitro* studies (e.g., Reich et al., 1990; Klein-Nulend et al., 1995; Johnson et al., 1996; Smalt et al., 1997; Jacobs et al., 1998).

The high density and extensive connections between osteocytes suggest that in ad-

dition to being the mechanosensors, osteocytes form a cellular communication network. Within a canaliculus, an osteocytic cell process is connected to a similar process of a neighboring osteocyte or osteoblast via gap junctions (Bennett and Goodenough, 1978; Doty, 1981; Jones et al., 1993; Civitelli, 1995; Moss, 1997b). The gap junctions enable the direct exchange of ions and small compounds between two cells, thus allowing a bone cell to communicate with neighboring cells. Linked by gap junctions in the lacunar-canalicular system, the osteocytes and osteoblasts are extensively interconnected, forming a three-dimensional connected cellular network (CCN). The CCN is suggested to function as a network of neurons, processing and integrating signals sensed by bone cells (Cowin et al., 1991; Moss, 1991). In order to investigate the mechanism of signal processing in the CCN, the determination of the stimulating signal on every bone cell in the CCN is necessary. This chapter presents the results of calculations with that objective.

The fluid shear stress is predicted in avian bones of two animal adaptation experiments, Gross et al. (1997) and Judex et al. (1997). For details, please see Chapter 1. A mathematical model based on the poroelastic model of Zeng et al. (1994) is developed in this chapter. The model has the loading conditions and bone geometry consistent with the adaptation experiments. The pore fluid pressure induced by bending and axial loading in the lacunar-canalicular porosity is first determined using the poroelastic model. Then the fluid shear stresses acting on osteocytic processes of every bone cell in the CCN are calculated from the gradient of pore fluid pressure.

3.2 Mathematical Formulation

Developing a realistic mathematical model of an experimental bone section requires knowledge of the bone's histological structure. While much literature exists relating to human and bovine bone microstructure, the experimental data employed here is from avian plexiform bone, which is of a different structure. The avian plexiform bone is modeled as a series of concentrically arranged alternate layers of mineralized tissue and blood plexies (Figure 3.2b). This model is based on the few descriptions of avian bone structure that could be located (Currey, 1960; Martin and Burr, 1989), along with a turkey bone we examined (Figure 3.1).

3.2.1 Fluid shear stress in the turkey bone

The experimental loading from the Gross et al. (1997) experiment involved a cyclic force $f(t)$ applied to the turkey radius through two pins with moment arm arm L, inducing both a bending moment and an axial force (Figure 3.2a). The plexiform cross-section of a long turkey bone is idealized as a set of concentric cylindrical sections (Figure 3.2b), with r_0 and r_i as the radius of the whole bone and the marrow cavity, respectively. A bone lamina is the mineralized area between any two vascular networks bounded by the radii r_{v1} and r_{v2}. Osteocytes are embedded in the bone lamina and are interconnected through canaliculi forming a connected cellular network (CCN). Osteocytes are assumed to be arranged in a rectangular array with a distance L_c between two osteocytes in the radial direction and a distance L_d in the circumferential direction in the CCN of a transverse cross section of the bone (Figure 3.2b). The bending induced bone fluid shear

stress acting on the surface of the osteocyte process within the canaliculi is a primary objective of the calculation (Figure 3.2c).

In order to predict the fluid shear stress, the normal stresses in the bone matrix due to the mechanical loading $f(t)$ have to be determined. The force $f(t)$ applied to the experimental bone acts in the z direction at point P on the y' axis, perpendicular to the neutral axis (Figure 3.2b). When the whole long bone section is subjected to the load $f(t)$, the sum of the three normal stresses σ_{kk} in the bone is given by

$$\sigma_{kk} = \sigma_0 + \frac{M_{x'}}{I_{y'}}y' + \frac{M_{y'}}{I_{x'}}x', \tag{3.2.1}$$

where $M_{x'}$, $M_{y'}$ are the components of the applied bending moment $M(= f(t) * L)$ about the x' and y' axes, respectively; $I_{x'} = I_{y'} = I$ are the area moments of inertia of the bone section; L is the length of the lever arm; $\sigma_0(= -f(t)/A)$ is the axial normal stress and A is the area of the bone cross section. Since the loading point of $f(t)$ lies on the y' axis, $M_{y'} = 0$, thus

$$\sigma_{kk} = -f(t)(\frac{1}{A} + \frac{L}{I}y'). \tag{3.2.2}$$

Using polar coordinates r, θ (corresponding to the x, y coordinates), and r', θ' (corresponding to x' and y' coordinates), we have:

$$\sigma_{kk} = -f(t)(\frac{1}{A} + \frac{L}{I}r'\sin\theta') = -f(t)[\frac{1}{A} + \frac{L}{I}r\sin(\theta + \gamma' - \pi)]. \tag{3.2.3}$$

The pore pressure p in the lacunar-canalicular porosity due to the applied loading can be calculated using the previously developed differential equation (Weinbaum et al., 1994):

$$c\nabla^2[\sigma_{kk} + \frac{3}{B}p] = \frac{\partial}{\partial t}[\sigma_{kk} + \frac{3}{B}p] \tag{3.2.4}$$

where $c(=r_0^2/\tau_r)$ is the pore pressure diffusion coefficient (Zeng et al., 1994); τ_r is the characteristic time of relaxation of the fluid pore pressure, and B is the Skempton parameter ($0 \leq B \leq 1$), which relates fluid pore pressure to the change of applied mechanical stress. From eq.(3.2.3) and eq.(3.2.4), the pore pressure p induced by loading $f(t)$ can be presented in polar coordinates as:

$$\frac{\partial^2 p}{\partial^2 r}+\frac{1}{r}\frac{\partial p}{\partial r}+\frac{1}{r^2}\frac{\partial^2 p}{\partial^2 \theta}-\frac{1}{c}\frac{\partial p}{\partial t}=\frac{B}{3c}[\frac{1}{A}+\frac{rL}{I}\sin(\theta+\gamma)](-\frac{df(t)}{dt}). \tag{3.2.5}$$

The applied bending load $f(t)$ used in the adaptation experiment of Gross et al. (1997) has a periodical trapezoidal waveform (Figure A1), which can be represented by a Fourier series in order to solve the pore pressure p in eq. (3.2.5) (see Appendix 2). Using eq.(A13) and the following dimensionless variables (see the Appendix 3),

$$R=\frac{r}{r_0}, \tau=\frac{ct}{{r_0}^2}, P=\frac{3p}{BT\sigma_r}, T=\frac{w{r_0}^2}{c}, N_0=1, N_m=\frac{Lr_0A}{I}, \sigma_r=\frac{F}{A}, \tag{3.2.6}$$

where F is the maximum magnitude of the loading $f(t)$, eq.(3.2.5) can be written in terms of the dimensionless pore pressure P as:

$$\frac{\partial^2 P}{\partial^2 R}+\frac{1}{R}\frac{\partial P}{\partial R}+\frac{1}{R^2}\frac{\partial^2 P}{\partial^2 \theta}-\frac{\partial P}{\partial \tau}=(N_0+N_mR\sin(\theta+\gamma))\sum_{n=1}^{\infty}\frac{nA_n}{F}\sin(nT\tau) \tag{3.2.7}$$

The solution of eq. (3.2.7) is:

$$\begin{aligned}P(R,\theta,\tau,n)=\sum_{n=1}^{\infty} Im\{[&\frac{-A_n}{iTF}(N_0+N_mR\sin(\theta+\gamma))+A_{0n}I_0(\sqrt{inT}R)+B_{0n}K_0(\sqrt{inT}R)\\&+(A_{1n}I_1(\sqrt{inT}R)+B_{1n}K_1(\sqrt{inT}R))\sin\theta\\&+(A_{2n}I_1(\sqrt{inT}R)+B_{2n}K_1(\sqrt{inT}R))\cos\theta)]e^{inT\tau}\}\end{aligned} \tag{3.2.8}$$

where I_1, K_1, I_0 and K_0 are modified Bessel functions of the first and the zeroth order, respectively. Parameters A_{0n}, B_{0n}, A_{1n}, B_{1n}, A_{2n}, B_{2n} can be determined (see Appendix

4) by the following boundary conditions at the two surfaces of the laminae:

$$P = 0 \quad \text{at} \quad R = R_{v1} = r_{v1}/r_0, \tag{3.2.9}$$

$$P = 0 \quad \text{at} \quad R = R_{v2} = r_{v2}/r_0, \tag{3.2.10}$$

and

$$\frac{\partial P}{\partial R} = 0 \quad \text{at} \quad R = 1. \tag{3.2.11}$$

The conditions applied are free fluid flow across the laminae surfaces (r_{v1} and r_{v2}), from the lacunar-canalicular porosity into the vascular porosity (i.e., the boundaries of the unfilled rings in Figure 3.2b), and no fluid flow at the periosteal surface.

The fluid shear stress s acting on the membrane surface of the osteocytic process is given in terms of the gradient in pore pressure p by Zeng et al. (1994):

$$s = \frac{b}{\gamma_1}\frac{\partial p}{\partial r}[A_3 I_1(\gamma_1/q) - B_3 K_1(\gamma_1/q)], \tag{3.2.12}$$

where A_3 and B_3 are parameters given in the Appendix, section 4, from Zeng et al. (1994). Substituting eq.(3.2.8) into eq.(3.2.12), we obtain the fluid shear stress s acting on the osteocytic process induced by periodic bending:

$$\begin{aligned} s = {} & \frac{BTFb}{3A\gamma_1 r_0}[A_3 I_1(\gamma_1/q) - B_3 K_1(\gamma_1/q)] \sum_{n=1}^{\infty} \{Im[\frac{-A_n}{iTF_{max}} N_m \sin(\theta + \dot{\gamma}) \\ & + (\sqrt{inT} A_{0n} I_1(\sqrt{inT}R) - B_{0n}\sqrt{inT} K_1(\sqrt{inT}R) \\ & + (\sqrt{inT} A_{1n} I_0(\sqrt{inT}R) - A_{1n}\frac{I_1(\sqrt{inT}R)}{R} - \sqrt{inT} B_{1n} K_0(\sqrt{inT}R) \\ & - B_{1n}\frac{K_1(\sqrt{inT}R)}{R}) \sin\theta + (\sqrt{inT} A_{2n} I_0(\sqrt{inT}R) - A_{2n}\frac{I_1(\sqrt{inT}R)}{R} \\ & - \sqrt{inT} B_{2n} K_0(\sqrt{inT}R) - B_{2n}\frac{K_1(\sqrt{inT}R)}{R}) \cos\theta) e^{inT\tau}]\}. \end{aligned} \tag{3.2.13}$$

3.2.2 Fluid shear stress in the rooster bone

In the rooster exercise experiment (Judex et al., 1997), the mid-diaphyseal tarsometatarsus was analyzed for bone formation (Figure 3.3). The bending and axial loading induced normal strain ε_{zz} along the axial z direction is:

$$\varepsilon_{zz} = E^{-1}(\frac{f(t)}{A} - \frac{M_x(t)}{I_x}y + \frac{M_y(t)}{I_y}x), \tag{3.2.14}$$

where E is the longitudinal modulus of elasticity of the bone, $f(t)$ is the axial loading, A is the cross sectional area, I_y and I_x are the area moments of inertia of the bone section measured in the rooster experiment, and $M_x(t)$ and $M_y(t)$ are the bending moments about the indicated axes.

Unlike the turkey experiment, where the bending and axial loading force is precisely controlled, the loading condition of the rooster experiment is established through the running of roosters on a treadmill; thus the cyclic force $f(t)$ and bending moments $M_x(t)$ and $M_y(t)$ are unknown. These three parameters can be determined based on three sets of values of the normal strains ε^i_{zz} $(i = 1, 2, 3)$ measured separately by three strain gauges attached at three locations $(x^i,\ y^i)$ on the surface of the bone cross section using the following equation:

$$\varepsilon^i_{zz} = E^{-1}(\frac{f(t)}{A} - \frac{M_x(t)}{I_x}y^i + \frac{M_y(t)}{I_y}x^i). \tag{3.2.15}$$

After determining $f(t)$, $M_y(t)$ and $M_x(t)$, the fluid shear stress in the lacunar-canalicular system of the rooster bone section can be predicted in the same manner as in the turkey bone section. The sum of the three normal stresses $\sigma_{kk}(t)$ is:

$$\sigma_{kk(t)} = \frac{1}{A}f(t) - \frac{M_x(t)}{I_x}y + \frac{M_y(t)}{I_y}x. \tag{3.2.16}$$

Using the following dimensionless variables,

$$X = \frac{x}{L_0}, Y = \frac{y}{L_0}, \tau = \frac{ct}{{L_0}^2}, P = \frac{3p}{BT\sigma_r}, T = \frac{w{L_0}^2}{c}, \tag{3.2.17}$$

where $\sigma_r = \frac{F(t)_{max}}{A}$ and $L_0 = max(x, y)$, eq.(3.2.4) can be written in terms of the dimensionless pore pressure P as:

$$\frac{\partial^2 P}{\partial X^2} + \frac{\partial^2 P}{\partial Y^2} - \frac{\partial P}{\partial \tau} = \frac{c}{wL_0\sigma_r}[\frac{1}{AL_0}\frac{dF(t)}{d\tau} - \frac{1}{I_x}\frac{dM_x(t)}{d\tau}Y + \frac{1}{I_y}\frac{dM_y(t)}{d\tau}X]. \tag{3.2.18}$$

Since the geometry of the rooster bone is irregular, a numerical method involving a grid and a time interval defined by dX, dY and $d\tau$ is used to solve eq. (3.2.18). Assuming $P(i, j, n)$ is the dimensionless pore pressure at time $\tau = n$ for the bone cell located at $X = i$, $Y = j$, eq.(3.2.18) can be written as a difference equation:

$$\frac{P(i+1,j,n) - 2P(i,j,n) + P(i-1,j,n)}{dX^2} + \frac{P(i,j+1,n) - 2P(i,j,n) + P(i,j-1,n)}{dY^2}$$
$$- \frac{P(i,j,n) - P(i,j,n-1)}{d\tau} = \frac{c}{wL_0\sigma_r}(\frac{1}{AL_0}\frac{dF(n)}{d\tau} - \frac{1}{I_x}\frac{dM_x(n)}{d\tau}j + \frac{1}{I_y}\frac{dM_y(n)}{d\tau}i). \tag{3.2.19}$$

From eq.(3.2.19), the numerical iteriation is:

$$P(i,j,n) = \frac{1}{\frac{-2}{dX^2} + \frac{-2}{dY^2} + \frac{-1}{d\tau}}\{\frac{c}{wL_0\sigma_{ref}}[\frac{1}{AL_0}\frac{dF(n)}{d\tau} - \frac{1}{I_x}\frac{dM_x(n)}{d\tau}j + \frac{1}{I_y}\frac{dM_y(n)}{d\tau}i]$$
$$- \frac{P(i,j,n-1)}{d\tau} - \frac{P(i+1,j,n) + P(i-1,j,n)}{dX^2} - \frac{P(i,j+1,n) + P(i,j-1,n)}{dY^2}\}. \tag{3.2.20}$$

The boundary conditions for the rooster bone section, the same as those for the turkey bone section (eq.(3.2.9)-(3.2.11)), can be represented in the numerical model as:

$$P(i,j,0) = 0, \tag{3.2.21}$$

$$P(i_{v1}, j_{v1}, n) = 0, \tag{3.2.22}$$

$$P(i_{v2}, j_{v2}, n) = 0, \tag{3.2.23}$$

$$\frac{\partial P(i_m, j_m, n)}{\partial r} = 0, \tag{3.2.24}$$

where eq.(3.2.21) defines the dimensionless pore pressure $P = 0$ at the start time $t = 0$ for all bone cells; eq.(3.2.22) and (3.2.23) show free fluid flow across the laminae surfaces (at locations of (i_{v1}, j_{v1}) and (i_{v2}, j_{v2})) from the lacunar-canalicular porosity into the vascular porosity, and eq.(3.2.24) shows no fluid flow at the periosteal surface.

The fluid shear stress s is obtained as the gradient of the pore pressure p:

$$s = \frac{b}{\gamma_1}\frac{\partial p}{\partial r}[A_3 I_1(\gamma_1/q) - B_3 K_1(\gamma_1/q)] \tag{3.2.25}$$

where

$$\partial r = \frac{2\sqrt{x^2 + y^2}}{L_0}\frac{1}{2x\partial x + 2y\partial y}. \tag{3.2.26}$$

3.2.3 Comparison of fluid shear stress to strain gradients and bone formation

In order to compare the predicted fluid shear stresses with the strain gradients and the bone formation across bone sectors obtained in the experiments, we employed s_{avg} to represent the averaged fluid shear stress acting on each bone sector. The s_{avg} at each bone sector is obtained by averaging the absolute value of the fluid shear stresses acting on every bone cell located within the bone sector. The linear correlation coefficient r is used to find how the averaged shear stress correlated with the absolute value of strain gradients and the bone formation across a bone section.

3.2.4 Model parameters

Most of the parameter values used in our model either can be obtained from the experiments (see Appendix 5 and 6) or have been estimated in Zeng et al. (1994) (see Appendix 3). However, parameters related to the histological structure of avian plexiform bone including the thickness of the lamina, the thickness of the vascular network, the distances between osteocytes in the radial and circumferential directions and the relaxation time τ_r, need to be determined. Observation of a turkey ulnar bone section by our research group shows that the thickness of a lamina is approximately 80 μm, the thickness of a vascular network is approximately 10 μm, the distance between two osteocytes in the radial direction L_c is approximately 10 μm and in the circumferential direction L_d is approximately 20 μm. These parameters are observed to be relatively constant through a cross section of the bone. Based on the size of the cross sections of the turkey radii and the rooster tarsometatarsuses, starting from the endosteal surface there are about 14 (for turkey bone) to 15 (for rooster bone) layers of laminae, 14 to 15 layers of vascular networks, and a partial lamina (with a thickness of 40 μm) at the periosteal surface. The longitudinal modulus of bone tissue elasticity is assumed to be 22.6 GPa (Gross et al., 1997). The characteristic time of relaxation of the fluid pore pressure τ_r is assumed to be 2 sec based on the experimental measurements from Salzstein and Pollack (1987).

3.3 Results

3.3.1 Fluid shear stress in turkey experiment

The predicted fluid shear stress s in the turkey experiment remains zero when the load is steady and reaches the maximal absolute value during loading and unloading (Figure 3.4), (see Figure A1 for applied loading). The sign change of s is due to the direction change of the fluid flow in the connected cellular network (CCN) caused by the sign change of the loading rate. The positive sign indicates that the fluid flows into the CCN, while the negative sign indicates that the fluid flows out of the CCN.

The maximum value of fluid shear stress s acting on every bone cell in the turkey CCN is non-uniformly distributed across the bone section (Figure 3.5). Within each lamina, due to the boundary conditions, the magnitude of the predicted fluid shear stress s along the radial direction is maximum at the boundary of the first vascular network, then it decreases linearly to zero at the midline of each lamina; at that point, it reverses and increases linearly with the opposite sign until reaching a maximum again at the boundary of the next vascular network. The circumferential locations of the maximum fluid shear stress s are along the y' axis (Figure 3.2) which is perpendicular to the neutral axis. Among laminae, the maximum fluid shear stress s occurs at the boundaries of the vascular networks and it increases with laminae away from the endosteal surface, reaching the maximum at the inner surface of the last partial lamina at the subperiosteal surface. In the lamina near the periosteal surface, the fluid shear stress s is the greatest at the boundary of the last vascular network and zero at the periosteal surface, where

no fluid flow is assumed to occur.

Across the turkey bone section, a strong correlation ($r_{coef} = 0.9$) is found between the averaged fluid shear stress s_{avg} and the absolute value of the radial strain gradient RG; however, no correlation is found between bone formation and s_{avg} ($r_{coef} = 0.02$), or betwen the bone formation and the absolute value of RG ($r_{coef} = 0.03$) (Figure 3.6).

3.3.2 Fluid shear stress in rooster experiment

In the rooster experiment, the cyclic force $f(t)$ calculated using eq.(3.2.15) ranged from -150 to 20 N over one loading cycle (Figure 3.7a), while the bending moments $M_x(t)$ and $M_y(t)$ ranged from -0.1 to 0.4 Nm (Figure 3.7b). The predicted fluid shear stress s of one rooster shows the maximal fluid shear stress during one running cycle is approximately 2 $dyne/cm^2$ (Figure 3.8). The sign change of s is due to the stepping and lifting motions related to the running.

The maximum value of fluid shear stress s acting on every bone cell in the rooster connected cellular network (CCN) illustrates a similar distribution to that in the turkey CCN (Figure 3.9). The magnitude of the predicted fluid shear stress s in the rooster bone along the radial direction is maximum at the boundary of a vascular network, then it decreases linearly to zero at the midline of each lamina and increases linearly with opposite sign until reaching a maximum again at the boundary of the next vascular network. Among laminae, the maximum fluid shear stress s occurs at the boundaries of the vascular networks and increases with laminae away from the endosteal surface, reaching the maximum at the inner surface of the last partial lamina at the subperiosteal

surface. In the lamina near the periosteal surface, the magnitude of fluid shear stress s is zero at the periosteal surface, where no fluid flow is assumed to occur.

The averaged shear stress s_{avg} and the radial strain gradients RG across the 12 bone sectors obtained in Judex et al. (1997) correlate to a certain extent ($r_{coef} = 0.62$). The bone formation in the rooster experiment is not related to the absolute value of s_{avg} ($r_{coef} = -0.47$) and is negatively correlated to the absolute value of RG ($r_{coef} = -0.85$) (Figure 3.10).

3.4 Discussion

Although the fluid shear stress is related (strongly in the turkey experiment and to some extent in the rooster experiment) to the radial strain gradients, there is no spatial correlation between the averaged fluid shear stress and the bone formation across bone sectors ($r_{coef} = 0.02$ for the turkey experiment and -0.47 for the rooster experiment). Our long-standing hypothesis is that the bone formation is not directly correlated with the averaged local fluid shear stress. Specifically we hypothesize that the bone formation is a result of the interpretation of a local decision-making process of the loading-induced signal distribution by the CCN. Based on the hypothesis, the distribution of the fluid shear stress in a CCN is more important than the local fluid shear stress in regulating bone formation. In the lamina near the periosteal surface of the turkey radius, the fluid shear stress is maximum on the osteocytes located at the boundary of the last layer of the vascular network, but is zero at the periosteal surface, where osteoblasts (bone forming cells) and bone lining cells are located and bone formation occurs. In this

situation, the signals have to be transmitted from the osteocytes excited by mechanical loading induced signals to those that did not receive a sufficiently strong signal from the fluid flow shear stress caused by the loading, including the osteoblasts located on the periosteal surface. If the signals regulating bone formation are processed by a CCN before reaching the osteoblasts, it is possible that the bone formation is not linearly related to the local fluid shear stress.

The extensive intercellular connection among bone cells is the basis of the hypothesis that the loading induced signals may be transmitted and integrated through intercellular communication before reaching bone forming cells to regulate bone adaptation. The interconnected structure of a CCN provides a suitable site for intercellular signal exchange and transmission. It is suggested that a CCN may function as a network with osteocytes as nodes and osteocytic processes as connections and that a CCN is operationally analogous to a network of neurons that permits parallel distributed signal processing (Cowin and Moss, 2000).

The interpretation of the influence of the CCN in processing the fluid shear stress data in the present situation is particularly important. The theory is that bone tissue adjusts its CCN to the stimulus that it customarily experiences. When the stimulus it experiences is no longer the same there is a period of adaptation of the CCN to the new stimulus. In the experiments, the turkey and rooster bones were subjected to normal loading up until having received a new mechanical loading (a particular and totally different loading in the turkey experiment and a higher magnitude and duration loading in the rooster experiment). Thus the bone adaptation that occurs is initially due to the new stimulus being interpreted by the CCN that is still tuned to the old stimulus.

How long it takes for the CCN to retune itself to the new stimulus is unknown, but it is not instantaneous. Since both experiments lasted for only 3-4 weeks, it is unclear if the retuning process of the CCN has been completed. Nonetheless, the predicted fluid shear stress distribution in the avian plexiform bone provides a basis for a study on the mechanism of the intercellular communication in the bone CCN and on the relation between the mechanical induced signals and bone formation.

This study is the first to predict the distribution of the fluid shear stress acting on every bone cell in a CCN across a whole bone section subjected to a cyclic bending and axial loading. A previously developed theoretical model by Zeng et al. (1994) predicted the fluid shear stress in the lacunar-canalicular system of an osteon subjected to loading that is either parallel or perpendicular to the osteonal axis. When fluid shear stress in a whole bone is considered rather than just in an osteon, in both normal physiological environments and bone adaptation experiments, there is bending in addition to the axial loading due to the shape and curvature of the whole bone section. The interest here is in whole bone so it is necessary to understand the fluid shear stress induced by both bending and axial loading. The predicted fluid shear stresses in the turkey and the rooster bone sections are in the range (0.2 to 20 $dyne/cm^2$) that osteocytes are reported to respond to (Ajubi et al., 1996; Klein-Nulend et al., 1997; Sterck et al., 1998; Bakker et al., 2001; Thi et al., 2002; Alford et al., 2003).

For the first time, the theoretically predicted fluid shear stress across a whole long bone section is compared to the strain gradients obtained in an animal adaptation experiment. The model shows a very strong correlation ($r_{coef} = 0.9$) between the predicted shear stress and the radial strain gradient in the turkey experiment by Gross et al. (1997).

This result is expected because the radial strain gradient is the driving force to the fluid shear stress acting on the osteocytic processes within the lacunar-canaliculi system in the radial direction. In our model, the radial direction is assumed to be the primary orientation of the lacunar-canalicular system based on a reasonable evaluation of the existing histological information about the lacunar-canaliculi system in avian bone. Note that the radial direction is the dominant orientation of the lacunar-canaliculi system in human osteonal bone. The fact that the correlation between the predicted fluid shear stress and the measured radial strain gradient is not so obvious in the rooster experiment most likely originates from the geometry of the bone section. The radial strain gradient measured by Judex et al. (1997) is defined as the difference between the midpoints of endosteal and periosteal surfaces enclosed by one bone sector. However, the exceedingly irregular shape of the bone cross section makes a significant difference between the radial direction of one sector and the direction perpendicular to both endosteal and periosteal surfaces of the sector.

It is also the first time that theoretically predicted fluid shear stress across a whole long bone section is compared to the bone response obtained in an animal adaptation experiment. We chose fluid shear stress as the mechanical stimulus because the fluid shear stress, compared to other mechanical parameters, is a physiological parameter that directly acts on and could be sensed by bone cells; this brings our computational model in Chapter 4 more close to the real mechanosensory system in bone. The absolute value of the predicted fluid shear stress is used in this study because of the reported dependence of bone cell response to the absolute value of fluid shear stress (Bakker et al., 2001; Cheng et al., 2001; Thi et al., 2002). Other mechanical parameters have

been compared to bone response using signed parameters. In a turkey ulna model, twenty-four mechanical parameters, including strain energy density, longitudinal shear stress and tensile principal stress/strain were compared to the bone response and the results were not successful (95% of 2880 permutations had $r_{coef} < 0.6$) (Brown et al., 1990). In Gross et al. (1997) and Judex et al. (1997), the circumferential strain gradient was found to be most closely related to the bone response ($r_{coef} = 0.6$ for the turkey experiment and 0.80 for the rooster experiment), compared to radial and longitudinal strain gradients. The combination of the strain gradient in three directions gave better results ($r_{coef} = 0.79$ for the turkey experiment and 0.85 for the rooster experiment). However, all the correlations in the above experiments are between local mechanical parameters and local bone response without taking into consideration the intercellular communication in the CCN, which may regulate local bone response based on mechanical stimuli acting on cells located at various regions. The circumferential strain gradient is more closely related to the bone response than the radial strain gradient, but it is not the driving force of fluid shear stress in the radially distributed lacunar-canalicular system in avian bone. The fluid shear stress acting on bone cells is most likely driven by the radial strain gradient, as suggested by the results in this study. It is possible that fluid flow induced signals could be sent in different directions in the CCN after being sensed by certain bone cells.

One of the limitations of this study is that the cross section of the turkey radius is assumed to be circular. We do not know the exact histological structure, but we do know that the turkey radius is only approximately circular in cross section. Another limitation is that fluid shear stress is assumed to be the stimulus of bone cells. This

assumption has not been proven and the fluid shear stress most likely is not the only stimulus that regulates bone response to mechanical loading.

In this study, a mathematical model based on avian plexiform bone microstructure is developed to predict the fluid shear stress distribution induced by bending and axial loading in a bone CCN. The model is applied to animal adaptation experiments and the results show a strong correlation between the predicted shear stress and the radial strain gradient obtained in the experiments. The unevenly distributed shear stress supports our hypothesis that the bone formation is not directly correlated to the averaged local fluid shear stress. This study provides a basis for the study of cellular communication in the bone CCN to be reported in Chapter 4.

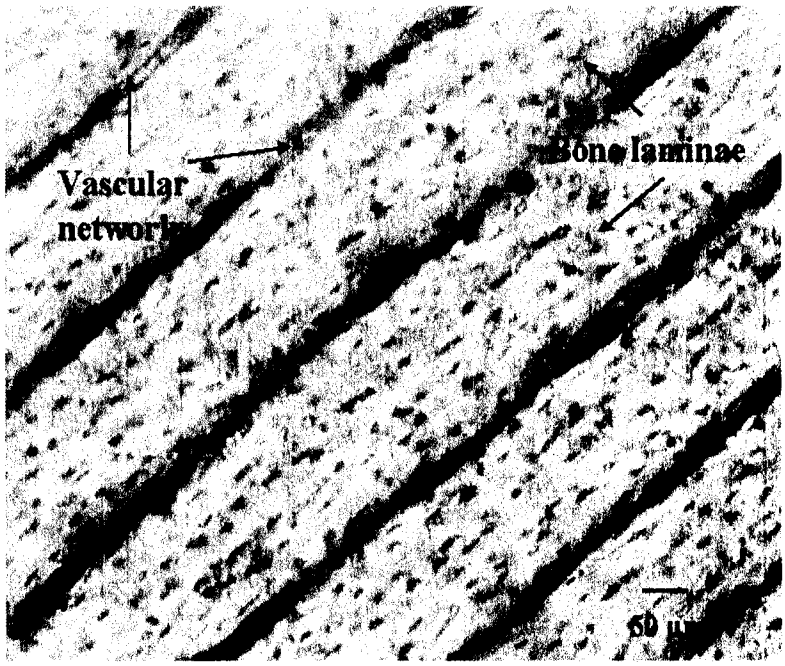

Figure 3.1: An image of the microstructure of a turkey ulna, which is composed of a series of concentrically arranged alternate layers of mineralized tissue (bone laminae) and blood plexies (vascular networks).

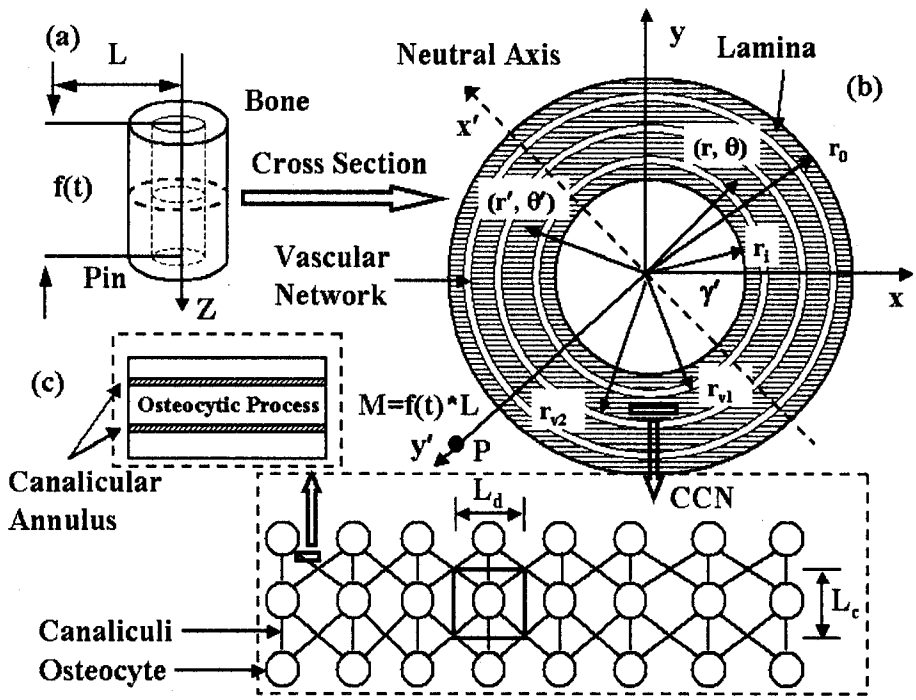

Figure 3.2: The idealized histological structure of the cross section of turkey plexiform bone. (a) As in Gross et al. (1997), the cyclic bending $f(t)$ is applied through two pins with moment arm L. (b) The cross section of the bone consists of a series of concentrically arranged laminae (horizontal-line-filled rings) and vascular networks (unfilled rings). The radius of the whole bone is r_0, and r_i represents the marrow cavity. Between any two vascular networks, located at radius r_{v1} and r_{v2}, is a bone lamina, where osteocytes are embedded and interconnected by canaliculi, forming a CCN. (c) Within each canaliculus, the fluid shear stress acting on the exterior surface of the membrane of the cell process is predicted.

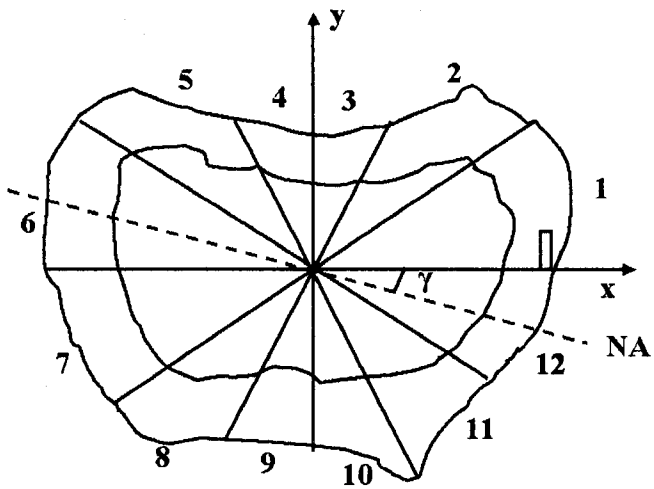

Figure 3.3: The cross section of a rooster tarsometatarsus with 12 equal pie sectors (adapted from Judex et al. (1997)). The small rectangular box is the domain whose shear stress is represented in Figure 3.9. γ is the angle between the x axis and the neutral axis (NA), and the z axis is normal to the plane of the section.

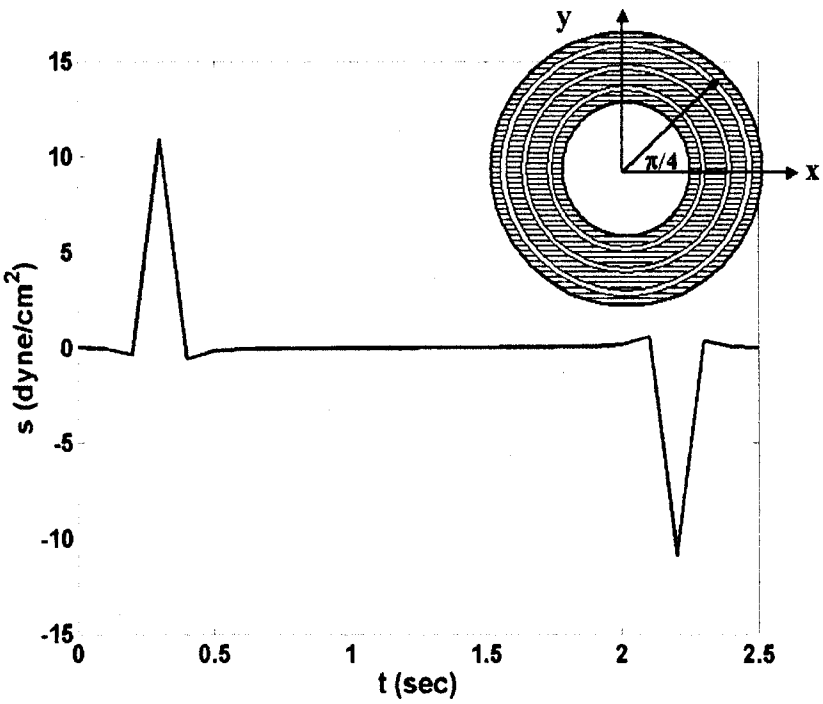

Figure 3.4: The fluid shear stress s (in $dyne/cm^2$) during one loading cycle in the turkey radius. s is plotted at one osteocyte, as an example, located at the inner surface of the lamina near the periosteal surface lamina with $r = 3.97\ mm$ and $\theta = \pi/4$ (shown schematically in the inserted figure). The maximum magnitude s_{max} occurs at $t = 0.3$ *sec* and $t = 2.2$ *sec* (see Figure A1 to relate the applied loading to the shear stress). The fluid shear stress acting on every osteocyte in the cellular network reaches the maximum at the same time.

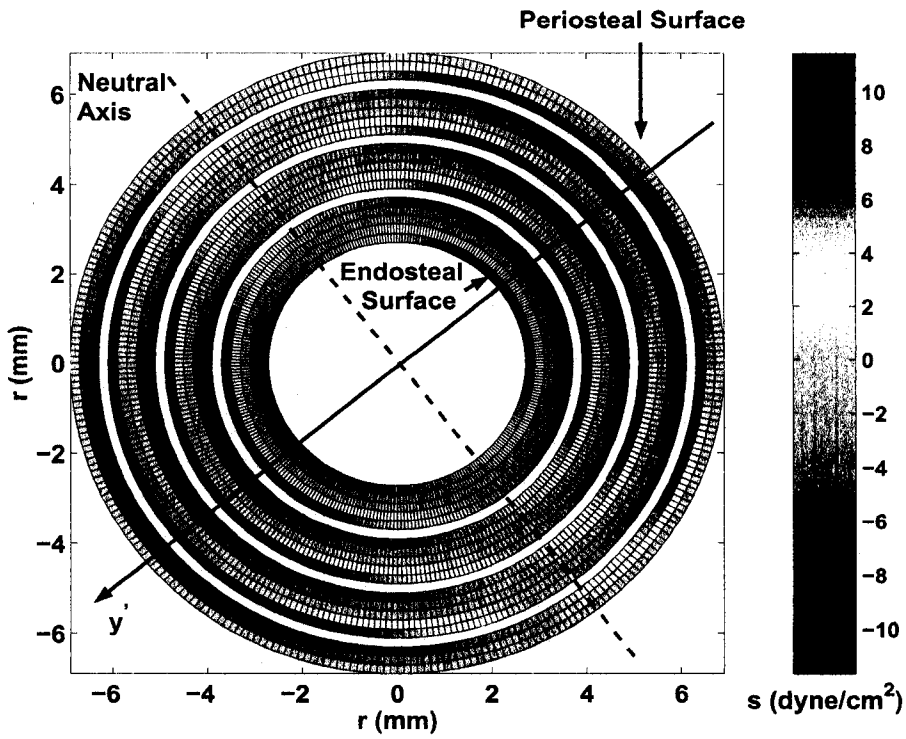

Figure 3.5: The distribution of the fluid shear stress s (in $dyne/cm^2$) acting on every bone cell in the CCN across the turkey radius section at $t = 0.3$ *sec*. For the purpose of a better presentation, only three laminae and the lamina near the periosteal surface are shown. The number of bone cells shown in each lamina is reduced and the thickness of laminae and vascular networks is enlarged.

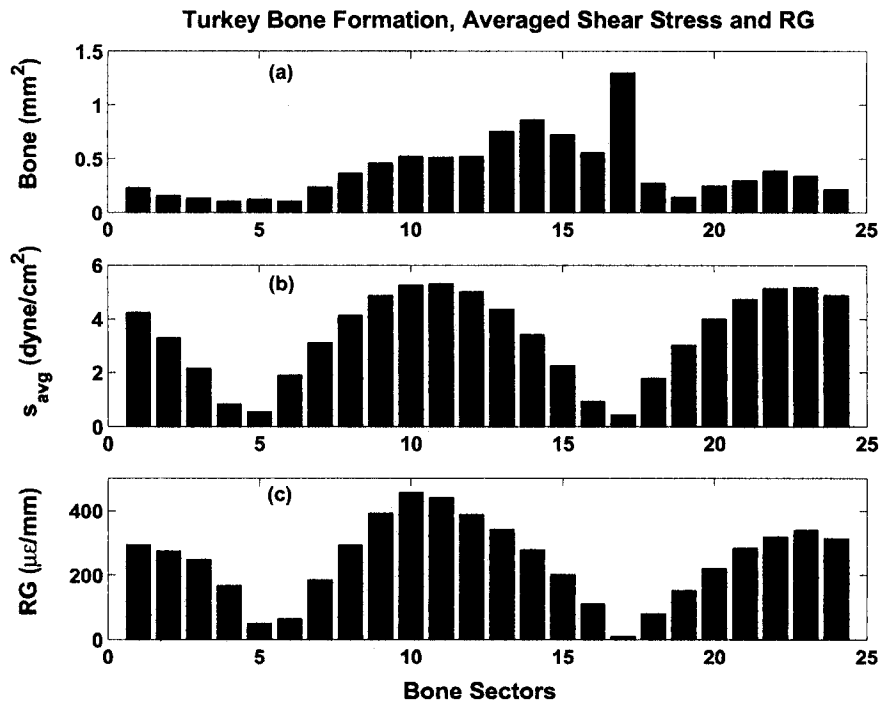

Figure 3.6: (a) The averaged bone formation (mm^2) (Gross et al., 1997), (b) the averaged absolute value of the shear stress s_{avg} ($dyne/cm^2$) and (c) the absolute value of the radial strain gradient RG ($\mu\varepsilon/mm$) (Gross et al., 1997) across the 24 bone sectors in the turkey experiment. A strong relation between s_{avg} and RG is found with the correlation coefficient $r_{coef} = 0.9$. The bone formation is not related to s_{avg} ($r_{coef} = 0.02$) or the absolute value of RG ($r_{coef} = 0.03$).

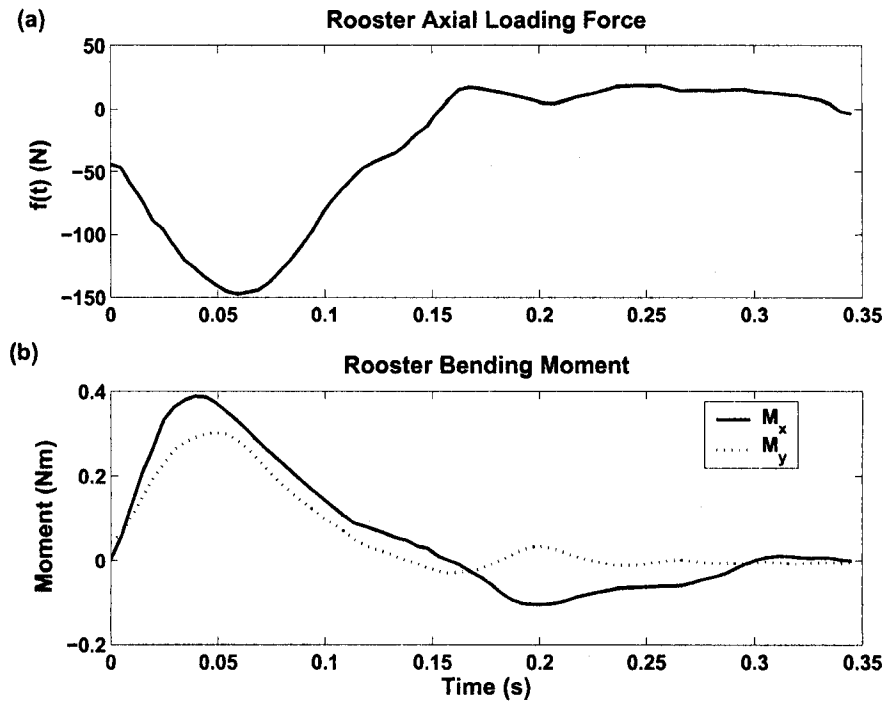

Figure 3.7: (a) The calculated loading force $f(t)$ (b) the calculated bending moments M_x and M_y applied to the rooster tarsometatarsus during one loading cycle.

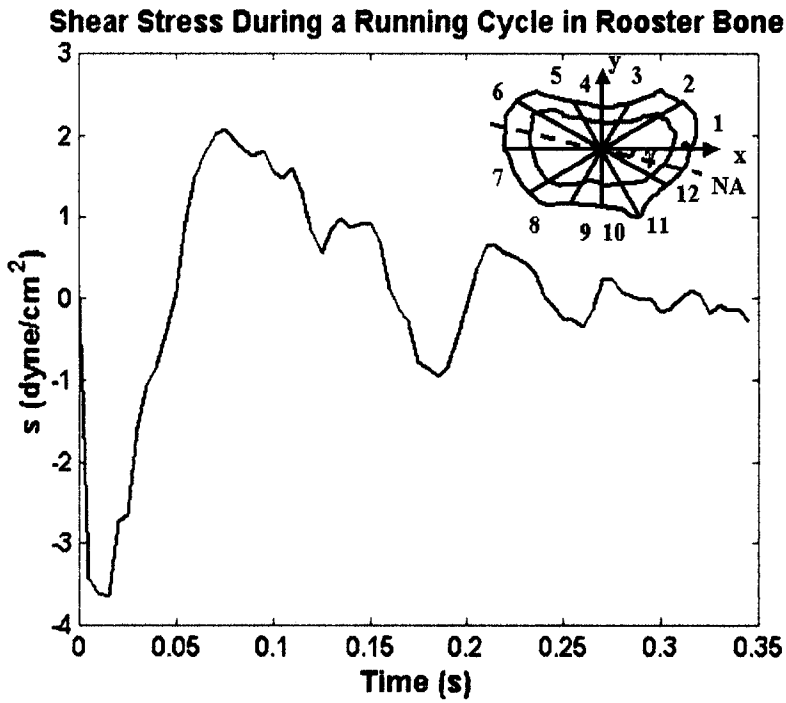

Figure 3.8: The predicted fluid shear stress s (in $dyne/cm^2$) during one running cycle. s is predicted at an osteocyte, as an example, located at $x = 8.4\ mm$ and $y = 0.0\ mm$ (shown as the black dot in the inserted figure) on the rooster bone cross section. The magnitude of shear stress reaches a maximum at $t = 0.08\ sec$. The fluid shear stress acting on every osteocyte in the cellular network reaches the maximum at the same time.

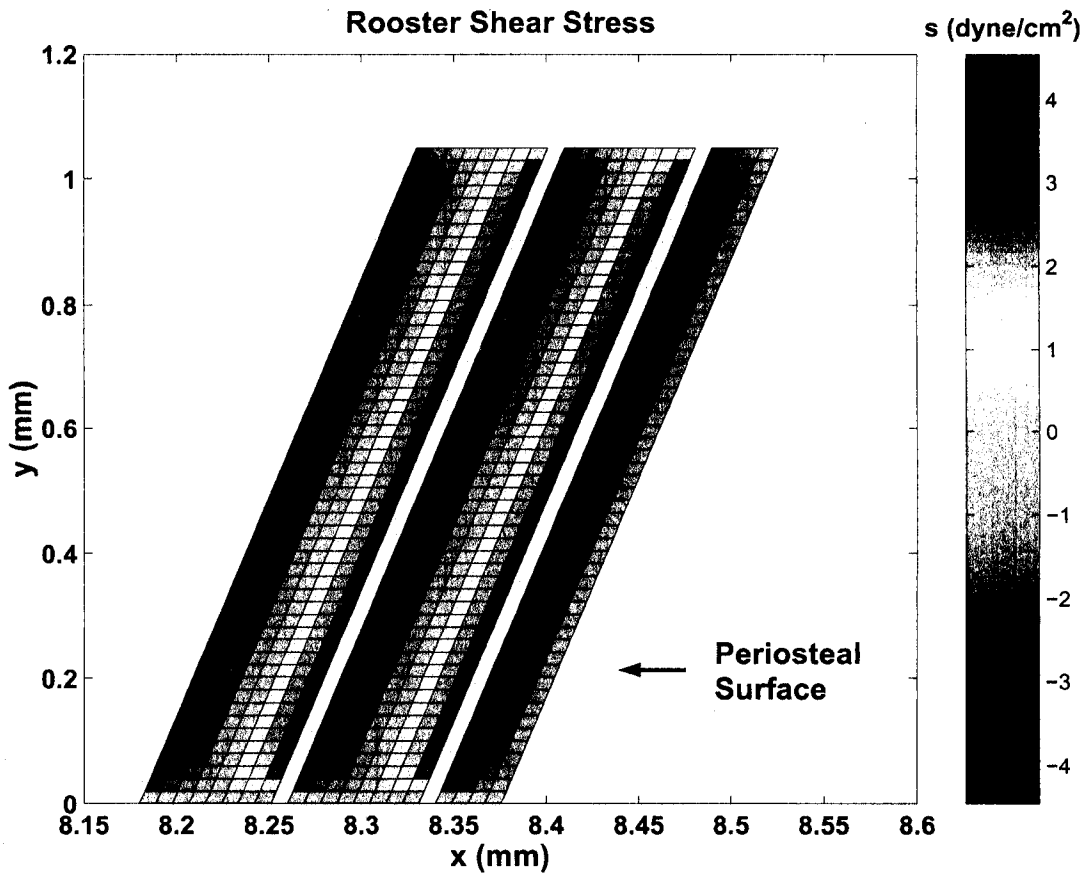

Figure 3.9: The distribution of the fluid shear stress s (in $dyne/cm^2$) acting on every cell in the rectangular box (Figure 3.3) on a rooster bone section. For the purpose of a better presentation, only two laminae and the lamina near the periosteal surface in the rectangular box are shown. The number of bone cells shown in each lamina is reduced and the thickness of laminae and vascular networks is enlarged.

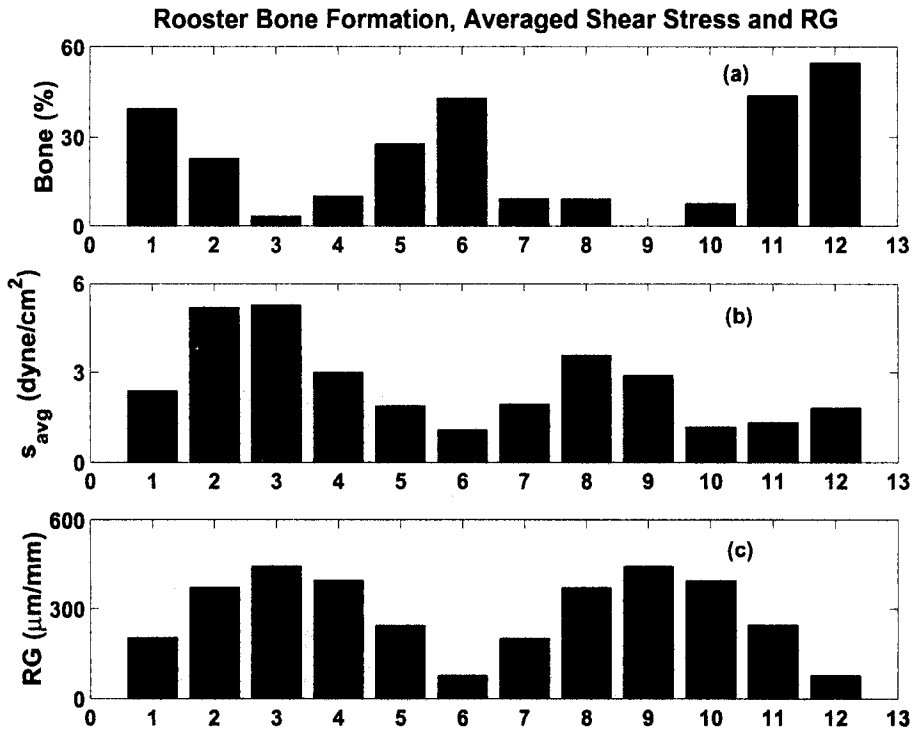

Figure 3.10: (a) The averaged bone formation percentage (Judex et al., 1997), (b) the average absolute value of the shear stress s_{avg} $(dyne/cm^2)$ and (c) the absolute value of the radial strain gradient RG $(\mu\varepsilon/mm)$ (Judex et al., 1997) across the 12 bone sectors in the rooster experiment. The correlation coefficient between s_{avg} and RG is 0.62. The bone formation is not related to s_{avg} ($r_{coef} = -0.47$) and is related negatively to the absolute value of RG ($r_{coef} = -0.85$).

Chapter 4 Development Of A Computational Connected Cellular Network To Study Bone Intercellular Communication

4.1 Introduction

Ever since the recognition (Wolff, 1892, 1986) that bone mass and structure can be influenced by mechanical loading, extensive research has been done to analyze the relationship between mechanical loading and bone adaptation. Koch (1917) hypothesized that bone is optimally designed to have a structure of maximum strength with minimum material. Harold Frost in his books (Frost, 1964, 1986) and many other publications accomplished the most extensive study of the mechanics and biology of bone adaptation to mechanical loading. Incorporating Frost's ideas Cowin and Hegedus (1976) and Hegedus and Cowin (1976) developed a theory of adaptive elasticity to employ as a model of bone adaptation. This theory was used to model a number of the bone remodeling animal experiments (Cowin et al., 1985).

Prior to 1990 the mechanistic models proposed to describe functional adaptation were phenomenological, or mechanistic. Phenomenological models attempt to simulate cause and effect (e.g., changed mechanical loading leading to changed bone architecture)

without a consideration of the intermediary mechanisms involved. Phenomenological models allow for conveniently testing the consequences of different hypotheses about bone adaptation. This approach is often useful for eliminating some assumptions that don't match experimental or clinical results and observations (e.g., only compressive static loading leads to bone formation) or stimulate further investigations (e.g., strain rates and spatial gradients may regulate adaptation). This and other phenomenological models for cortical and cancellous bone adaptation have recently been reviewed by (Hart, 2001).

Mechanistic models, on the other hand, start instead with parameters (e.g., bone cell activities and microenvironment) that are linked to portions of the biological processes involved in bone maintenance, turnover, and repair. These models, currently less developed than some of the phenomenological models because they are more complex, may lead to successfully linking mechanical and biological causes and effects. These models offer the promise of not only extending the descriptive and predictive capabilities of phenomenological models, but may offer insights into manipulation of the bone response, and development of pharmacological therapeutic agents. A mechanistic model for bone adaptation is described in a series of papers over the last decade (Cowin et al., 1991; Weinbaum et al., 1994; Cowin et al., 1995; You et al., 2001). This mechanistic model relates the effect of mechanical load applied to a whole bone to the bone fluid flow around the cells buried in the bone and, most significantly, to the bone adaptation process. As overview of these model concepts in the light of the relevant experimental data is presented in Cowin and Moss (2000).

The mechanistic model described above predicts that the maximum cellular stimula-

tory signal for bone mechanosensation occurs at the places where the fluid flow creates the greatest force on the cells buried in the bone matrix, the osteocyte. This location is not the location where the bone deposition or resorption is needed or, indeed, occurs. To explain this apparent inconsistency it is suggested that bone may function as a mechanosensory and mechanotransduction system where the loading induced signals are transmitted and integrated before regulating bone adaptation (Cowin et al., 1991; Moss, 1991; Aarden et al., 1994; Duncan and Turner, 1995; Burger and Klein-Nulen, 1999b; Bloomfield, 2001; Turner et al., 2002). This implies that the relationships may be nonlinear and that the response to mechanical loading may be a coordinated result of signal integration in bone tissue.

In the first chapter, bone tissue was described as an extensively connected cellular network (CCN) with osteocytes as sensor cells and osteoblasts and osteoclasts as action cells. Osteocytes and osteoblasts are interconnected through cell processes in the lacunar-canalicular system, establishing intercellular communication between neighboring cells. The signal transmitted through the intercellular pathways involve any or all of the following processes: cellular electrical events through gap junctions initiated by stretch and voltage activated ion channels (K^+, Ca^{2+}, Na^+ and Cs^+) and action potentials (Ypey et al., 1992; Rawlinson et al., 1996; Mikuni-Takagaki, 1999); circulating hormones (parathyroid hormone, growth hormone, estrogen and androgen) (Kasperk et al., 1990; Inaoka et al., 1995; Jagger et al., 1996; Lean et al., 1996; Chow et al., 1998); and local hormones (cytokines and growth factors) (Allen and Boxhorn, 1989; Greene and Allen, 1991; Seino, 1994). Intercellular communication through gap junctions has been shown experimentally in osteocytes (Jones et al., 1993; Palumbo et al., 1990), os-

teoblasts (Doty, 1981; Chiba et al., 1994; Donahue et al., 1995; Lecanda et al., 1998; Saunders et al., 2001; Romanello et al., 2003) and between osteocytes and osteoblasts (Doty, 1981; Yellowley et al., 2000).

A bone CCN has been presented as a network with osteocytes as nodes and osteocytic cell processes as connections (Cowin et al., 1991; Moss, 1991). Each osteocyte, which functions as an information-processing unit with nonlinear capability, is connected via gap junctions to its neighbors. Cells in a CCN are organized in layers and the cell processes of all osteocytes in all layers have identical functions. The loading induced signal continues to propagate through the network until it reaches osteoblasts on the bone surfaces, where it regulates the site and magnitude of bone formation. The hypothesis that osteocytes may exhibit certain capabilities of neurons is supported by the reported possible involvement of the neurotransmitter glutamate, an important transmitter in the central neural system, in intercellular communication among bone cells (Mason et al., 1997; Patton et al., 1998; Gu and Publicover, 2000; Hinoi et al., 2001; Huggett et al., 2002) and the evidence of short- and long-term memory exhibited by bone cells and tissue (Turner et al., 2002; Spencer and Genever, 2003).

To a large extent osteocytes as signal-sensing units and most likely signal-processing units function very much like the computational elements in an artificial neural network (ANN). A computational element that is a mathematical approximation of a biological neuron (and an osteocyte as well) sums weighted input signals, compares with a threshold, and then passes a new signal through a nonlinearity known as the activation function (Figure 4.1). The weights represent the connection strength between computational elements. In biological neuronal systems, comprehensive tasks such as classifi-

cation, pattern recognition and information processing are performed through learning, which involves adjustments of the thresholds and the synaptic connections, or weights, between neurons. Analogously, a bone CCN most likely is able to adjust the thresholds and weights, or connection strength of gap junctions, between osteocytes to regulate the bone adaptation response induced by mechanical loading.

The objective of this study is to develop a computational connected cellular network (CCCN) with its structure and connection mimicking the bone CCN to emulate the information-processing ability of a cluster of interconnected osteocytes. An algorithm that enables the network to adjust its thresholds and weights is designed specifically for the CCCN to extract the intercellular communication pattern by correlating loading stimulus at the cellular level with experimentally obtained bone formation data from Gross et al. (1997) and Judex et al. (1997). The loading stimulus at the cellular level is hypothesized to be the bone fluid shear stress acting on the osteocytic processes and is computed by the mathematical model developed in the previous chapter.

4.2 Development of a computational connected cellular network (CCCN) for bone structure

The development of the bone CCCN consists of two parts: 1) development of a network architecture similar to that of a bone CCN, and 2) design of an algorithm to adjust cell thresholds and connection weights.

4.2.1 CCCN structure

As discussed in the previous chapter, the development of the CCCN is based upon two avian animal experiments (Gross et al., 1997; Judex et al., 1997). So the architecture of the CCCN mimics the structure of avian plexiform bone, which consists of a series of concentrically arranged alternate layers of mineralized tissue and blood plexies (Figure 4.2). Osteocytes are located and interconnected within the layers of mineralized tissue, whereas there are no osteocytes in the vascular networks.

The structure of the CCCN is idealized as a 2-D grid (Figure 4.2). Each node of the CCCN grid represents one osteocyte, which is assumed to be connected with six of its nearest neighbor cells through gap junctions in the lacunar-canalicular system. Due to lack of experimental data and reports on osteocytic neighbor connection in avian bones, this assumption is based on observations in human bones, where the connections are concentrated within the nearest neighbor cells and are mainly in the radial direction of the bone section (Garven, 1965; Rasmussen and Bordier, 1975; Curtis et al., 1985). The connection strength between osteocytes is represented by weights. Although there are no osteocytes in the vascular networks, it has been experimentally observed that osteocytic processes are able to cross the vascular network, connecting the osteocytes in one lamina with those in the next one (Currey, 1960). We assume that osteocytes between bone laminae are connected in the same manner as the osteocytes within one lamina.

4.2.2 CCCN algorithm

The CCCN computational algorithm is developed by modifying the back-propagation (BP) network learning algorithm A carefully designed BP network is capable of capturing any functional relationship between input and output data. However, it is not a suitable network for a CCCN in that the structure of a BP network is different from that of a CCCN. In a BP network, a computational element in one layer is connected with every element of the next higher layer, while an osteocyte in a CCCN is connected only with its neighboring osteocytes. The connection structure of a CCCN provides pathways for signal transmission in all directions whereas, in a BP network there is a clearly defined signal propagation direction namely, forward direction. Unlike the BP neural network where the network architecture and signal propagation directions are fixed, CCCN connection patterns and signal propagation directions evolve over computational cycles.

The CCCN algorithm consists of two steps: initialization, which is only done once, and computational cycles, which repeat until a preset error value is reached (Figure 4.3). The object of initialization is to assign initial values to network parameters. A computational cycle is defined as the use of an entire set of data once to compute network parameters. There are five parts in one computational cycle: 1) cell parameter reset, 2) output computation, 3) error computation, 4) computation of changes in network parameters, and 5) network parameter update.

In the CCCN algorithm, a cell can be in one of three possible states: resting (0), active (1), or post-active (-1). An integer denoted as the activation order is assigned to

every cell to indicate the order in which the cell is activated. If a cell is among the set of cells activated by loading induced bone fluid shear stress, then the activation order of that cell is 1. The cells with the activation order equal to 1 are directly activated cells, as opposed to indirectly activated cells, which are activated by signals transmitted from neighboring cells.

We assume that loading induced signals propagate from an active cell to a resting cell (there is no signal transmission between two active cells) and that a cell in a post-active state cannot receive any signals from its neighboring cells. This assumption is borrowed from neuronal studies and experiments (Churchland and Sejnowski, 1992) as there is no available experimental information so far for bone cells.

With a bone cell $C(i,j)$ at location (i,j) in a 2-D grid of a CCCN, we associate the following parameters:

- $S(i,j)$ is the cell state
- $O(i,j)$ is the output of the cell
- $L(i,j)$ is the activation order of the cell
- $W^n(i,j,p,q)$ is the connection weight between $C(i,j)$ and its neighbor cell $C(p,q)$
- $T_l^n(i,j)$ is the loading threshold that fluid shear stress has to surpass in order to be sensed by $C(i,j)$. The subscript l denotes loading.
- $T_s^n(i,j)$ is the signal threshold that the received signals have to surpass in order for $C(i,j)$ to generate a response. The subscript s denotes signal.

Among the above parameters, three are cell parameters ($S(i,j)$, $O(i,j)$ and $L(i,j)$) and the other three are network parameters ($W^n(i,j,p,q)$, $T_l^n(i,j)$, and $T_s^n(i,j)$). The values of network parameters in one computational cycle are computed based on the respective values of the previous computational cycle. For better presentation, superscript n is used to denote the cycle dependency of the network parameters. The cell parameters are independent from cycle to cycle.

Initialization: This is applied once at the very beginning of the computation. All cell parameters are set to 0 and all network parameters are assigned random initial values.

Computational Cycle: As mentioned before, there are five parts in one computational cycle (Figure 4.3). The first four parts are applied to one randomly picked input-output data pair and the changes in cell and network parameters are computed. The first four parts repeat for the next data pair until the whole data set is exhausted. The network parameters are updated in the last part. The five parts are summarized below:

1) Cell parameter reset: The cell parameters, namely cell state, output, and activation order of every cell in the network are reset to 0.

2) Output computation: Consider a resting cell $C(i,j)$ at the nth computational cycle. The output $O(i,j)$ of $C(i,j)$ can be obtained by:

$$O(i,j) = \begin{cases} f_m[F(i,j) - T_l^n(i,j)], \text{if } L_{max} = 0 \\ \\ f_s[\sum_{p,q \in N(i,j)} O(p,q)W^n(i,j,p,q) - T_s^n(i,j)], \text{otherwise} \end{cases} \quad (4.2.1)$$

where f_m and f_s are activation functions (see Figure 4.1), f_m is the mechanosensory function that transforms fluid shear stress into signals sensed by bone cells, f_s is the signal communication function that describes cell response to received signals, $F(i,j)$ is the absolute value of the shear stress acting on cell $C(i,j)$, L_{max} is the maximum value of the activation order of the network, $N(i,j)$ is the neighborhood of $C(i,j)$, and (p,q) is the location of an activated cell in the neighborhood of $C(i,j)$. The output of other resting cells in the network is computed in the same manner.

After computing the output of every resting cell in the network, the state of all previously activated cells is set to the post-active state before updating the state of the resting cells:

$$\text{If} \begin{cases} L(i,j) = 0 \\ O(i,j) > 0 \end{cases} \text{ then: } \begin{cases} S(i,j) = 1 \\ L(i,j) = L(p,q) + 1. \end{cases}$$

$$\text{If } O(i,j) \leq 0, \text{ then: } \begin{cases} S(i,j) = 0 \\ L(i,j) = 0 \\ O(i,j) = 0. \end{cases} \tag{4.2.2}$$

This part of the computation for one input-output pair of data is repeated until no cell in the network is in the active state.

A hyperbolic tangent function, one of the most commonly used activation functions in artificial neural networks (Haykin, 1999), is used as the mechanosensory function f_m

and the signal communication function f_s:

$$f_m(x) = A_m tanh(B_m x) \tag{4.2.3}$$

$$f_s(x) = A_s tanh(B_s x), \tag{4.2.4}$$

where A_m and A_s are magnitude parameters to control the output magnitude, and B_m and B_s are slope parameters of the functions. The optimal value set of the parameters (1.7 for A_m and A_s, 0.67 for B_m and B_s) are determined by trial and error.

3) Error computation: The error between the computed bone formation and the experimentally measured bone formation is estimated for the cells located in the last row of the CCCN, which represent the osteoblasts on the periosteal surface of the bone section. The experimentally measured bone formation was divided into several sectors (24 for turkeys and 12 for roosters) across the bone sections by Gross et al. (1997) and Judex et al. (1997). The computed bone formation B_k by the CCCN in sector k is assumed to be the average output of cells in the sector.

$$B_k = \frac{\sum_{j \in k} O(M, j)}{D} \tag{4.2.5}$$

where M denotes the last row of the network, and D is the total number of cells located in sector k. The error signal $e(M, j)$ of $C(M, j)$ in sector k is:

$$e(M, j) = B_k - BM_k \tag{4.2.6}$$

where BM_k is the experimentally measured bone formation of sector k.

4) Computation of changes in network parameters: The changes in network parameters are computed for all cells that participate in activating osteoblasts that have not

produced the desired amount of bone formation. The participating cells are traced through the propagation pathways and the structure of the network with the participating cells can be determined (Figure 4.4). The sign (increase or decrease) of the network parameter change is defined by the sign of the local gradient $\delta(i,j)$ in the weight space of $C(i,j)$. If cell (i,j) is in the last row $(i = M)$ of the CCCN, the local gradient is:

$$\delta(i,j) = e(i,j)f'[\sum_{p,q\in N(i,j)} W^n(i,j,p,q)O(p,q)]. \tag{4.2.7}$$

For a cell located in the interior part of the network, the local gradient is:

$$\delta(i,j) = f'[\sum_{p,q\in N(i,j)} W^n(i,j,p,q)O(p,q)] * \sum_{s,t\in N(p,q)} W^n(p,q,s,t)O(s,t). \tag{4.2.8}$$

In eq.(4.2.7) and (4.2.8), f' is the first derivative of f, which is the mechanosensory function (f_m) if $C(i,j)$ is a directly activated cell, or the signal communication function (f_s) if $C(i,j)$ is an indirectly activated cell.

To compute the changes in network parameters, we employ the "Manhattan" updating step derived from the RPROP (Resilient backpropagation) update rule (Riedmiller and Braun, 1993):

$$\Delta W^n(i,j,p,q) = -\eta^n(i,j) * sign[-\delta(i,j)O(p,q)] \tag{4.2.9}$$

$$\Delta T_l^n(i,j) = \eta^n(i,j) * sign[-\delta(i,j)] \tag{4.2.10}$$

$$\Delta T_s^n(i,j) = \eta^n(i,j) * sign[-\delta(i,j)], \tag{4.2.11}$$

where $\eta^n(i,j)$ is the learning rate that controls the rate of change for $C(i,j)$ in the nth computational cycle. This completes the computation for one pair of data. The same computation repeats for the next randomly picked input-output data pair until the whole data set is exhausted.

5) Network parameter update: The final step of a computational cycle is to update the weights and thresholds:

$$W^{n+1}(i,j,p,q) = W^n(i,j,p,q) + \Delta W^n_{avg}(i,j,p,q), \tag{4.2.12}$$

$$T^{n+1}_l(i,j) = T^n_l(i,j) + \Delta T^n_{lavg}(i,j) \tag{4.2.13}$$

$$T^{n+1}_s(i,j) = T^n_s(i,j) + \Delta T^n_{savg}(i,j), \tag{4.2.14}$$

where $\Delta W^n_{avg}(i,j,p,q)$, $T^n_{lavg}(i,j)$ and $T^n_{savg}(i,j)$ are the averaged change in connection weights, loading threshold, and signal threshold of $C(i,j)$ for the whole data set, respectively.

To speed up the error minimization process, the learning rate $\eta^{n+1}(i,j)$ is adjusted based on the previous value as:

$$\eta^{n+1}(i,j) = \begin{cases} \gamma^+\eta^n(i,j) & \text{if } \Delta W^n_{avg}(i,j,p,q) * \Delta W^{n-1}_{avg}(i,j,p,q) > 0 \\ \gamma^-\eta^n(i,j) & \text{if } \Delta W^n_{avg}(i,j,p,q) * \Delta W^{n-1}_{avg}(i,j,p,q) < 0 \\ \eta^n(i,j) & \text{otherwise} \end{cases} \tag{4.2.15}$$

where γ^+ and γ^- are growth/shrinking factors ($0 < \gamma^- < 1 < \gamma^+$). In this study, $\gamma^+ = 1.2$, $\gamma^- = 0.5$, and $10^{-6} \leq \eta^n(i,j) \leq 1$ are determined by trial and error.

We use the averaged error percentage per sector of an entire data set, denoted by E_s, to compare to a specified preset error value E_p, which sets the stop point for network computation. This signals the end of one computational cycle.

With the updated weights and thresholds as the starting values, the next computational cycle starts. This process is repeated as long as the error percentage E_s remains

above the preset value E_p. When $E_s \leq E_p$, the updated weights show the connection patterns between cells and the threshold values indicate the sensitivities of each cell.

4.3 Experiments with the network

The developed algorithm for the CCCN is applied to the turkey and rooster CCCNs created using the actual sizes of the experimental turkey and rooster bone sections. Experiments with the networks and the measurements of network parameters are described below.

4.3.1 The sizes of the turkey and rooster CCCNs

The sizes of the turkey and rooster CCCNs depend on the sizes of the turkey and rooster bone cross sections and the distance between osteocytes in the respective connected cellular networks (CCN). In the previous chapter, the distance between turkey osteocytes in the circumferential and radial direction was observed to be approximately 20 and 10 μm, respectively. We assume the same for the rooster CCCN in absence of such experimental data. Based on the size of turkey and rooster bone cross sections measured in the experiments (Gross et al., 1997; Judex et al., 1997), the turkey CCCN is estimated to be a grid of 122 rows and 1054 columns (128,588 osteocytes) and the rooster CCCN is estimated to be a grid of 131 rows and 2427 columns (317,937 osteocytes) (Figure 4.5(a)-(c)).

4.3.2 The input and output of the CCCNs

The CCCN uses the distribution of bone fluid shear stress obtained in the previous chapter as the input and the bone formation measured from the turkey and rooster experiments (Gross et al., 1997; Judex et al., 1997) as the output. In the previous chapter, a strong correlation ($r_{coef} = 0.9$) was found between the computed averaged shear stress and the radial strain gradient obtained in the turkey experiment. This strong correlation makes it possible to calculate the individual shear stress distribution for each of the nine experimental turkeys (one turkey is taken out of the data set because there was no bone response) based on the individual radial strain gradient obtained in the turkey experiment. There are two loading conditions in the turkey experiment: loading group A (four turkeys) in which the loading pins were rotated 89 degrees from those of loading group B (five turkeys) (Figure 4.6). The fluid shear stress and bone formation corresponding to each anatomic site, i.e., the 24 bone sectors, of the nine turkeys are used as nine input-output pairs for the turkey CCCN. Two pairs of input and output from the turkey experiment are shown in Figure 4.5.

The computed fluid shear stress distribution in one rooster bone serves as the input for all five roosters because the correlation between the predicted averaged shear stress and the radial strain gradient is not very strong ($r_{coef} = 0.6$). The measured bone formation and radial strain gradient data from the experiment (Judex et al., 1997) were collected separately from different roosters, which makes it difficult to obtain the individual shear stress distribution for each of the five experimental roosters. The fluid shear stress and bone formation corresponding to each anatomic site, i.e. the 12 bone sectors, of the five

roosters are used as five input-output pairs for the rooster CCCN. One pair of input and output from the rooster experiment is shown in Figure 4.5.

4.3.3 Experiment one: Cell population responsible for regulating bone formation

This experiment is designed to investigate the cell population responsible for regulating bone response and the maxiumum propagation of the loading induced signals in the CCCN. The cells that perceive the loading induced signals and participate in regulating bone formation at the periosteal surface are defined as essential cells. Starting from the activated osteoblasts at the last row of the CCCN, the locations of the essential cells can be determined by tracing back the cells that participate in activating the osteoblasts. We measure and report the number of times an essential cell is activated (activation frequency) for three groups: turkey loading groups A and B and the rooster group. The maximum distances that signals propagate in the radial and circumferential directions in the CCCNs of the three groups are also reported.

4.3.4 Experiment two: Averaged network parameters and shear stress

The second experiment of the CCCN is designed to show how network parameters, namely two thresholds (T_l and T_s) and connections weights (W), change under different values of fluid shear stress. The network parameters and shear stress are averaged

in the radial direction and presented along the circumferential direction of the bone cross sections. This is because the absolute value of fluid shear stress varies in the circumferential direction with the local bending moments. The absolute value of fluid shear stress does not remain constant in the radial direction (it is large near the vascular networks and close to zero at the midline of each bone lamina); however, the change is linear and is not related to local bending moments.

4.3.5 Experiment three: Effect of the network parameters on bone formation

For the third experiment of the CCCN, three tests are designed to explore the roles of the three network parameters in regulating bone formation at the periosteal surface. The three tests are designed by assigning one parameter to one of a series of constants, one at a time, while adjusting the other two. The degree of influence of the three parameters in regulating bone response is evaluated by the error percentage E_s of the network obtained from the three tests. If one parameter has more control over the network, assigning a constant value to that parameter will lead to a larger error percentage in the network results.

The series of constants assigned to loading and signal thresholds for the turkey and rooster CCCNs are from 0 to 6.8 $dyne/cm^2$ with an interval of 1.13 $dyne/cm^2$, and from 0 to 1.2 (out of a maximum value of 10.2) with an interval of 0.1, respectively. The series of constants were determined by testing the network results so that bone formation at the periosteal surface occurs. The series of constants assigned to connection weights

is from 0.1 to 1 (out of a maximum value of 1) with an interval of 0.05. The signal thresholds and the connection weights are unitless.

4.4 Results

The designed CCCN algorithm successfully self-adjusts the network parameters to make the error percentage E_s decrease to a minimum value within a reasonable number of computational cycles (Figure 4.7). The error percentage E_s decreases from 114% to 2.56% for the turkey CCCN and from 93% to 14.6% for the rooster CCCN.

4.4.1 Cell population responsible for regulating bone formation

The cells responsible for regulating bone formation, the essential cells, vary with location relative to the neutral axis in the connected cellular network (CCN) (Figure 4.8(a)-(b)). Essential cells are located in the lamina near the periosteal surface and in the inner laminae (towards the endosteal surface) near the neutral axis. Fewer cells located in inner laminae in the rooster CCN join with the cells located in the last lamina to regulate bone formation, as compared to the turkey CCN (Figure 4.8(c)). No essential cell is found at the endosteal surface in the three loading groups.

Loading induced signals propagate a much longer distance in the circumferential direction than in the radial direction of the turkey and rooster CCCNs. The averaged maximum signal propagation distance (not shown in Figure 4.8) in the radial direction is approximately 540 μm in turkey group A, 260 μm in turkey group B, and 110 μm

in the rooster group. The maximum signal propagation distance in the circumferential direction is approximately 450 μm in turkey group A, 1130 μm in turkey group B, and 200 μm in the rooster group.

4.4.2 Averaged network parameters and shear stress

The network results show that the averaged network parameters vary with the averaged magnitude of fluid shear stress. The averaged loading threshold T_l ranges from 0 to 18 $dyne/cm^2$ for turkey group B, 0 to 12.8 $dyne/cm^2$ for turkey group A, and 2.5 to 14.0 $dyne/cm^2$ for the roosters. The loading threshold T_l is relatively large in areas receiving large fluid shear stress and is relatively small in areas receiving small fluid shear stress (Figures 4.9-4.11(b)).

The averaged signal threshold T_s has the same relationship with fluid shear stress as the averaged loading threshold T_l. The averaged signal threshold ranges (out of a maximum value of 10.2) from 0 to 0.8 for turkey group B, 0 to 0.9 for turkey group A, and 0 to 3.0 for roosters. T_s is relatively large in areas receiving large fluid shear stress and small in areas receiving small fluid shear stress (Figures 4.9-4.11(c)).

The relationship between fluid shear stress and the averaged connection weights is opposite to that of the loading and signal thresholds. Relatively weak connection weights are observed in areas receiving large fluid shear stress and strong connection weights are observed in areas receiving small fluid shear stress (Figures 4.9-4.11(d)).

4.4.3 Effect of the network parameters on bone formation

The results of the three designed tests show that loading threshold (T_l) plays a more important role in regulating bone formation than signal threshold (T_s) and connection weights (W) (Figure 4.12). A constant loading threshold generates a larger percentage error (minimum 21.1% for roosters and 5.9% for turkeys, compared to a constant signal threshold (minimum 15.3% for roosters and 2.64% for turkeys) and connection weights (minimum 14.7% for roosters and 2.7% for turkeys).

Compared to the percentage error generated with free parameters (minimum 14.6% for the rooster and 2.56% for the turkeys), assigning the loading threshold to a constant generates a larger percentage error, while assigning the signal threshold and connection weights to a constant did not influence significantly the network results.

4.5 Discussion

Cell population: Most of the cells responsible for perceiving stimulus (the essential cells) are located in the lamina near the periosteal surface and in the inner laminae near the neutral axis. This is not a surprising result when the fluid shear stress distribution is studied closely. The absolute value of the shear stress is maximum at the location close to the vascular network in the lamina near the periosteal surface. The shear stress is strong enough to directly activate some osteocytes in the lamina, which is very close to the periosteal surface where the osteoblasts are located. This decreases the possibility of other cells in the inner bone lamina from being involved in regulating bone formation

because the osteoblasts most likely are activated by signals transmitted from the closely located activated osteocytes. In the areas near the neutral axis, the locations of essential cells are observed diverging into the inner laminae of neighboring areas. This is because the shear stress in the areas near the neutral axis is not strong enough to directly activate local osteocytes. In order to activate osteoblasts near the neutral axis, the osteocytes in neighboring areas (including both inner laminae and the lamina near the periosteal surface) where the shear stress is stronger have to send signals to cells located near the neutral axis.

The locations of essential cells suggested by the network indicate that the bone formation occurring at the periosteal surface of the turkey and rooster CCCNs does not require participation of cells located at the endosteal surface. This is consistent with the observation that no bone formation is found at the endosteal surface in both the turkey and rooster experiments (Gross et al., 1997; Judex et al., 1997). To our knowledge, this is the first time that the cell population responsible for perceiving loading induced stimulus of bone formation at the periosteal surface is identified via computational modeling.

Signal propagation distance: The network result of the averaged maximum signal propagation distance in the turkey CCN indicates the integration of loading induced signal in the CCN. The hypothesis that loading induced signal is integrated in a bone CCN is originated from the observation of signal attenuation in intercellular propagation reported in in vitro experiments (Enomoto et al., 1992; Demer et al., 1993; D'Andrea and Vittur, 1997). Compared to the experimentally obtained maximum propagation distance (320 μm, Jeansonne et al. (1979)) of the signal transmitted from a single activated bone cell, the averaged maximum propagation distance of signals in turkey group A and B

is much longer (450-1130 μm), except in the radial direction of turkey group B (260 μm). This indicates the possibility of the signal integration in the turkey bone CCN. The averaged maximum signal propagation distance in the rooster CCN is much shorter (110-200 μm), compared to that of the turkey CCN, which suggests that the signal integration in the rooster CCN is more concentrated within local signals.

An important network result is that the loading induced signals propagate a much longer distance in the circumferential direction than in the radial direction of the CC-CNs. This leads us to believe that fluid shear stress induced signals propagate and are integrated to a larger degree in the circumferential direction than in the radial direction. Based on observations of human bone (Garven, 1965; Rasmussen and Bordier, 1975; Curtis et al., 1985), the canalicular channels in avian bones are assumed to be mainly in the radial direction. Since the distribution pattern of canaliculi coincides with that of the osteocyte processes (Kamioka et al., 2001), the fluid flow through the lacunar-canalicular system creating shear stress sensed by osteocytes is predominantly in the radial direction. The network result shows that the fluid shear stress induced signal is transmitted mainly in the circumferential direction, which may be the reason why the experimentally measured radial strain gradient (driving force of fluid flow in the radial direction) does not correlate well with the bone formation in the space domain. Signal integration observed in the network may explain the result that the combination of circumferential, radial and longitudinal strain gradients shows a much better correlation than any of the three strain gradients (Gross et al., 1997; Judex et al., 1997). The network result supports the hypothesis that loading induced signals propagate in connected cellular networks and that bone response is a coordinated result of signal integration in

the networks.

Averaged network parameters and shear stress: The averaged cell sensitivities (which are negatively related to the loading and signal thresholds) and the connection weights are found to be inversely correlated with the averaged fluid shear stress across the bone section. The network result shows that the thresholds of cells responding to mechanical stimulus varies for cells in the same bone tissue. This result is consistent with experimental reports (Hsieh et al., 2001), in which the strain threshold was found to have a large value where the loading strains were typically higher and a smaller value where the loading strains were lower. It has been proposed that bone cells are able to accommodate their mechanical loading conditions, adjusting osteocyte sensitivity differently in different loading areas (Turner, 1991). When a bone cell experiences repeated loading for a certain duration, its loading threshold will increase and a larger loading is needed to have it activated. Both the turkey and rooster experiments have animals subjected to a certain loading condition for a few weeks. It is reasonable to assume that bone cells adjust or change the loading and signal threshold (sensitivities) according to the fluid shear stress received.

Loading thresholds: Loading threshold is suggested to play a more important role in regulating bone response to mechanical loading, compared to the signal threshold and connection weights. This is a reasonable result as the loading threshold determines the strength of signals sensed by osteocytes and the distribution of directly activated cells, which control to a certain extent the signal propagation patterns in the network. Compared to the loading threshold, the signal threshold and connection weights have less control over the network based on the results of this study. The limited number

of animal data sets and the large sizes of the turkey and rooster CCCNs could be a reason why assigning a constant to the signal threshold and connection weights did not generate considerable errors.

Differences of the results between the turkey and the rooster CCCNs: The difference in the error percentage between the turkey and the rooster CCCNs is most likely caused by the difference in the sizes of two CCCNs, in the number of data sets and loading conditions between the two animal groups. The size of the rooster CCCN is much larger than that of the turkey CCCN and the number of the data sets of the rooster CCCN (5) is smaller than that of the turkey CCCN (9). This difference makes it more difficult to correlate input and output data in the rooster CCCN than in the turkey CCCN. There are two types of loading regimens (loading group A and B) in the turkey data set and one type of loading in the rooster data set. Having more loading regimens in the data sets enables the turkey CCCN to collect more information, as opposed to the rooster CCCN, which uses one type of loading regimen. With more bone cells involved in the computation, the turkey model has a better chance to generate a better result. Ideal data sets for such a network to extract a nonlinear relationship between input and output data should include different representatives of the network to different loading environments, so that the data sets are good generations of the network responses to different environments (Anderson and Rosenfeld, 1988).

The difference in the method of loading application might account for the difference of essential cell population between the turkey and rooster groups. The natural loading history of the turkey radius has not been fully quantified; however, the magnitude of peak strain in the turkey experiment was in the measured physiological loading range

of the rooster ulna due to natural wing flapping (Rubin and Lanyon, 1987). The two loading conditions applied through an invasive method to the turkey radius most likely induced shear stress distribution patterns different from the physiological distribution. The loading condition applied to the roosters was induced by an exercise model of running on a treadmill. Quantification of the loading history of roosters indicates that the exercise model in the rooster experiment induces a similar shear stress distribution pattern with a higher magnitude compared to normal weight bearing activities such as walking and running (Konieczynski et al., 1998). The difference in the essential cell population between the turkey and rooster groups could reflect the difference in how bone cellular networks react to external loadings with different patterns and magnitudes.

Summary: The CCCN is the first computational model that bridges the gap in understanding mechanical loading induced signals at the cellular level with bone response at the tissue level by extracting intercellular communication patterns from animal experiments. This computational approach for the first time identifies the cell population responsible for perceiving loading stimulus. With limited animal data sets, CCCNs extract a distinct intercellular communication pattern in which the averaged cell sensitivities and connection weights are inversely correlated with the averaged fluid shear stress across the bone section. The loading threshold is found to play an important role in regulating bone formation at the periosteal surface. The developed algorithm for the CCCN provides a unique and important tool to analyze intercellular communication and to discover the underlying relationship between input and output data in biological structures.

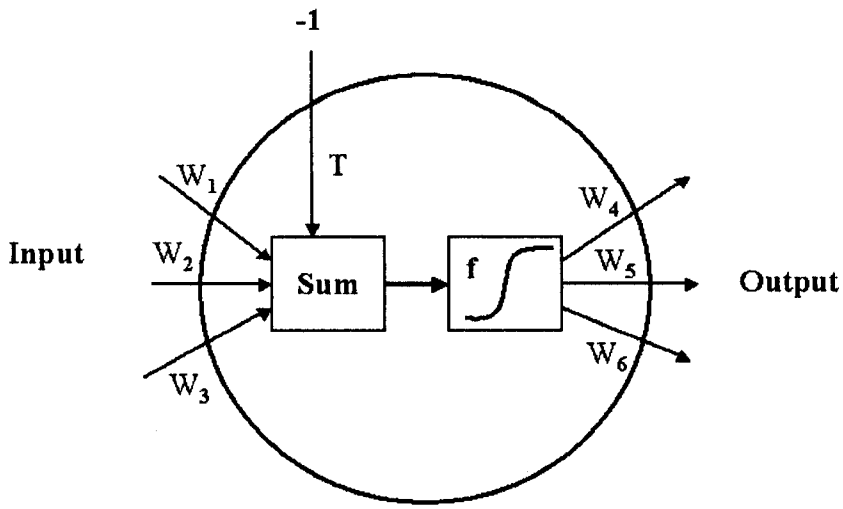

Figure 4.1: The signal processing procedure of a computational element. The element sums the weighted input, compares with the threshold T and sends out a new signal through a nonlinear active function f. W_{1-6} are weights.

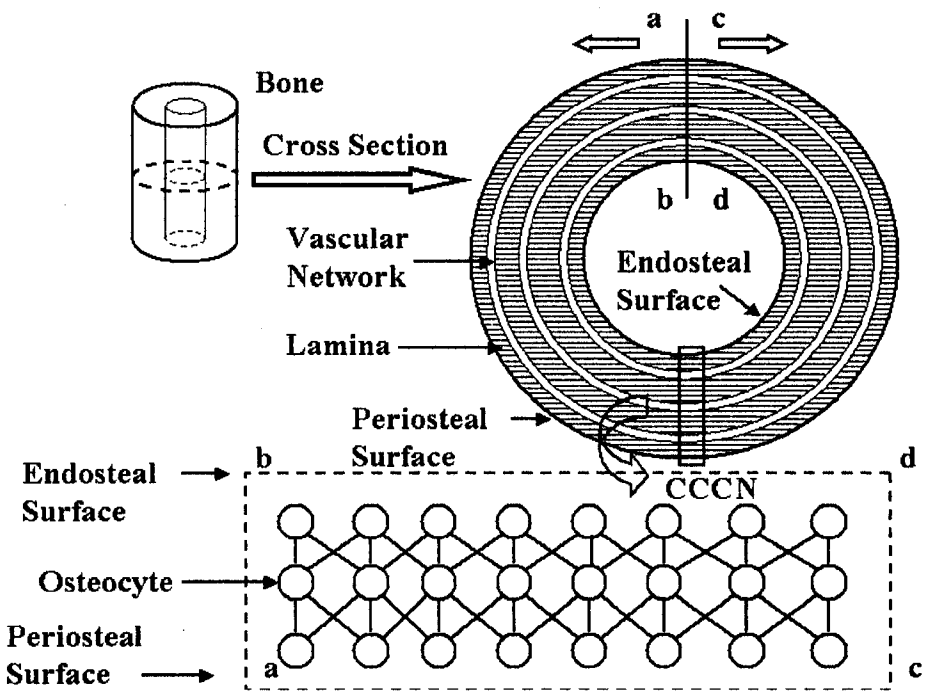

Figure 4.2: The connected cellular network in a bone cross section is idealized to be a 2-D grid. The annular cross section of the bone is "cut open" from the line at the top of the section and topologically mapped to be a 2-D rectangular grid with the top layer as the endosteal surface and the bottom layer as the periosteal surface. The radial direction of the bone cross section is along the *ba* or *dc* direction and the circumferential direction is along the *bd* or *ac* direction. Osteocytes are located and interconnected within the concentrically arranged laminae (horizontal-line-filled rings). There are no osteocytes in the vascular networks (unfilled rings). The osteocytes located on the line *ba* are connected in the same manner with those located on the line *dc*. (Laminae and osteocytes are not drawn to scale.)

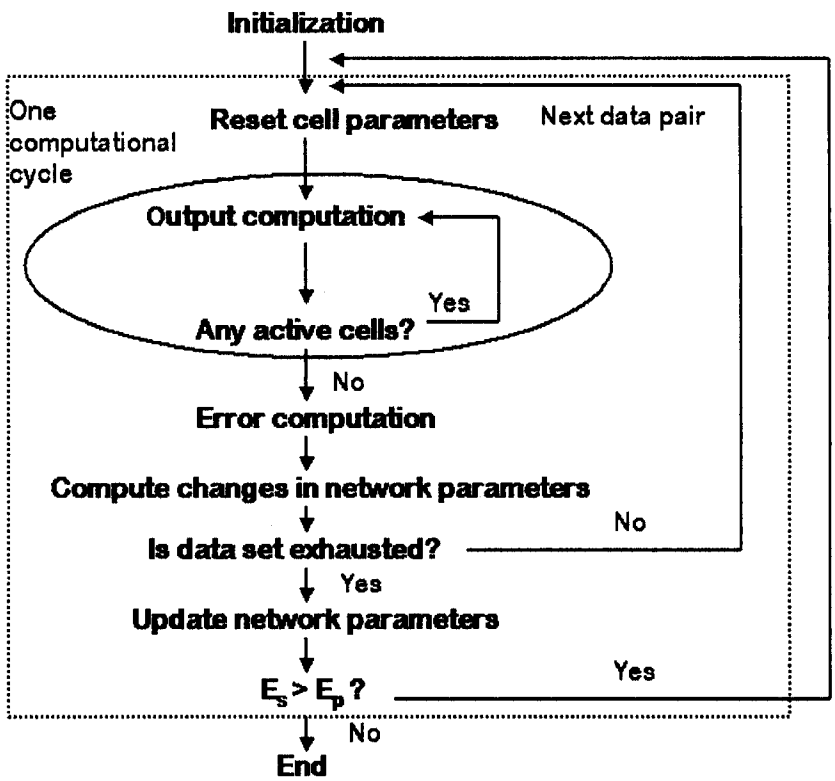

Figure 4.3: A diagram of the CCCN algorithm.

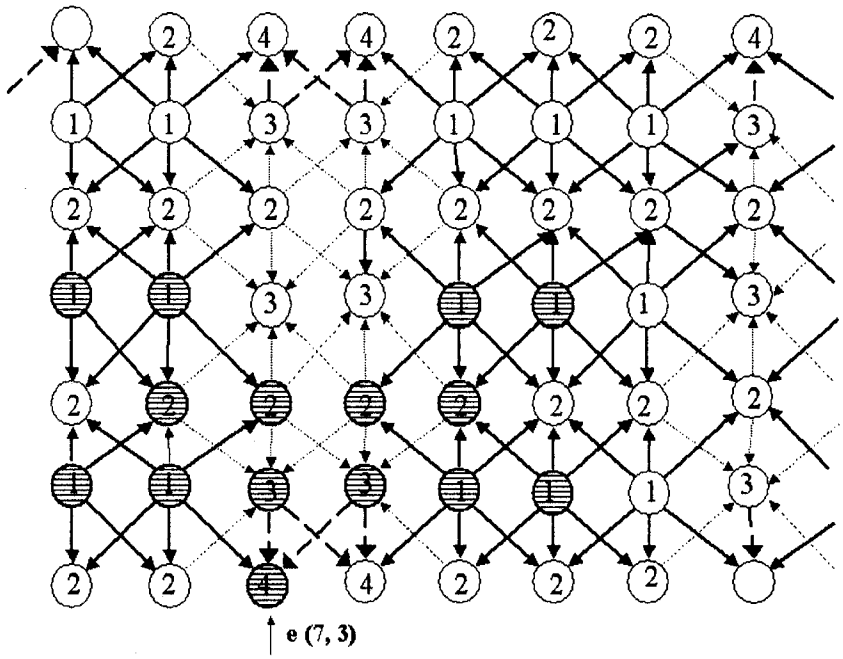

Figure 4.4: A diagram of signal propagation in a sample 7 x 8 network. The circles represent bone cells and the arrows show the direction of signal propagation from cell to cell. The numbers are the activation orders of the cells. Cells without activation orders are in the resting state. The signals sent from the directly activated cells (activation order equal to 1), represented by solid arrows, are transmitted to neighboring cells. Signals transmitted from indirectly activated cells with activation order equal to 2 and 3 are represented by dotted arrows and bold dashed arrows, respectively. The cells (filled with horizontal lines) participating in an error signal generated at the last row of the network $e(7,3)$ can be traced back through signal propagation pathways.

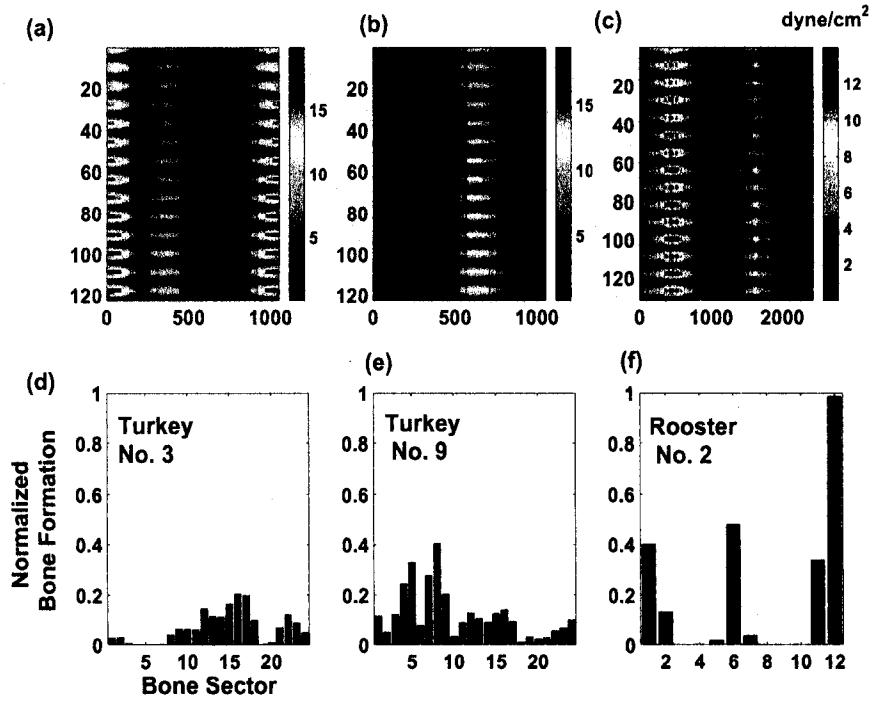

Figure 4.5: Network Input and output. (a)-(c) are the fluid shear stress distribution of turkey No. 3, No. 9 and rooster No. 2, respectively, obtained in the previous chapter. Every pixel in the images represents one osteocyte/cell where the absolute value of fluid shear stress received is color-coded with red representing the largest values (20 $dyne/cm^2$ for turkeys and 14 $dyne/cm^2$ for roosters) and blue representing the smallest value (0 $dyne/cm^2$ for all animals). In the image, the horizontal axis is the circumferential direction and the vertical axis is the radial direction of the bone section. The top row is the endosteal surface and the bottom row is the periosteal surface. This spatial presentation of the bone cross section will be used for all CCCNs in this chapter. (d)-(f) are normalized bone formation at the periosteal surface for each bone sector (24 sectors for turkeys and 12 sectors for roosters) for turkey No. 3 and No. 9 and rooster No. 2, respectively.

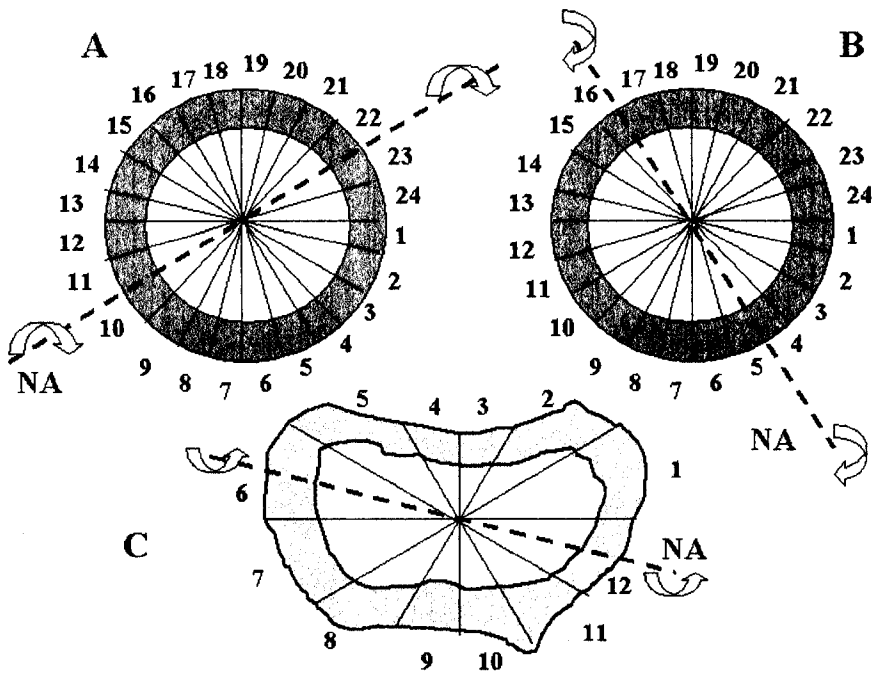

Figure 4.6: Loading conditions in the turkey (Gross et al., 1997) and the rooster (Judex et al., 1997) experiments. Two loading conditions in the turkey experiment with the loading pattern of group A (four turkeys) rotated 89 degrees from that of group B (five turkeys). One loading condition in the rooster experiment (five roosters) (C). The cross section of the turkey bone is divided into 24 equal angle sectors and rooster bone is divided into 12 equal angle sectors. NA is the neutral axis.

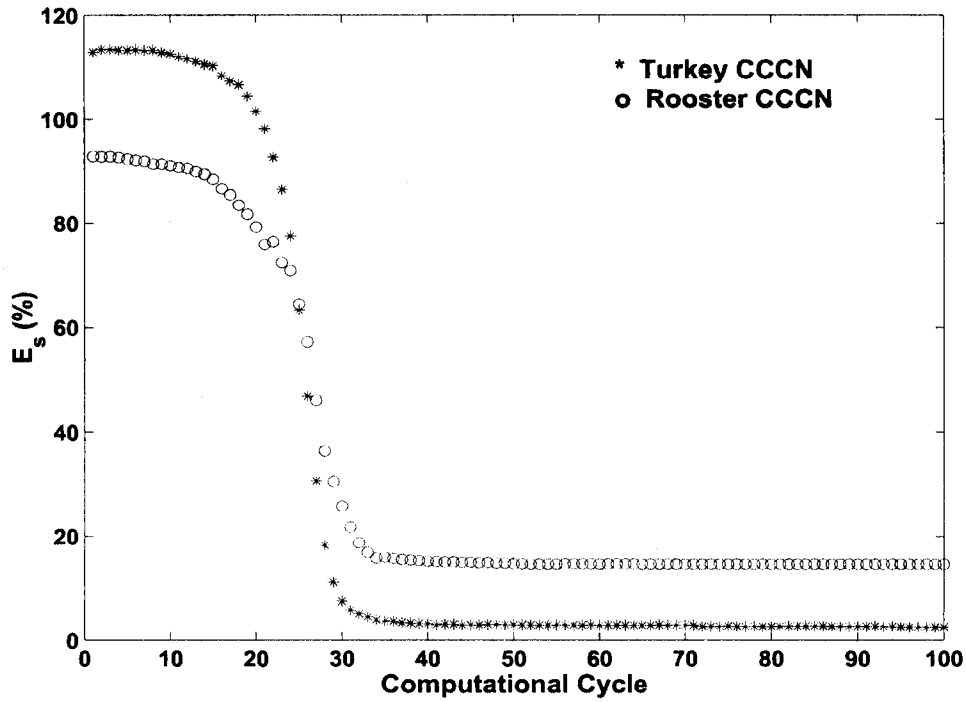

Figure 4.7: Error percentage E_s plotted for each computational cycle.

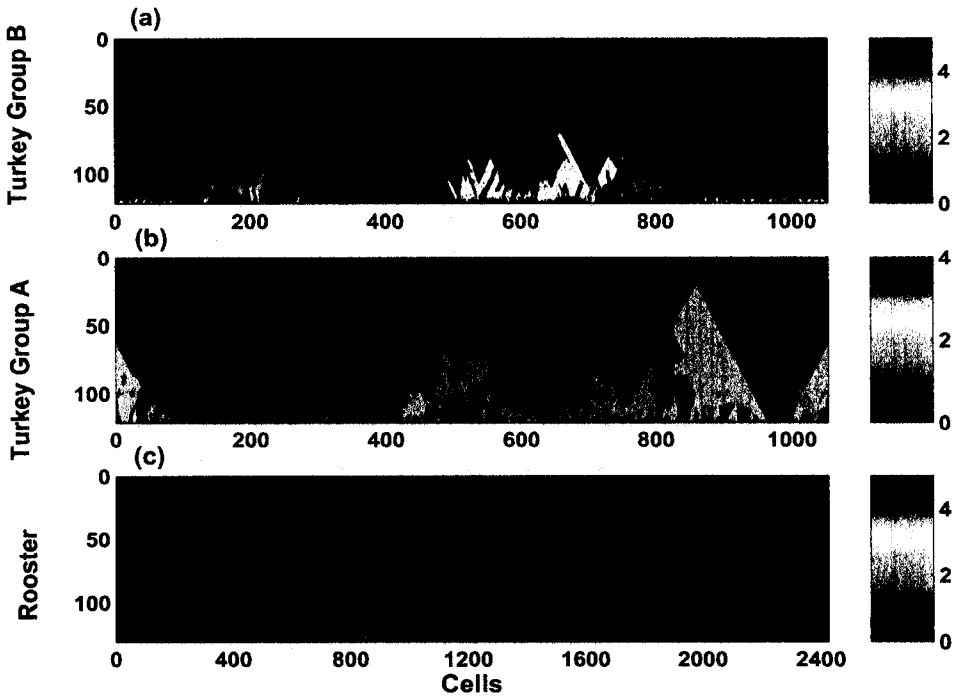

Figure 4.8: The essential cells in turkey (a, b) and rooster (c) CCCNs. Every pixel in the images represents the activation frequency of the essential cell in the loading group. Red represents high activation frequency and blue represents low activation frequency.

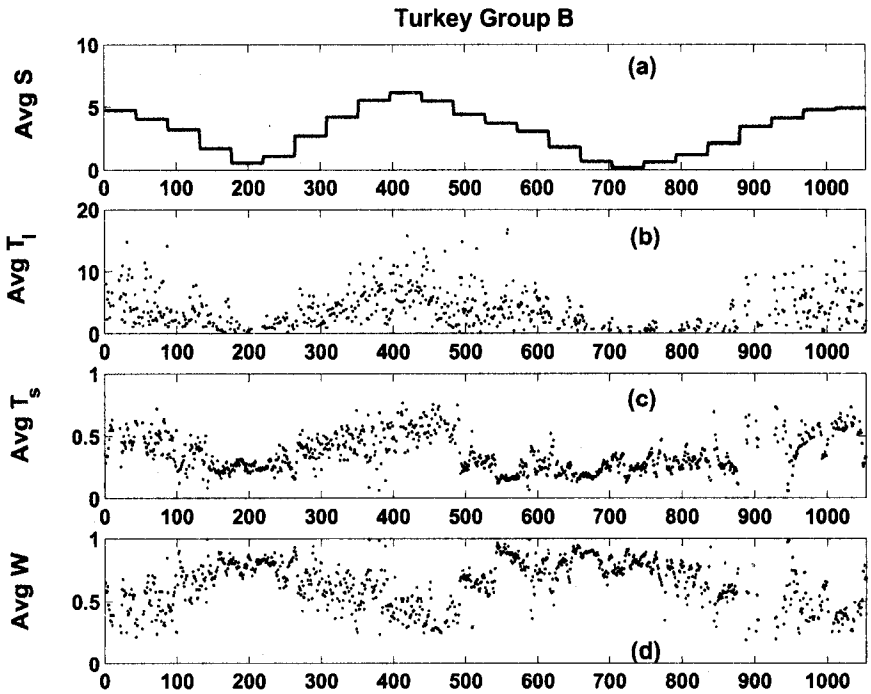

Figure 4.9: The averaged values of (b) the loading threshold T_l in $dyne/cm^2$, (c) the signal thresholds T_s, (d) the connection weights W, compared to (a) the averaged absolute value of fluid shear stress in $dyne/cm^2$ for turkey group B. Both T_s and W are unitless.

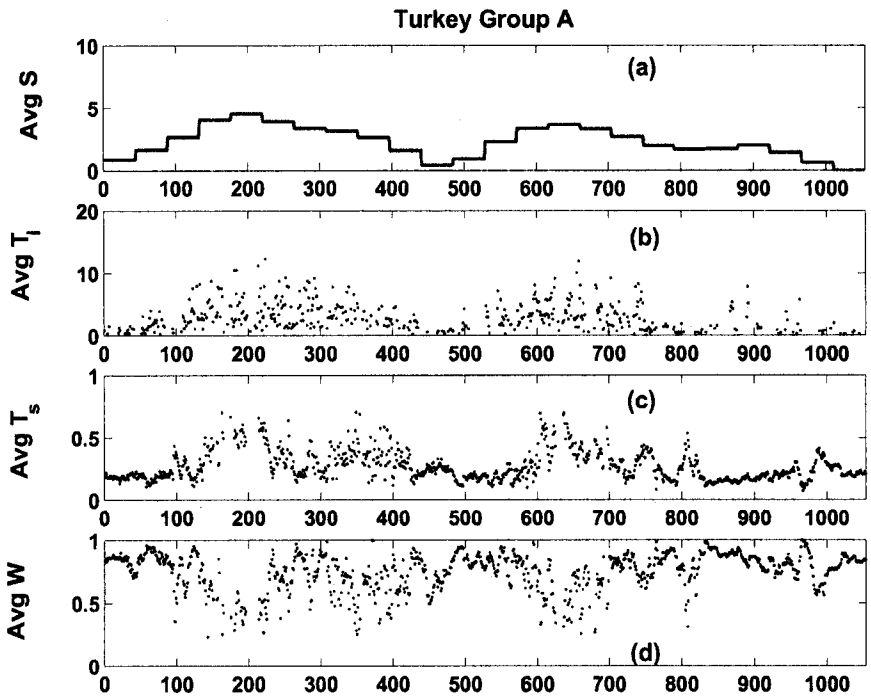

Figure 4.10: The averaged values of (b) the loading threshold T_l in $dyne/cm^2$, (c) the signal thresholds T_s, (d) the connection weights W, compared to (a) the averaged absolute value of fluid shear stress in $dyne/cm^2$ for turkey group A. Both T_s and W are unitless.

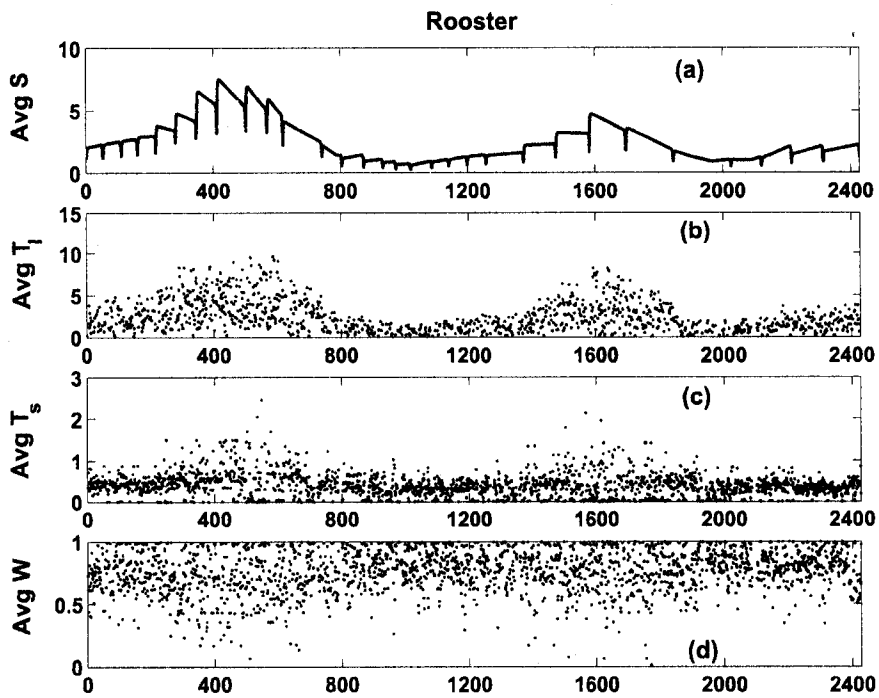

Figure 4.11: The averaged values of (b) the loading threshold T_l in $dyne/cm^2$, (c) the signal thresholds T_s, (d) the connection weights W, compared to (a) the averaged absolute value of fluid shear stress in $dyne/cm^2$ for turkey group B. Both T_s and W are unitless.

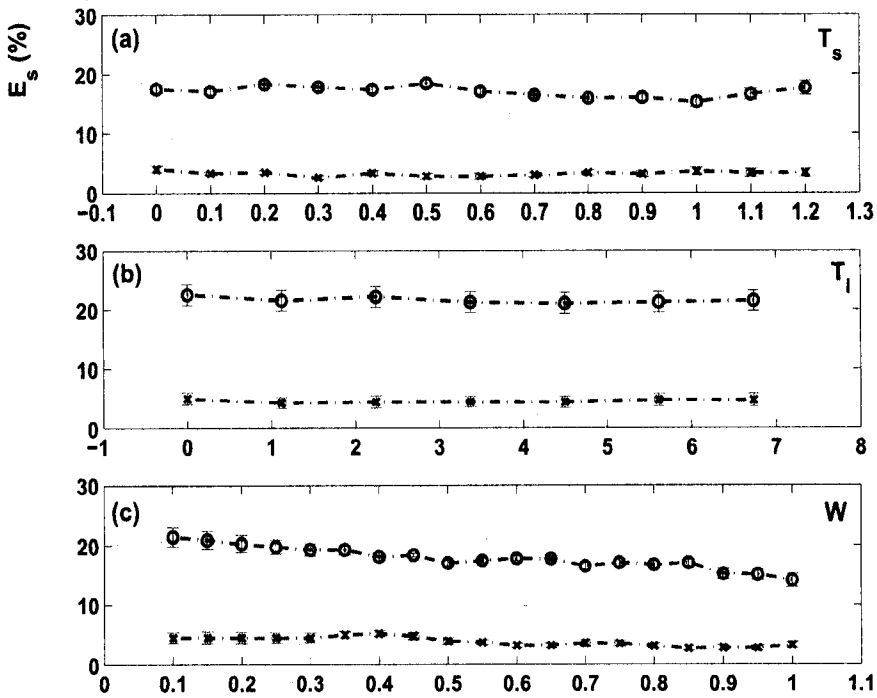

Figure 4.12: The results of the three tests designed to explore the roles of the three network parameters. The error percentage is plotted with (a) the signal threshold T_s, (b) the loading threshold T_l (in $dyne/cm^2$), and (c) the connection weight W assigned to a series of constants. * is the turkey group, including both group A and group B, o is the rooster group.

Chapter 5 Final Remarks and Future Work

In this dissertation we developed a computational connected cellular network (CCCN) model to explore how bone cells perceive mechanical loading induced signals through intercellular communication. This study is based on the hypothesis that loading induced signals are transmitted and integrated in a connected cellular network (CCN) before reaching bone surfaces where adaptation occurs. The nonlinearity of bone response in the space domain to mechanical loading is shown in Chapter 2, where a back-propagation neural network captures the underlying relationship between several loading parameters and bone formation. In Chapter 3, fluid shear stress, a mechanical loading induced stimulus suggested to be the signal sensed by bone cells, is obtained by a mathematical model based on avian bone microstructure. The averaged absolute value of the shear stress shows no linear correlation with experimental bone formation in the space domain. The results of both Chapter 2 and 3 support the hypothesis that the bone CCN is a site where loading induced signals are not only transmitted but also integrated within the network before regulating bone response.

The CCCN model is developed in Chapter 4, where the cell population that is responsible for perceiving the loading induced signal and distinct intercellular communication patterns are observed. The much more irregularly located essential cells in the turkey group, compared to that in the rooster group, is in agreement with the observation found

in Chapter 1 that the relationship between the loading parameters and bone formation in the turkey group is much more complicated than the rooster group. This suggests that the loading method may play an important role in bone response to mechanical loading. Intercellular communication patterns in bone CCNs are computationally emulated for the first time. Loading threshold of bone cells is found to play an important role in regulating avian bone formation. Much is known about the response of bone cells to fluid shear stress; however, the signal (cell response) propagation and communication subsequently in a bone CCN have never been investigated before.

The proposed CCCN model provides a unique and important tool to analyze intercellular communication and to discover the underlying relationship between input and output data in biological structures. For future investigation in intercellular communication and in designing experiments to validate the results of the CCCN, a few ideas are presented here.

- The signals transmitted through intercellular pathways in a bone CCN involve electrical events through gap junctions and diffusion of biochemical signals such as circulating and local hormones. In this study, only the signals associated with gap junctions were taken into consideration. The CCCN model would be more close to a bone CCN in biological functions if both electrical and biochemical signals were taken into consideration, either with two separate networks or with one network integrated by two mechanisms of signal transmission.

- The network revealed cell population responsible for bone response may be validated if an in vivo experiment can be designed to compare bone response to a

certain pattern of mechanical loading with or without blocking the gap junctions of osteocytes in the bone laminae near the periosteal surface.

- It would be interesting if bone responses to different patterns of mechanical loading applied through a noninvasive method can be collected. With varied sets of data, one can use the proposed CCCN model to explore and study essential cells, and the extent to which connection strength and signal threshold regulate bone response may be identified more clearly.

- Bone formation is time dependent. This dictates investigation of the evolution of intercellular communication in the time domain. Bone adaptation experiments can be designed so that the bone response with certain time information can be collected. This will help to specify the time duration a bone CCN takes for the intercellular communication to reach a steady state and to study the change of the intercellular communication in long-term loading. It would be interesting to study how this model can be modified to take dynamics into account. Such a model can be frozen in time to study static properties.

- The special features of the proposed CCCN, such as the local connections, cell states and the evolving structures of the network, make it different from the conventional learning networks. Mathematical analysis of the proposed CCCN needs to be done to find out how the network evolves with computational cycles and what kind of mathematical function the network approximates.

Appendix 1. BP Network Algorithm

Glossary:

- M: the number of neurons in layer $l-1$
- N: the number of training data sets
- K: the number of layers in the BP network
- $x(n)$: input vector $(1 \leq n \leq N)$
- $d(n)$: the corresponding desired output of $x(n)$ $(1 \leq n \leq N)$ at the output layer (the last layer)
- y_i^l: the output of neuron i in the layer l
- w_{ji}^l: the connection weights between neuron j in layer l and neuron i in layer $l-1$
- f: the activate function of neuron j in layer l
- δ_j^l: local gradients of the neuron j in layer l

There are three steps in BP network algorithm, namely initialization, forward computation and backward computation.

Initialization: Assign the connection weights and thresholds with random numbers generated from a uniform distribution function.

Forward computation: In this step, the computed output of the whole network and the error signal are calculated. First, the local input of every neuron in every layer is computed by following equation:

$$z_j^l(n) = \sum_{i=0}^{M} w_{ji}^l(n) y_i^{l-1}(n) \tag{A1}$$

where $z_j^l(n)$ is the local input of neuron j in layer l from neuron i in the previous layer; and $y_i^{l-1}(n)$ is the output of neuron i in the previous layer $l-1$. When $i = 0$, we define $y_0^{l-1}(n) = +1$; and $w_{j0}^l(n) = b_j^l(n)$ becomes the threshold of neuron j in layer l.

Second, equation (2) gives the local output $y_i^{l-1}(n)$ of neuron j in layer l, which can be fed to neurons in the next layer.

$$y_j^l(n) = f_j^l(z_j^l(n)) \tag{A2}$$

Two special cases need to be addressed:

- If $l = 1$ (i.e. neuron j is in the first layer, or the input layer), then the local output of the first layer is the input vector.

$$y_j^0(n) = x_j(n) \tag{A3}$$

- If $l = K$ (i.e. neuron j is in the last layer, or the output layer), then the local output of the last layer is the computed network output, $o_j(n)$:

$$y_j^K(n) = o_j(n) \tag{A4}$$

Finally, the error signal is computed:

$$e_j(n) = d_j(n) - o_j(n) \tag{A5}$$

Backward computation: In this step, the weights are adjusted according to the generalized delta rule:

$$\delta_j^l(n) = \begin{cases} e_j^K(n) f_j'(z_j^K(n)) & \text{if neuron j is in ouput layer } K \\ f_j'(z_j^l(n)) \sum_q \delta_q^{l+1}(n) w_{qj}^{l+1}(n) & \text{if neuron j is in hidden layer l} \end{cases} \tag{A6}$$

where q is the number of neurons in layer $l+1$.

The weights, w_{ji}^l, of the network in layer l can be adjusted:

$$w_{ji}^l(n+1) = w_{ji}^l(n) + \eta \delta_j^l(n) y_i^{l-1}(n) \tag{A7}$$

where η is the learning-rate parameter, which controls the amount of changes to the weights between two consecutive iterations. The smaller η is, the slower rate of learning is. On the other hand, a too-large η can speed up the learning procedure, but it may lead a network into oscillation.

With the adjusted weights, a BP network begins iterations of the forward and backward computations using next training data set until the error signal is sufficiently small.

Appendix 2. Fourier series of the loading in Gross et al. (1997)

The loading variation is specified by a trapezoidal function $f(t)$, $0 < t < 2t_1 + t_2 + 2t_3$, such that

$$f(t) = \begin{cases} 0 & 0 < t < t_1 \\ k(t - t_1) & t_1 < t < t_1 + t_3 \\ F & t_1 + t_3 < t < t_1 + t_3 + t_2 \\ k(t_1 + t_2 + 2t_3 - t) & t_1 + t_2 + t_3 < t < t_1 + t_2 + 2t_3 \\ 0 & t_1 + t_2 + 2t_3 < t < 2t_1 + t_2 + 2t_3 \end{cases} \tag{A8}$$

where k is the loading rate, F is the peak loading magnitude, and t_1, t_2, and t_3 are time durations shown in Figure A1. A Fourier series representation which describes eq.(A8) as well as its periodic extensions to all other values of t is:

$$f(t) = \frac{A_0}{2} + \sum_{n=1}^{\infty} [A_n \cos(nwt) + B_n \sin(nwt)] \tag{A9}$$

where $w = 2\pi/T_t$, and $T_t = 2t_1 + 2t_3 + t_2$ is the loading period.

The Fourier constants are:

$$A_0 = \frac{2F(t_2 + t_3)}{T_t} \tag{A10}$$

$$A_n = \frac{2k}{T_t n^2 w^2}\{\cos[nw(t_1 + t_3)] - \cos(nwt_1) + \cos[nw(t_1 + t_2 + t_3)]$$

$$- \cos[nw(t_1 + t_2 + 2t_3)]\} \tag{A11}$$

$$B_n = 0 \tag{A12}$$

Thus eq.(A9) can be written as:

$$f(t) = \frac{A_0}{2} + \sum_{n=1}^{\infty} A_n \cos(nwt). \tag{A13}$$

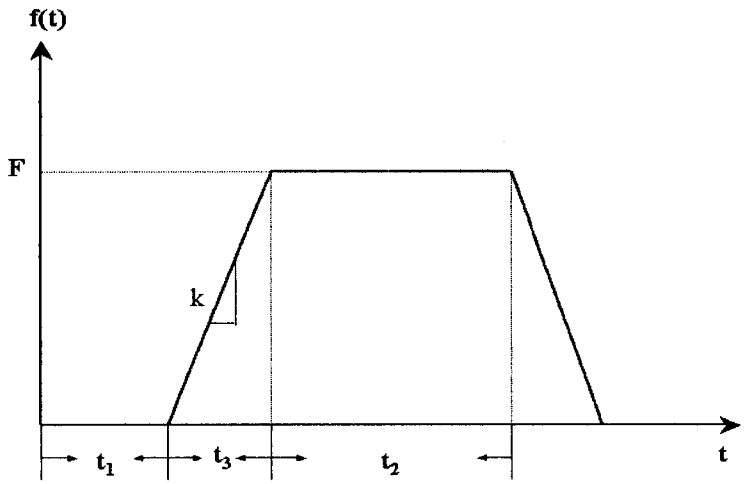

Figure A1: The trapezoidal loading function $f(t)$ employed in the turkey experiment (Gross et al., 1997) ($t_1 = 0.26$ *sec*, $t_2 = 1.8$ *sec*, $t_3 = 0.09$ *sec*, $k = 120$ N/sec and $F = 10.8$ N).

Appendix 3. Parameter Values Adopted from Zeng et al. (1994)

- a is the radius of the osteocytic process (=50 nm)
- B is a Skempton pore pressure parameter (=0.53)
- b is the radius of the canaliculus (=100 nm)
- γ_1 is a dimensionless parameter ($= b/\sqrt{k_p}$)
- q is the ratio of b to a (=2)
- c ($= r_0^2/\tau_r$) is the diffusion coefficient in the differential equation governing the pore fluid pressure
- τ_r is the characteristic time of relaxation of the fluid pore pressure
- a_0 is the radius of the fiber traversing the annular region between the osteocytic process and the canaliculus wall (=1 nm)
- Δ is the open space between the transverse fibers in the channel between the cytoplasmic process and the wall of the canaliculus (=7 nm)
- k_p is the cell process channel scale Darcy law permeability constant for fluid flow through the mid-section of a cell process channel filled with transverse fibers ($= 0.0572{a_0}^2(\Delta/a_0)^{2.377}$)
- μ is bone fluid viscosity

- d is the half thickness of bone specimen used in the experiment $(d = (r_0 - r_i)/2)$
- $n_c/(L_c L_d)$ is the number of canaliculi in an area L_c by L_d

Appendix 4. Parameters in Pore Pressure Solution

$$A_{0n} = \frac{AnN_0}{iTF} \frac{K_0(\sqrt{inT}R_{v2}) - K_0(\sqrt{inT}R_{v1})}{I_0(\sqrt{inT}R_{v1})K_0(\sqrt{inT}R_{v2}) - I_0(\sqrt{inT}R_{v2})K_0(\sqrt{inT}R_{v1})} \tag{A14}$$

$$B_{0n} = \frac{AnN_0}{iTF} \frac{I_0(\sqrt{inT}R_{v1}) - I_0(\sqrt{inT}R_{v2})}{I_0(\sqrt{inT}R_{v1})K_0(\sqrt{inT}R_{v2}) - I_0(\sqrt{inT}R_{v2})K_0(\sqrt{inT}R_{v1})} \tag{A15}$$

$$A_{1n} = \frac{AnN_m}{iTF} R_{v2}\cos\gamma \frac{R_{v1}K_1(\sqrt{inT}R_{v2}) - R_{v2}K_1(\sqrt{inT}R_{v1})}{R_{v2}I_1(\sqrt{inT}R_{v1})K_1(\sqrt{inT}R_{v2}) - R_{v2}I_1(\sqrt{inT}R_{v2})K_1(\sqrt{inT}R_{v1})} \tag{A16}$$

$$B_{1n} = \frac{AnN_m}{iTF} R_{v2}\cos\gamma \frac{R_{v2}I_1(\sqrt{inT}R_{v1}) - R_{v1}I_1(\sqrt{inT}R_{v2})}{R_{v2}I_1(\sqrt{inT}R_{v1})K_1(\sqrt{inT}R_{v2}) - R_{v2}I_1(\sqrt{inT}R_{v2})K_1(\sqrt{inT}R_{v1})} \tag{A17}$$

$$A_{1n} = \frac{AnN_m}{iTF} R_{v2}\sin\gamma \frac{R_{v1}K_1(\sqrt{inT}R_{v2}) - R_{v2}K_1(\sqrt{inT}R_{v1})}{R_{v2}I_1(\sqrt{inT}R_{v1})K_1(\sqrt{inT}R_{v2}) - R_{v2}I_1(\sqrt{inT}R_{v2})K_1(\sqrt{inT}R_{v1})} \tag{A18}$$

$$B_{1n} = \frac{AnN_m}{iTF} R_{v2}\sin\gamma \frac{R_{v2}I_1(\sqrt{inT}R_{v1}) - R_{v1}I_1(\sqrt{inT}R_{v2})}{R_{v2}I_1(\sqrt{inT}R_{v1})K_1(\sqrt{inT}R_{v2}) - R_{v2}I_1(\sqrt{inT}R_{v2})K_1(\sqrt{inT}R_{v1})} \tag{A19}$$

$$A_3 = \frac{K_0(\gamma_1) - K_0(\gamma_1/q)}{I_0(\gamma_1/q)K_0(\gamma_1) - I_0(\gamma_1)K_0(\gamma_1/q)} \tag{A20}$$

$$B_3 = \frac{I_0(\gamma_1/q) - I_0(\gamma_1)}{I_0(\gamma_1/q)K_0(\gamma_1) - I_0(\gamma_1)K_0(\gamma_1/q)} \tag{A21}$$

Appendix 5. Parameter Values Adopted from Gross et al. (1997)

- L is the moment arm length (=13.2 cm)
- r_0 is the radius of the whole bone (=4.0 mm)
- r_i is the radius of the marrow cavity (=2.7 mm)
- γ is the angle between the neutral axis and the x axis (=62±2.5 *degrees*)

Appendix 6. Parameter Values Adopted from Judex et al. (1997)

- I_y is the area moment of inertia of the bone section (=92.1 mm^4)
- I_x is the area moment of inertia of the bone section (=170.56 mm^4)

Bibliography

Aarden, E. M., Burger, E. H. and Nijweide, P. J. Function of osteocytes in bone. *J Cell Biochem.* 55(3):287-299, 1994.

Ajubi N. E., Klein-Nulend J., Nijweide P. J., Vrijheid-Lammers T., Alblas M. J. and Burger E. H. Pulsating fluid flow increases prostaglandin production by cultured chicken osteocytes–a cytoskeleton-dependent process. *Biochem Biophys Res Commun.* 225(1):62-68, 1996.

Alford A. I., Jacobs C. R. and Donahue H. J. Oscillating fluid flow regulates gap junction communication in osteocytic MLO-Y4 cells by an ERK1/2 MAP kinase-dependent mechanism small star, filled. *Bone.* 33(1):64-70, 2003.

Allen R. E. and Boxhorn L. K. Regulation of skeletal muscle satellite cell proliferation and differentiation by transforming growth factor-beta, insulin-like growth factor I., and fibroblast growth factor. *J Cell Physiol.* 138(2):311-315, 1989.

Anderson J. A. and Rosenfeld E. *Neurocomputing: Foundations of Research.* Cambridge, MA: MIT Press, 1988.

Bakker A. D., Soejima K., Klein-Nulend J. and Burger E. H. The production of nitric oxide and prostaglandin E(2) by primary bone cells is shear stress dependent. *J Biomech.* 34(5):671-677, 2001.

Basu M., Mi L. Y., Fritton S. P. and Cowin S. C. A Biologically Motivated Computational Learning Model. *NATO Advanced Study Institute on Learning, Theory*

and Practice. K. U. Leuven, Belgium, July 8-21, 2002

Bennett M. V. L. and Goodenough D. A. Gap junctions: Electronic coupling and intercellular communication. *Neurosci Res Program Bull.* 16: 373-485, 1978.

Bloomfield S. A. Cellular and molecular mechanisms for the bone response to mechanical loading. *Int J Sport Nutr Exerc Metab.* 11 Suppl:S128-S136, 2001.

Brown T. D., Pedersen D. R., Gray M. L., Brand R. A. and Rubin C. T. Toward an identification of mechanical parameters initiating periosteal remodeling: a combined experimental and analytic approach. *J Biomech.* 23(9):893-905, 1990.

Burger E. H. and Klein-Nulen J. Responses of bone cells to biomechanical forces in vitro. *Adv Dent Res.* 13:93-98, 1999.

Burger E. H. and Klein-Nulen J. Mechanotransduction in bone–role of the lacunocanalicular network. *FASEB J.* 13 Suppl:S101-S112, 1999.

Burr D. B., Martin R. B., Schaffler M. B. and Radin E. L. Bone remodeling in response to in vivo fatigue microdamage. *J Biomech.* 18(3):189-200, 1985.

Carter D. R. Mechanical loading histories and cortical bone remodeling. *Calcif Tissue Int.* 36 Suppl 1:S19-S24, 1984.

Carter D. R., Fyhrie D. P. and Whalen R. T. Trabecular bone density and loading history: regulation of connective tissue biology by mechanical energy. *J Biomech.* 20(8):785-794, 1987.

Cheng B., Zhao S., Luo J., Sprague E., Bonewald L. F. and Jiang J. X. Expression

of functional gap junctions and regulation by fluid flow in osteocyte-like MLO-Y4 cells. *J Bone Miner Res.* 16(2):249-259, 2001.

Chiba H., Sawada N., Oyamada M., Kojima T., Iba K., Ishii S. and Mori M. Hormonal regulation of connexin 43 expression and gap junctional communication in human osteoblastic cells. *Cell Struct Funct.* 19(3):173-177, 1994.

Chow J. W., Fox S., Jagger C. J. and Chambers T. J. Role for parathyroid hormone in mechanical responsiveness of rat bone. *Am J Physiol.* 274(1 Pt 1):E146-54, 1998.

Churches A. E. and Howlett C. R. Functional adaptation of bone in response to sinusoidally varying controlled compressive loading of the ovine metacarpus. *Clin Orthop.* 168:265-280, 1982.

The Computational Brain. MIT Press, Cambridge, Mass, 1992.

Civitelli R., Beyer E. C., Warlow P. M., Robertson A. J., Geist S. T. and Steinberg T. H. Connexin43 mediates direct intercellular communication in human osteoblastic cell networks. *J Clin Invest.* 91(5):1888-1896, 1993.

Civitelli R. Cell-cell communication in bone. *Calcif Tissue Int.* 56(Suppl.1):S29-S31, 1995.

Cowin S. C. and Hegedus D. H. Bone remodeling I: theory of adaptive elasticity. *J. Elasticity.* 6(3):313-326, 1976.

Cowin S. C. and Van Buskirk W. C. Surface bone remodeling induced by a medullary pin. *J Biomech.* 12(4):269-276, 1979.

Cowin S. C. and Firoozbakhsh K. Bone remodeling of diaphysial surfaces under constant load: theoretical predictions. *J Biomech.* 14(7):471-484, 1981.

Cowin S. C., Hart R. T., Balser J. R. and Kohn D. H. Functional adaptation in long bones: establishing in vivo values for surface remodeling rate coefficients. *J Biomech.* 18(9):665-684, 1985.

Cowin S. C., Moss-Salentijn L. and Moss M. L. Candidates for the mechanosensory system in bone. *J Biomech Eng.* 113:191-197, 1991.

Cowin S. C., Weinbaum S. and Zeng Y. A case for bone canaliculi as the anatomical site of strain generated potentials. *J Biomech.* 28:1281-1297, 1995.

Cowin S. C. Bone poroelasticity. *J Biomech.* 32(3):217-238, 1999.

Cowin S. C. and Moss M. L. Mechanosensory mechanisms in bone. *Textbook of Tissue Engineering.* Lanza R., Langer R., Chick W (eds), 2nd edition, Academic Press, San Diego, 723-738, 2000.

Cullen D. M., Smith R. T. and Akhter M. P. Time course for bone formation with long-term external mechanical loading. *J Appl Physiol.* 88(6):1943-1948, 2000.

Cullen D. M., Smith R. T. and Akhter M. P. Bone-loading response varies with strain magnitude and cycle number. *J Appl Physiol.* 91(5):1971-1976, 2001.

Currey J. D. Differences in the blood-supply of bone of different histological types. *J of Microscopical Science.* 101:351-370, 1960.

Curtis T. A., Ashrafi S. H. and Weber D. F. Canalicular communication in the cortices of human long bones. *Anat Rec.* 212:336-344, 1985.

D'Andrea P. and Vittur F. Propagation of intercellular Ca2+ waves in mechanically stimulated articular chondrocytes. *FEBS Lett* . 400(1):58-64, 1997.

Demer L. L., Wortham C. M., Dirksen E. R. and Sanderson M. J. Mechanical stimulation induces intercellular calcium signaling in bovine aortic endothelial cells. *Am J Physiol.* 264(6 Pt 2):H2094-H2102, 1993.

Dodds R. A., Ali N., Pead M. J. and Lanyon L. E. Early loading-related changes in the activity of glucose 6-phosphate dehydrogenase and alkaline phosphatase in osteocytes and periosteal osteoblasts in rat fibulae in vivo. *J Bone Miner Res* . 8(3):261-267, 1993.

Donahue H. J., McLeod K. J., Rubin C. T., Andersen J., Grine E. A., Hertzberg E. L. and Brink P. R. Cell-to-cell communication in osteoblastic networks: cell line-dependent hormonal regulation of gap junction function. *J Bone Miner Res.* 10(6):881-889, 1995.

Doty S. B. Morphological evidence of gap junctions between bone cells. *Calcif Tissue Int.* 33:509-512, 1981.

Duncan R. L. and Turner C. H. Mechanotransduction and the functional response of bone to mechanical strain. *Calcif Tissue Int.* 57(5):344-358, 1995.

Enomoto K., Furuya K., Yamagishi S. and Maeno T. Mechanically induced electrical and intracellular calcium responses in normal and cancerous mammary cells. *Cell Calcium.* 13(8):501-511, 1992.

Freemont A. J. Basic bone cell biology. *Int J Exp Path.* 74: 411-416, 1993.

French A. S. Mechanotransduction. *Annu Rev Physiol.* 54:135-152, 1992.

Frost H. M. *Dynamics of Bone Remodeling in Bone Biodynamics.* Ed, Frost H. M., Little and Brown, Boston, 1964.

Frost H. M. A determinant of bone architecture: the minimum effective strain. *Clin Orthop.* 175:286-292, 1983.

Frost H. M. Intermediary Organization of the Skeleton, Vols. I and II, CRC Press, Boca Raton, FL, 1986

Frost H. M. Skeletal structural adaptations to mechanical usage (SATMU): 2. Redefining Wolff's law: the remodeling problem. *Anat Rec.* 226(4):414-422, 1990.

Garven H. S. D. *A Student's Histology.* Williams and Wilkins, Baltimore, 1965.

Greene E. A. and Allen R. E. Growth factor regulation of bovine satellite cell growth in vitro. *J Anim Sci.* 69(1):146-152, 1991.

Gross T. S., Edwards J. L., McLeod K. J. and Rubin C. T. Strain gradients correlate with sites of periosteal bone formation. *Bone Miner.* 12:982-988, 1997.

Gu Y. and Publicover S. J. Expression of functional metabotropic glutamate receptors in primary cultured rat osteoblasts. Cross-talk with N-methyl-D-aspartate receptors. *J Biol Chem.* 275(44):34252-34259, 2000.

Harrigan T. P. and Hamilton J. J. Bone strain sensation via transmembrane potential changes in surface osteoblasts: loading rate and microstructural implications. *J Biomech.* 26(2):183-200, 1993.

Hart R. T., Davy D. T. and Heiple K. G. Mathematical modeling and numerical solutions for functionally dependent bone remodeling. *Calcif Tissue Int 36 Suppl.* 1: S104-109, 1984.

Hart R. L. Bone modeling and remodeling: theories and computation. *Bone Mechanics Handbook.* Cowin S. C. Ed., CRC Press, Boca Raton, FL.

Haykin S. *Neural Networks : A Comprehensive Foundation.* Upper Saddle River, NJ:Prentice Hall.

Hegedus D. M. and Cowin S. C. Bone remodeling, II: small strain adaptive elasticity. *J. of Elasticity.* 6: 337-352, 1976.

Hillsley M. V. and Frangos J. A. Bone tissue engineering: the role of interstitial fluid flow. *Biotechnology and Bioengineering.* 43: 573-581, 1994.

Hinoi E., Fujimori S., Nakamura Y. and Yoneda Y. Group III metabotropic glutamate receptors in rat cultured calvarial osteoblasts. *Biochem Biophys Res Commun.* 281(2):341-346, 2001.

Ho T. and Basu M. Measuring the complexity of classification problems. *Proceedings of the International Conf. Pattern Recognition.* Barcelona, Spain, Sept. 3-8, 2000.

Hsieh Y. F., Robling A. G., Ambrosius W. T., Burr D. B. and Turner C. H. Mechanical loading of diaphyseal bone in vivo: the strain threshold for an osteogenic response varies with location. *J Bone Miner Res.* 16:2291-2297, 2001.

Huggett J. F., Mustafa A., O'neal L. and Mason D. J. The glutamate transporter GLAST-1 (EAAT-1) is expressed in the plasma membrane of osteocytes and is responsive to extracellular glutamate concentration. *Biochem Soc Trans.* 30(Pt 6):890-893.

Huiskes R., Weinans H., Grootenboer H. J., Dalstra M., Fudala B. and Slooff T. J. *Adaptive bone-remodeling theory applied to prosthetic-design analysis. J Biomech.* 20:1135-1150,

Hung C. T., Pollack S. R., Reilly T. M. and Brighton C. T. Real-time calcium response of cultured bone cells to fluid flow. *Clin Orthop.* 313:256-269, 1995.

Inaoka T., Lean J. M., Bessho T., Chow J. W., Mackay A., Kokubo T. and Chambers T. J. Sequential analysis of gene expression after an osteogenic stimulus: c-fos expression is induced in osteocytes. *Biochem Biophys Res Commun.* 217(1):264-70, 1995.

Jacobs C. R., Yellowley C. E., Davis B. R., Zhou Z., Cimbala J. M. and Donahue H. J. Differential effect of steady versus oscillating flow on bone cells. *J Biomech.* 31(11): 969-976, 1998.

Jagger C. J., Chow J. W. and Chambers T. J. Estrogen suppresses activation but enhances formation phase of osteogenic response to mechanical stimulation in rat bone. *J Clin Invest.* 98(10):2351-2357, 1996.

Jeansonne B. G., Feagin F. F., McMinn R. W., Shoemaker R. L. and Rehm W. S. Cell-to-cell communication of osteoblasts. *J Dent Res* 58(4): 1415-1423, 1979.

Jee W. S. S. Structure and function of bone tissue. *Orthopaedics, Principles of Basic and Clinical Science.* Bronner F. and Worrell R. V., Eds, CRC Press, Boca Raton, FL., 1999

Jiang J. X. and Cheng B. Mechanical stimulation of gap junctions in bone osteocytes is mediated by prostaglandin E2. *Cell Commun Adhes.* 8(4-6):283-288, 2001.

Johnson D. L., McAllister T. N. and Frangos J. A. Fluid flow stimulates rapid and continuous release of nitric oxide in osteoblasts. *Am J Physiol.* 271:205-208, 1996.

Johnson K. A., Skinner G. A. and Muir P. Site-specific adaptive remodeling of Greyhound metacarpal cortical bone subjected to asymmetrical cyclic loading. *Am J Vet Res.* 62(5):787-793, 2001.

Jones D. B., Nolte H., Scholubbers J. G., Turner E. and Veltel D. Biochemical signal transduction of mechanical strain in osteoblast-like cells. *Biomaterials.* 12(2):101-110, 1991.

Jones S. J., Gray C., Sakamaki H., Arora M., Boyde A., Gourdie R. and Green C. The incidence and size of gap junctions between bone cells in rat calvaria. *Anat Embryol (Berl).* 187:343-352, 1993.

Judex S., Gross T. S. and Zernicke R. G. Strain gradients correlate with sites of exercise-induced bone-forming surfaces in the adult skeleton. *Bone Miner.* 12:1737-1745, 1997.

Kamioka H., Honjo T. and Takano-Yamamoto T. A three-dimensional distribution of osteocyte processes revealed by the combination of confocal laser scanning microscopy and differential interference contrast microscopy. *Bone.* 28(2):145-9, 2001

Kasperk C., Fitzsimmons R., Strong D., Mohan S., Jennings J., Wergedal J. and Baylink D. Studies of the mechanism by which androgens enhance mitogenesis and differentiation in bone cells. *J Clin Endocrinol Metab.* 71(5):1322-9, 1990.

Klein-Nulend J., van der Plas A., Semeins C. M., Ajubi N. E., Frangos J. A., Nijweide P. J. and Burger E. H. Sensitivity of osteocytes to biomechanical stress in vitro. *FASEB J.* 9:441-445, 1995.

Klein-Nulend J., Burger E. H. and Semeins C. M., Raisz L. G. and Pilbeam C. C. Pulsating fluid flow stimulates prostaglandin release and inducible prostaglandin G/H synthase mRNA expression in primary mouse bone cells. *J Bone Miner Res.* 12(1):45-51, 1997.

Koch J. C. The laws of bone architecture. *Am J Anat.* 21:177-298, 1917.

Konieczynski D. D., Truty M. J. and Biewener A. A. Evaluation of a bone's in vivo 24-hour loading history for physical exercise compared with background loading. *J Orthop Res* 16(1):29-37, 1998.

Lanyon L. E. and Hartman W. Strain related electrical potentials recorded in vitro and in vivo. *Calcif Tissue Res.* 22(3):315-327, 1977.

Lean J. M., Mackay A. G., Chow J. W. and Chambers T. J. Osteocytic expression

of mRNA for c-fos and IGF-I: an immediate early gene response to an osteogenic stimulus. *Am J Physiol.* 270(6 Pt 1):E937-45, 1996.

Lecanda F., Towler D. A., Ziambaras K., Cheng S. L., Koval M., Steinberg T. H. and Civitelli R. Gap junctional communication modulates gene expression in osteoblastic cells. *Mol Biol Cell.* 9(8):2249-2258, 1998.

Loitz B. J. and Zernicke R. F. Strenuous exercise-induced remodelling of mature bone: relationships between in vivo strains and bone mechanics. *J Exp Biol.* 170:1-18, 1992.

Martin R. B. The effects of geometric feedback in the development of osteoporosis. *J Biomech.* 5(5):447-455, 1972.

R. B. Martin and D. B. Burr A hypothetical mechanism for the stimulation of osteonal remodeling by fatigue damage. *J Biomechanics.* 15:137-139, 1982.

Martin R. B. and Burr D. B. *Structure, function, and adaptation of compact bone.* Raven Press.

Mason D. J., Suva L. J., Genever P. G., Patton A. J., Steuckle S., Hillam R. A. and Skerry T. M. Mechanically regulated expression of a neural glutamate transporter in bone: a role for excitatory amino acids as osteotropic agents. *Bone.* 20(3):199-205, 1997.

Mattheck C. and Huber-Betzer H. CAO: Computer simulation of adaptive growth in bones and trees. *Computers in Biomedicine.* Held K. D., Brebbia C. A.,

Ciskowski R. D., Eds, Computational Mechanics Publications, Southampton, 291-296, 1991

McDonald F., Yettram A. L., MacLeod K. The response of bone to external loading regimens. *Med Eng Phys.* 16:384-397, 1994.

Mi L. Y., Basu M., Fritton S. P. and Cowin S. C. Study of site-specific bone formation using a neural network model. *Proceedings of the IEEE-INNS-ENNS International Joint Conference on Neural Networks.* 3: 641-654, 2000.

Mi L. Y., Basu M., Fritton S. P. and Cowin S. C. Simulation of the bone cellular network using a neural network model. *Annals of Biomedical Engineering.* 28(S1): S-49, 2000

Mi L. Y., Basu M., Fritton S. P. and Cowin S. C. Computational connected cellular Network A novel learning system to study bone formation. *Proceedings of the IEEE-INNS-ENNS International Joint Conference on Neural Networks.* 3: 1693-1647, 2001.

Mi L. Y., Basu M., Fritton S. P. and Cowin S. C. Bone fluid motion induced by bending and axial loading in bone: analysis of an adaptation study. *Transactions of the 48th Meeting of the Orthopaedic Research Society.* 27:573, 2002.

Mi L. Y., Basu M., Fritton S. P. and Cowin S. C. A learning algorithm for computational connected cellular network. *Proceedings of the 9th International Conference on Neural Information Processing.* 1: 503-506, 2002.

Mi L. Y., Fritton S. P., Basu M., and Cowin S. C. Analysis of Avian Bone Response

to Mechanical Loading. Part One: Distribution of Bone Fluid Shear Stress Induced by Bending and Axial Loading. *Biomech Model Mechanobiol.* (submitted), 2004

Mi L. Y., Basu M., Fritton S. P., and Cowin S. C. Analysis of Avian Bone Response to Mechanical Loading. Part Two: Development of a Computational Connected Cellular Network (CCCN) to Study Bone Intercellular communications. *Biomech Model Mechanobiol.* (submitted), 2004

Mikuni-Takagaki Y. Mechanical responses and signal transduction pathways in stretched osteocytes. J Bone Miner Metab 17(1) : 57-60, 1999.

Mosley J. R. and Lanyon L. E. Strain rate as a controlling influence on adaptive modeling in *response to dynamic loading of the ulna in growing male rats. Bone.* 23:313-318, 1998.

Moss M. L. Bone as a connected cellular network: modeling and testing. *Topics in Biomedical Engineering.* Ross G (ed), New York: Pergamon Press, 117-119, 1991.

Moss M. L. and Cowin S. C. Mechanosensory mechanisms in bone. *Principles of Tissue Engineering.* Lanza R., Langer R., Chick W (eds), Landes Company, 645-659, 1997

Moss M. L. The functional matrix hypothesis revisited. 2. The role of an osseous connected cellular network. *Am J Orthod Dentofacial Orthop.* 112:221-226, 1997.

O'Connor J. A., Lanyon L. E., MacFie H. The influence of strain rate on adaptive bone. *remodelling. J Biomech.* 15:767-782, 1982.

Ogata T. Fluid flow induces enhancement of the Egr-1 mRNA level in osteoblast-like cells: involvement of tyrosine kinase and serum. *J Cell Physiol.* 170(1):27-34, 1997.

Owan I., Burr D. B., Turner C. H., Qiu J., Tu Y., Onyia J. E. and Duncan R. L. Mechanotransduction in bone: osteoblasts are more responsive to fluid forces than mechanical strain. *Am J Physiol.* 273(3 Pt 1):C810-C815, 1997

Palumbo C., Palazzini S. and Marotti G. Morphological study of intercellular junctions during osteocyte differentiation. *Bone.* 11(6):401-406, 1990.

Patton A. J., Genever P. G., Birch M. A., Suva L. J. and Skerry T. M. Expression of an N-methyl-D-aspartate-type receptor by human and rat osteoblasts and osteoclasts suggests a novel glutamate signaling pathway in bone. *Bone.* 22(6):645-649, 1998.

Piekarski K. Analysis of bone as a composite material. *Internatinoal J Eng Sci.* 11:557-565, 1973.

Piekarski K. and Munro M. Transport mechanism operating between blood supply and osteocytes in long bones. *Nature.* 269(5623):80-82, 1977.

Pollack S. R., Petrov N., Salzstein R., Brankov G. and Blagoeva R. An anatomical model for streaming potentials in osteons. *J Biomech.* 17(8):627-636, 1984.

Pead M. J., Suswillo R., Skerry T. M., Vedi S. and Lanyon L. E. Increased 3H-uridine levels in osteocytes following a single short period of dynamic bone loading in vivo. *Calcif Tissue Int.* 43(2):92-96, 1988.

Pead M. J., Skerry T. M., Lanyon L. E. Direct transformation from quiescence to bone formation in the adult periosteum following a single brief period of bone loading. *J Bone Miner Res.* 3:647-656, 1988.

Prendergast P. J. and Taylor D. Prediction of bone adaptation using damage accumulation. *J Biomech.* 27(8):1067-1076, 1994.

Qin Y. X., Rubin C. T. and McLeod K. J. Nonlinear dependence of loading intensity and cycle number in the maintenance of bone mass and morphology. *J Orthop Res.* 16:482-489, 1998.

Qin Y. X., Kaplan T., Saldanha A. and Rubin C. Fluid pressure gradients, arising from oscillations in intramedullary pressure, is correlated with the formation of bone and inhibition of intracortical porosity. *J Biomech.* 36(10):1427-1437, 2003.

Raab-Cullen D. M., Akhter M. P., Kimmel D. B. and Recker R. R. Bone response to alternate-day mechanical loading of the rat tibia. *J Bone Miner Res.* 9(2):203-211, 1994.

Rasmussen H. and Bordier P. *The Physiological and Cellular Basis of Metabolic Bone Disease.* Williams and Wilkins, Baltimore, 1975.

Rawlinson S. C., Pitsillides A. A. and Lanyon L. E. Involvement of different ion channels in osteoblasts' and osteocytes' early responses to mechanical strain. *Bone.* 19(6):609-14, 1996.

Reich K. M., Gay C. V. and Frangos J. A. Fluid shear stress as a mediator of

osteoblast cyclic adenosine monophosphate production. *J Cell Physiol.* 143:100-104, 1990.

Reich K. M. and Frangos J. A. Effect of flow on prostaglandin E2 and inositol trisphosphate levels in osteoblasts. *Am J Physiol.* 261(3 Pt 1):C428-C432

Riedmiller M. and Braun H. A Direct Adaptive Method for Faster Backpropagation Learning: The RPROP Algorithm. *Proc. of the IEEE Int. Conf. on Neural Networks.* 586-591, 1993

Robling A. G., Hinant F. M., Burr D. B. and Turner C. H. Improved bone structure and strength after long-term mechanical loading is greatest if loading is separated into short bouts. *J Bone Miner Res.* 17(8):1545-1554, 2002.

Romanello M., Veronesi V., D'Andrea P. Mechanosensitivity and intercellular communication in HOBIT osteoblastic cells: a possible role for gap junction hemichannels. *Biorheology.* 40(1-3,):119-121, 2003.

Rubin C. T. and Lanyon L. E. Regulation of bone formation by applied dynamic loads. *J Bone Joint Surg Am.* 66(3):397-402, 1984.

Rubin C. T. and Lanyon L. E. Regulation of bone mass by mechanical strain magnitude. *Calcif Tissue Int.* 37:411-417, 1985.

Rubin C. T. and Lanyon L. E. Osteoregulatory nature of mechanical stimuli: function as a determinant for adaptive remodeling in bone. *J Orthop Res.* 5(2):300-310, 1987.

Salzstein R. A. and Pollack S. R. Electromechanical potentials in cortical bone–II. Experimental analysis. *J Biomech.* 20(3):271-280, 1987.

Saunders M. M., You J., Trosko J. E., Yamasaki H., Li Z., Donahue H. J. and Jacobs C. R. Gap junctions and fluid flow response in MC3T3-E1 cells. *Am J Physiol Cell Physiol.* 281(6):C1917-1925, 2001.

Seino Y. Cytokines and growth factors which regulate bone cell function. *Acta Astronaut.* 33:131-6, 1994.

Skedros J. G., Hunt K. J., Hughes P. E. and Winet H. Ontogenetic and regional morphologic variations in the turkey ulna diaphysis: implications for functional adaptation of cortical bone. Anat Rec 273A(1):609-629, 2003.

Skerry T. M., Bitensky L., Chayen J. and Lanyon L. E. Early strain-related changes in enzyme activity in osteocytes following bone loading in vivo. *J Bone Miner Res.* 4(5):783-788, 1989.

Smalt R., Mitchell F. T., Howard R. L. and Chambers T. J. Induction of NO and prostaglandin E2 in osteoblasts by wall-shear stress but not mechanical strain. *Am J Physiol.* 273(4 Pt 1):E751-E758

Spencer G. J. and Genever P. G. Long-term potentiation in bone - a role for glutamate in strain-induced cellular memory? *BMC Cell Biol.* 31, 4(1):9, 2003

Srinivasan S., Weimer D. A., Agans S. C., Bain S. D. and Gross T. S. Low-magnitude mechanical loading becomes osteogenic when rest is inserted between each load cycle. *J Bone Miner Res.* 17(9):1613-20, 2002.

Sterck J. G., Klein-Nulend J., Lips P. and Burger E. H. Response of normal and osteoporotic human bone cells to mechanical stress in vitro. *Am J Physiol.* 274(6 Pt 1):E1113-E1120.

Thi M. M., Kojima T., Cowin S. C., Weinbaum S. and Spray D. C. Fluid shear stress remodels expression and function of junctional proteins in cultured bone cells. *Am J Physiol Cell Physiol.* 284(2):C389-403, 2003.

Turner C. H. Toward a mathematical description of bone biology: the principle of cellular accommodation. *Calcif Tissue Int.* 65:466-481, 1991.

Turner C. H., Forwood M. R., Rho J. Y. and Yoshikawa T. Mechanical loading thresholds for lamellar and woven bone formation. *J Bone Miner Res.* 9(1):87-97, 1994.

Turner C. H., Owan I. and Takano Y. Mechanotransduction in bone: role of strain rate. *Am J Physiol.* 269(3 Pt 1):E438-E442

Turner C. H., Robling A. G., Duncan R. L. and Burr D. B. Do bone cells behave like a neuronal network? *Calcif Tissue Int.* 70(6):435-442, 2002.

Weinbaum S., Cowin S. C. and Zeng Y. A model for the excitation of osteocytes by mechanical loading-induced bone fluid shear stresses. *J Biomech.* 27:339-360, 1994.

Westbroek I., Ajubi N. E., Alblas M. J., Semeins C. M., Klein-Nulend J., Burger E. H. and Nijweide P. J. Differential stimulation of prostaglandin G/H synthase-2

in osteocytes and other osteogenic cells by pulsating fluid flow. *Biochem Biophys Res Commun.* 268(2):414-419, 2000.

Williams J. L., Iannotti J. P., Ham A., Bleuit J. and Chen J. H. Effects of fluid shear stress on bone cells. *Biorheology.* 31:163-170, 1994.

Wolff J. Das Gesetz der Transformation der Knochen. Berlin, Hirschwald.

Wolff J. *The Law of Bone Remodelling.* Berlin, Springer.

Yellowley C. E., Li Z., Zhou Z., Jacobs C. R. and Donahue H. J. Functional gap junctions between osteocytic and osteoblastic cells. *J Bone Miner Res.* 15(2):209-217, 2000.

You L., Cowin S. C., Schaffler M. B. and Weinbaum S. A model for strain amplification in the actin cytoskeleton of osteocytes due to fluid drag on pericellular matrix. *J Biomech.* 34(11):1375-1386, 2001.

Ypey D. L., Weidema A. F., Hold K. M., Van der Laarse A., Ravesloot J. H., Van Der Plas A. and Nijweide P. J. Voltage, calcium, and stretch activated ionic channels and intracellular calcium in bone cells. *J Bone Miner Res 7 Suppl.* 2:S377-87, 1992.

Zaman G., Pitsillides A. A., Rawlinson S. C., Suswillo R. F., Mosley J. R., Cheng M. Z., Platts L. A., Hukkanen M., Polak J. M. and Lanyon L. E. Mechanical strain stimulates nitric oxide production by rapid activation of endothelial nitric oxide synthase in osteocytes. *J Bone Miner Res.* 14(7):1123-1131,

Zeng Y., Cowin S. C. and Weinbaum S. A fiber matrix model for fluid flow and streaming potentials in the canaliculi of an osteon. *Ann Biomed Eng.* 22:280-292, 1994.

Ziambaras K., Lecanda F., Steinberg T. H. and Civitelli R. Cyclic stretch enhances gap junctional communication between osteoblastic cells. *J Bone Miner Res.* 13(2):218-228, 1998.